NANOPARTICLE TECHNOLOGIES TO CURE AND PREVENT INFECTIOUS DISEASES

Thesis by

Magnus Adrian Gero Hoffmann

In Partial Fulfillment of the Requirements for
the Degree of
Doctor of Philosophy

CALIFORNIA INSTITUTE OF TECHNOLOGY
Pasadena, California

2022
(Defended October 26, 2021)

Magnus Adrian Gero Hoffmann
ORCID: 0000-0003-4923-9568

ABSTRACT

Despite almost 40 years of intensive research, there is still no curative treatment for HIV-1/AIDS. Anti-retroviral therapy (ART) prolongs the life expectancy of HIV-1-infected individuals but is associated with side effects, and multiple drugs need to be given in combination to prevent the development of viral resistance. In addition, treatment must continue for the lifetime of the individual due to the existence of a long-lived latent proviral reservoir. While a "sterilizing" cure remains difficult to achieve due to difficulties associated with identifying and clearing latently-infected cells, recent research has focused on designing a "functional" cure, i.e., a therapeutic strategy that enables long-term suppression of HIV-1 replication and remission of symptoms in the absence of ART. The work presented here describes a new therapeutic direction for the development of a functional cure against HIV-1. This approach is based on the hypothesis that HIV-1 is unable to escape from a nanoparticle (NP)-based decoy that presents clusters of the HIV-1 receptor CD4, because CD4-NPs mimic viral target cells more accurately than soluble CD4-based inhibitors and permit high-avidity interactions with trimeric HIV-1 Env proteins. We demonstrate that CD4-NPs are >10,000-fold more potent than soluble CD4 (sCD4) and prevent viral escape in vitro. AAV-mediated delivery of self-assembling CD4-NPs produced stable CD4-NP serum concentrations in mice that were almost 1,000-fold higher than concentrations required to neutralize HIV-1 in vitro, suggesting that these concentrations could be therapeutic. Viral challenge studies in non-human primates are underway to evaluate the potential of this therapeutic strategy.

As an alternative approach to generate decoys against HIV-1, we generated engineered red blood cells (RBCs) that expressed viral receptors and potently inhibited HIV-1 infection of target cells in vitro. Because RBCs do not contain nuclei or functional organelles required for protein translation, infection of engineered RBCs represents a dead-end for a lentivirus such as HIV-1, which must integrate into the host cell genome as part of its lifecycle. We generated stable erythroid progenitor cell lines that continuously produced HIV-1 receptor-expressing RBCs that could be administered to HIV-1-infected individuals. As RBCs vastly outnumber CD4+ T-cells, HIV-1's main target cells, and have extended lifetimes, only a fraction of an individual's RBCs would need to be replaced with the engineered RBC viral traps in order to suppress HIV-1 infection in vivo.

My work on CD4-NP therapeutics against HIV-1 also led to the invention and development of the EBR NP technology that is ideally suited for vaccine design applications. This technology can be used to modify any type of membrane protein to self-assemble into enveloped virus-like NPs without the need for additional proteins. EBR NP assembly is induced by inserting a short amino acid sequence into the cytoplasmic tail of the membrane protein, which was designed to recruit host proteins from the endosomal sorting complex required for transport (ESCRT) pathway. We applied this technology to design protein NP-based vaccines against Severe Acute Respiratory Syndrome coronavirus 2 (SARS-CoV-2), which elicited potent serum neutralizing antibody responses in mice. The EBR NP technology is also ideally suited for the development of hybrid vaccine approaches that allow genetic encoding of protein-based NPs, thereby combining attributes of mRNA and protein-based NP vaccines. Pilot studies demonstrated that mRNA and DNA vaccines encoding the self-assembling SARS-CoV-2 spike-EBR construct elicited ~10-fold higher neutralizing

antibody responses than mRNA and DNA vaccines encoding the unmodified spike protein. This hybrid approach has the potential to substantially enhance the potency of mRNA vaccines and could become a leading vaccine platform technology. Future applications for the EBR NP technology are discussed, including the development of a universal coronavirus vaccine to prevent future pandemics, and engineering EBR NPs to mRNA vaccines or therapeutic cargoes for efficient and targeted delivery.

PUBLISHED CONTENT AND CONTRIBUTIONS

Chapter 2:

Hoffmann, M.A.G., Bar-On, Y., Yang, Z., Gristick, H.B., Gnanapragasam, P.N.P, Vielmetter, J., Nussenzweig, M.C. and Bjorkman, P.J., 2020. Nanoparticles presenting clusters of CD4 expose a universal vulnerability of HIV-1 by mimicking target cells. *Proceedings of the National Academy of Sciences*, *117*(31), pp.18719-18728. https://doi.org/10.1073/pnas.2010320117

M.A.G.H. was the lead researcher on this project, designed the experiments, generated the reagents, performed the experiments, analyzed the data, and wrote the manuscript.

Chapter 4:

Hoffmann, M.A.G., Kieffer, C. and Bjorkman, P.J., 2021. In vitro characterization of engineered red blood cells as viral traps against HIV-1 and SARS-CoV-2. *Molecular Therapy-Methods & Clinical Development*, *21*, pp.161-170. https://doi.org/10.1016/j.omtm.2021.03.003

M.A.G.H. was the lead researcher on this project, designed the experiments, generated the reagents, performed the experiments, analyzed the data, and wrote the manuscript.

TABLE OF CONTENTS

Acknowledgements.....iii
Abstract iv
Published Content and Contributions.....v
Table of Contents..... vi

Chapter 1: Introduction 1
Discovery of HIV 1
HIV epidemiology and genetic diversity 3
HIV-1 structure, genome, and lifecycle 8
HIV-1 transmission, pathogenesis, and clinical progression 17
Treatment of HIV-1/AIDS 19
Barriers and strategies for the development of an HIV-1 cure 22
Thesis overview 26

Chapter 2: Nanoparticles presenting clusters of CD4 expose a universal vulnerability of HIV-1 by mimicking target cells 28
Abstract 29
Introduction 31
Results 33
Discussion 43
Methods and materials 49
Figures 59
Supplementary materials 71
Supplementary figures and tables 76

Chapter 3: AAV-mediated delivery of nanoparticle decoys to functionally cure HIV-1 89
Abstract 90
Introduction 92
Results 95
Discussion 100
Methods 102
Figures 108

Chapter 4: In vitro characterization of engineered red blood cells as viral traps against HIV-1 and SARS-CoV-2. 114
Abstract 115
Introduction 117
Results 118
Discussion 125

Methods 129
Figures 139
Supplementary figures 146

Chapter 5: EBR nanoparticle technology and AAV-mediated delivery of self-assembling CD4 nanoparticles 152
Abstract 153
Research challenge 156
EBR nanoparticle technology 160
Future directions 167
Figures 181

Bibliography 194

Chapter 1

INTRODUCTION

Discovery of HIV

On June 5, 1981, a report published by the US Centers for Disease Control and Prevention (CDC) described five cases of Pneumocystis carinii pneumonia (PCP), a rare opportunistic lung infection that only occurs in severely immunocompromised individuals[1]. All patients were young homosexual men without previous health problems. On the same day, the CDC received reports of gay men presenting with a rare form of skin cancer, Kaposi's sarcoma[2], which is associated with a weakened immune system. By the end of 1981, 270 cases of severe immunodeficiency among homosexual men were reported, and by 1982 the CDC estimated that tens of thousands may be affected by the disease[3]. The symptoms predominantly affected homosexual males, heroin users, Haitians, and hemophiliacs, which led the CDC to introduce the name "4H disease". From September 1982, the CDC started to use the term acquired immune deficiency syndrome (AIDS)[3].

In 1983, a retrovirus later known as human immunodeficiency virus type 1 (HIV-1) was identified as the causative agent of AIDS[4]. At the time, many potential causes of the disease had been proposed such as fungi, chemicals, and autoimmunity, but a number of observations pointed towards a virus[5]. Firstly, there were reports of AIDS cases in patients with hemophilia who received filtered clotting factors suggesting that the causative agent can be transferred through blood and has to be smaller than bacteria or fungi. Secondly, the

disease was marked by a decrease in the levels of CD4+ T-lymphocytes, a specific type of immune cell involved in the adaptive immune response[6], suggesting that the causative agent specifically targets this cell type. Moreover, lymphotropic retroviruses had been shown to induce AIDS-like symptoms in animal models[5], and human T-cell leukemia virus (HTLV), a retrovirus that specifically infects T-lymphocytes, had recently been discovered[7].

HIV-1 was first isolated from a French patient with early-stage AIDS symptoms such as lymphadenopathy in Luc Montagnier's laboratory at the Pasteur Institute[4]. T-lymphocytes were derived from a lymph node biopsy and cultured in the presence of interleukin-2. The culture supernatant exhibited reverse transcriptase activity, a class of enzymes found in retroviruses that copy RNA into DNA[8,9]. Electron micrographs showed virus particles budding from cells that were morphologically and antigenically distinct from HTLV[4]. Importantly, T-cells from healthy donors could be infected with the virus-containing supernatant, but not other cell types such as B-lymphocytes and fibroblasts. Luc Montagnier and Françoise Barre-Sinoussi, the lead scientist on this project, received the Nobel Prize for the isolation and characterization of HIV-1 in 2008.

The causal link between HIV-1 and AIDS was substantiated by studies from Robert Gallo's group at the National Cancer Institute[10] and a research team at the University of California, San Francisco, led by Jay Levy[11], which independently reported the isolation of HIV-1 from larger groups of AIDS patients. Gallo's team achieved another breakthrough as they were able to infect a cell line with HIV-1, which enabled scientists to study and characterize the virus. This early work laid the foundation for the development of HIV-1

blood tests and life-saving therapeutics. Despite enormous progress over the last 40 years since the start of the epidemic, HIV-1/AIDS remains a major public health issue and a highly active field of research with many unanswered questions.

HIV epidemiology and genetic diversity

By the end of 2019, more than 75 million people have become infected since the start of the epidemic, and 32.7 million people have died from AIDS-related causes[12]. The World Health Organization (WHO) estimated that there were 38 million people living with HIV worldwide[13] with almost 70% of infected people living in sub-Saharan Africa (Fig. 1). Although infection and death rates have steadily decreased, every year 1.7 million people become newly infected with HIV and 690,000 people die of AIDS-related illnesses[12]. In 2014, the Joint United Nations Programme on HIV/AIDS (UNAIDS) proposed an ambitious 90-90-90 treatment targets: i) 90% of infected people know their HIV status; ii) 90% of infected people who know their HIV status have access to anti-retroviral therapy (ART); iii) viral suppression is achieved in 90% of patients receiving ART[12]. As of 2019, approximately 81% of people living with HIV were aware that they had been infected and 67% of knowingly-infected people received ART (Fig. 2). Viral suppression was achieved in only 59% of treated individuals likely due to poor adherence and ineffective drug combinations, which allow HIV to replicate and acquire escape mutations leading to drug resistance (Fig. 2). Despite intensive efforts, these results suggest that it will be difficult to control the HIV epidemic in the absence of a vaccine and/or cure.

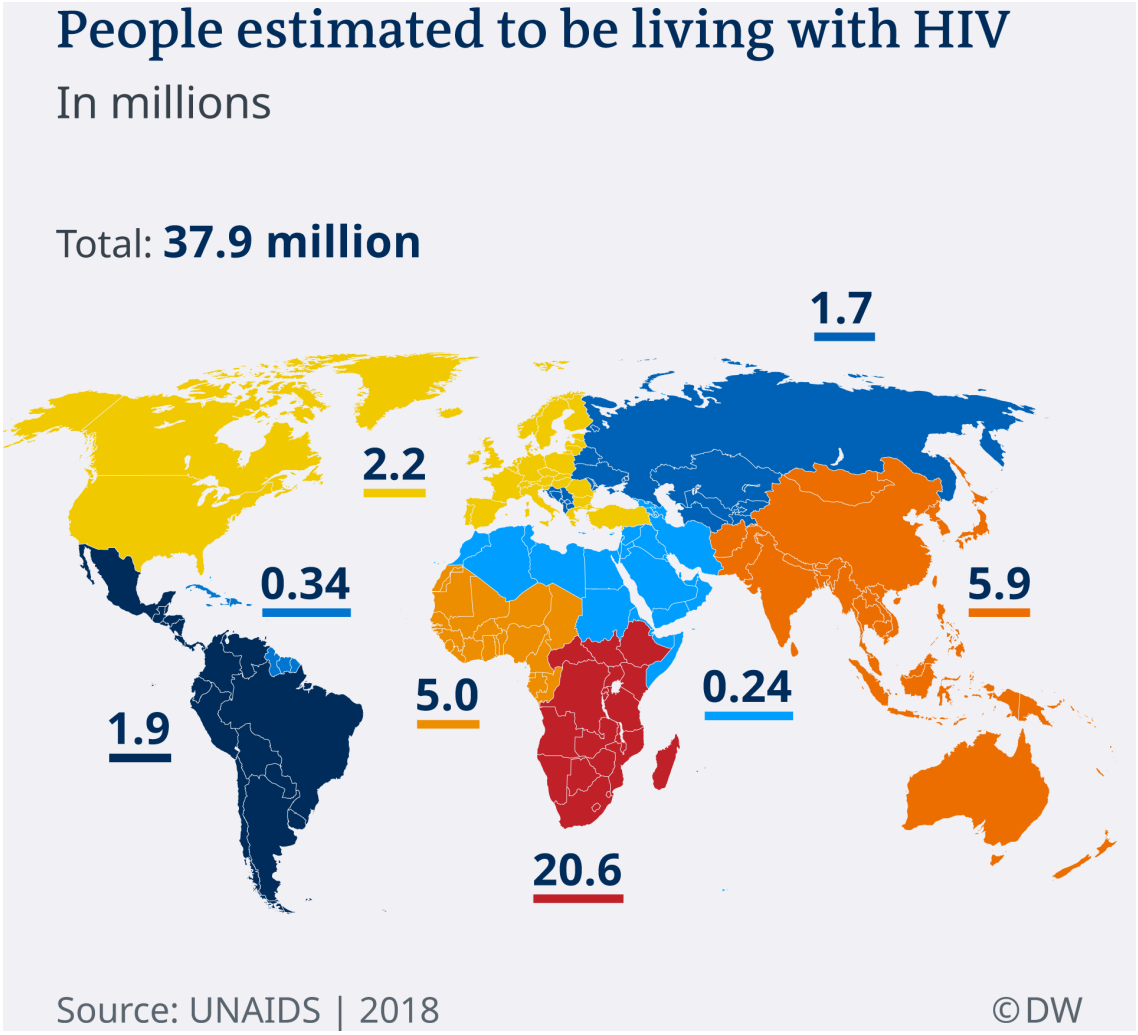

Figure 1. Worldwide distribution and prevalence of HIV-1/AIDS.

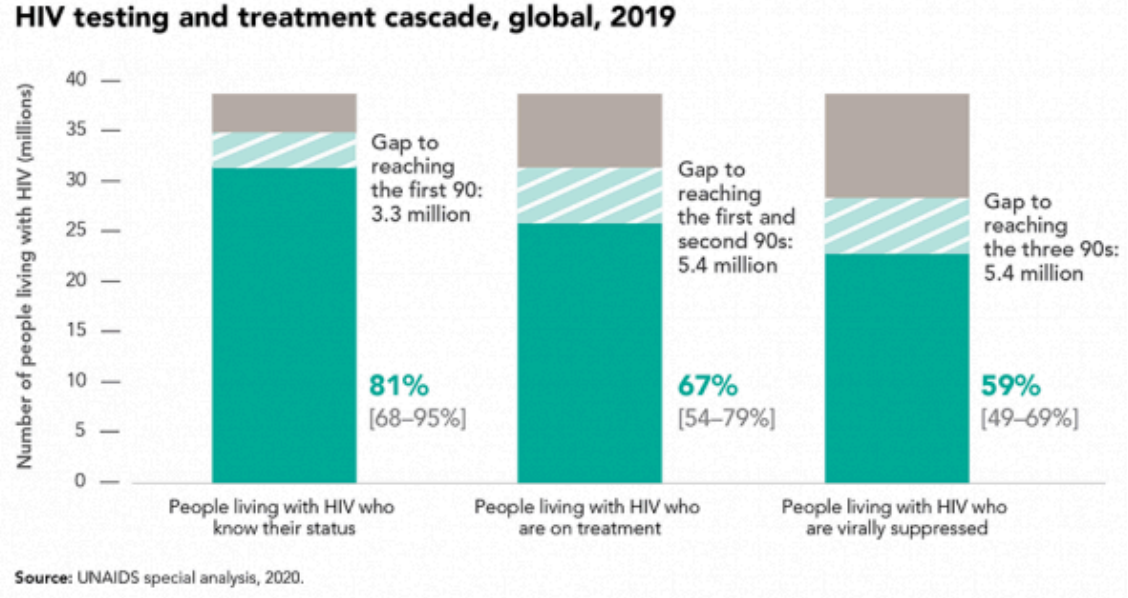

Figure 2. 90-90-90 treatment targets proposed by UNAIDS.

The genetic diversity of HIV represents one of the biggest roadblocks to achieving global treatment targets, as well as the development of an effective vaccine or cure. There are two major types of HIV, HIV-1 and HIV-2 (Fig. 3). While HIV-1 was discovered by Barre-Sinoussi and Montagnier in 1983[4], HIV-2 was found in 1986 in Western Africa[14]. HIV-1 and HIV-2 are morphologically similar and can both cause AIDS in infected patients, but HIV-1 is far more prevalent, infectious, and virulent than HIV-2[15]. It was later discovered that HIV-1 and HIV-2 are closely related to simian lentiviruses that infect chimpanzees[16] and sooty mangabeys[17], respectively, suggesting that the HIV/AIDS epidemic was the consequence of zoonotic transfer events from non-human primates to humans[18]. The genomes of HIV-1 and HIV-2 contain ~55% nucleotide sequence identity, and the amino acid sequences for viral proteins Gag, Pol, and Env share ~54%, ~55%, and ~35% sequence identity, respectively[19].

HIV-1 has been classified into four distinct lineages, groups M, N, O, and P, which resulted from independent cross-species transmission events (Fig. 3)[20]. Group M was discovered first and accounts for ~99% HIV-1 infections worldwide[20]. HIV-1 group M has been subdivided into 9 clades, A, B, C, D, F, G, H, J, and K, and numerous circulating recombinant forms (CRFs) have been identified that were derived from recombination events between different subtypes[21]. Clade C is the most prevalent subtype in Southern Africa, East Africa, and India, accounting for almost 50% of all global infections, while clade B predominates in North America, Western Europe, and Australasia (Fig. 4)[22].

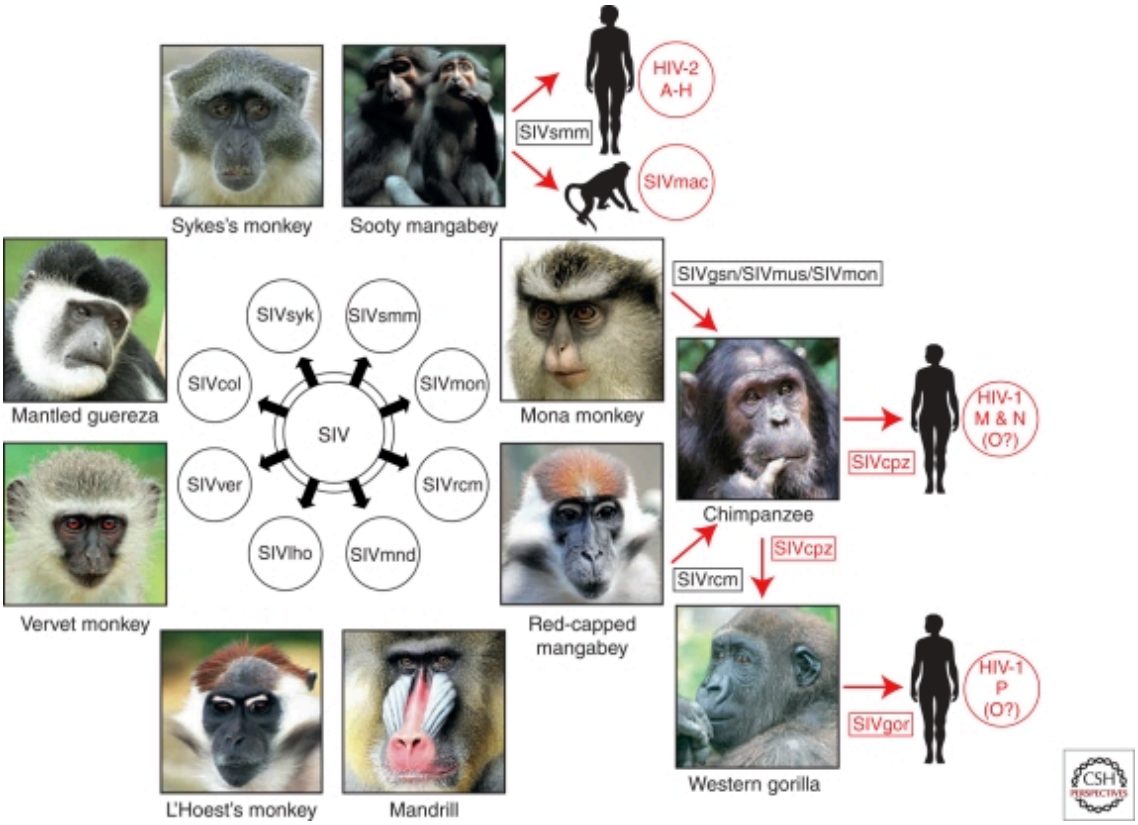

Figure 3. Origins of different HIV-1 lineages.

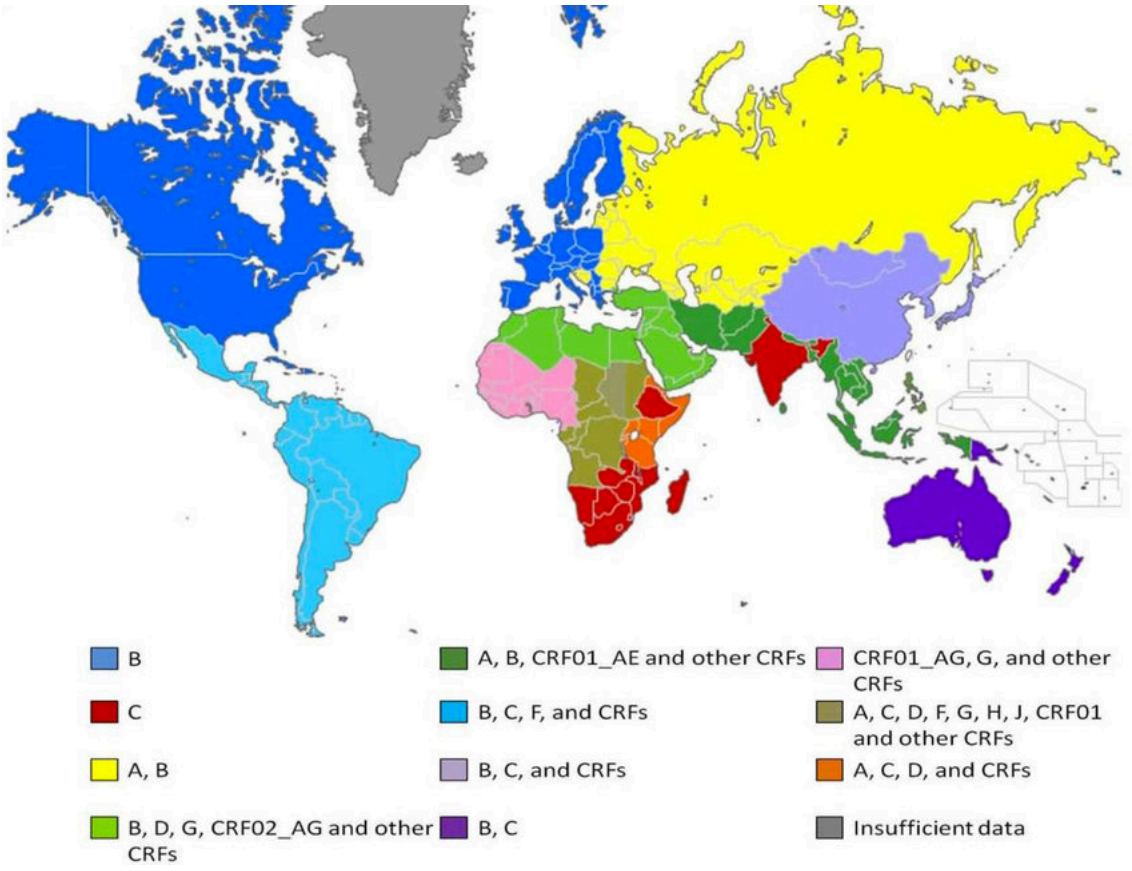

Figure 4. Prevalence and distribution of HIV-1 Group M clades and circulating recombinant forms.

Genetic variation within group M subtypes is generally 15-20% compared to 25-35% variation between group M subtypes[23]. The *gag* and *pol* genes are more conserved with 8-10% sequence variation, while up to 40% variation has been found for *env*[23]. The enormous degree of genetic diversity of HIV-1 has been driven by two main mechanisms. Firstly, the error-prone HIV-1 enzyme reverse transcriptase (RT) frequently introduces mutations when it converts the retroviral RNA genome into double-stranded DNA[24], an important step in the HIV-1 lifecycle. The mutation rate of HIV-1 has been estimated to be 10^5-10^6 times faster

than for eukaryotic genomic DNA, corresponding to 0.1-1 mutations per synthesized HIV-1 genome[25]. The second strategy HIV-1 employs to generate diversity is genetic recombination. Each HIV-1 virus particle contains two copies of single-stranded RNA, which allows RT to frequently switch between templates during reverse transcription. During each replication cycle, between two and twenty recombination events can occur[26], which leads to extensive reshuffling of genetic information and facilitates the rapid evolution of drug-resistant HIV-1 variants[27].

HIV-1 structure, genome, and lifecycle

HIV-1 belongs to the genus *lentivirus*, a subgroup within the *retroviridae* family. HIV-1 is an enveloped virus with a diameter of ~120 nm that contains two copies of a single-stranded, positive-sense RNA genome (Fig. 5). The RNA molecules interact with the nucleocapsid protein p7 and are enclosed by a conical capsid composed of 2,000 copies of the p24 protein[28]. The HIV-1 capsid also contains a small number of copies of the viral enzymes reverse transcriptase, integrase, and protease, which are essential for the HIV-1 lifecycle. The viral protein p17 forms a matrix that surrounds the capsid and provides support for the lipid bilayer envelope. On the surface of the virion, ~7-14 copies of the envelope glycoprotein (Env) are displayed[29], a trimeric protein composed of gp120-gp41 heterodimers. Env interacts with cellular receptors to mediate viral entry into target cells.

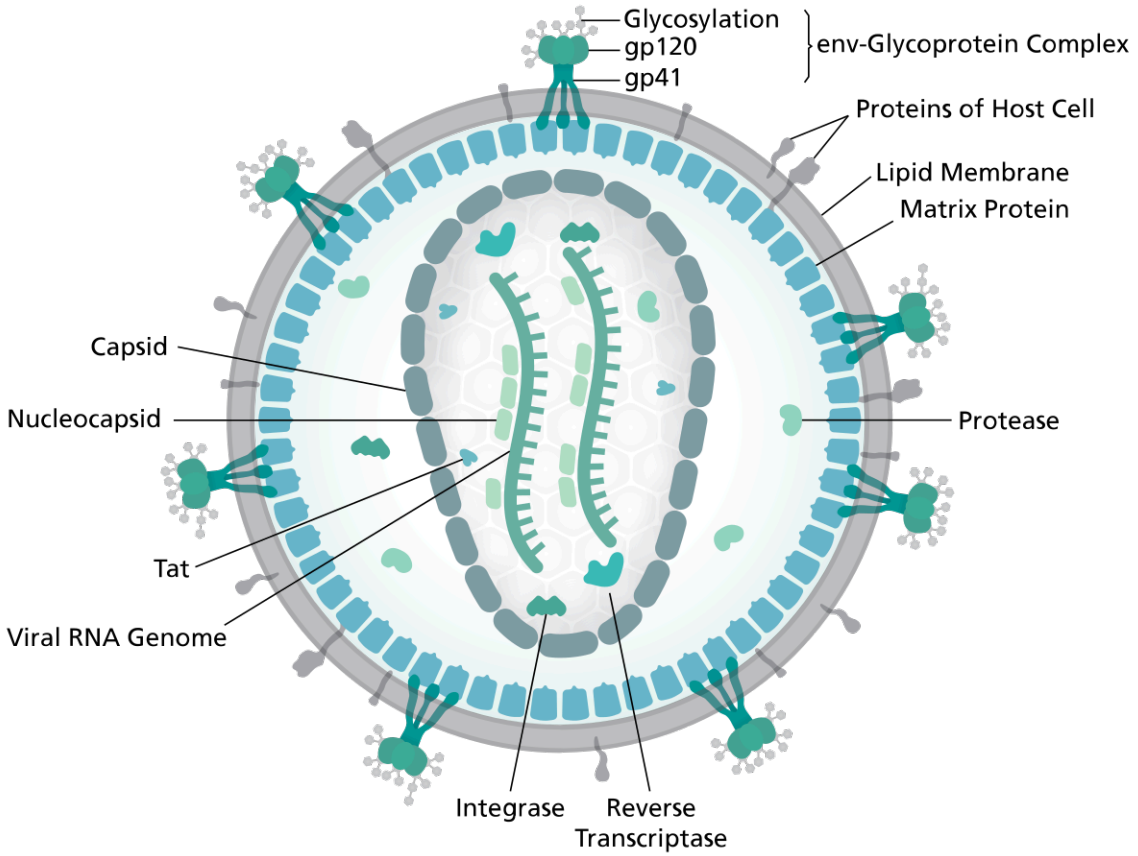

Figure 5. Schematic outlining the structure and components of HIV-1.

The HIV-1 lifecycle comprises seven distinct stages: 1) attachment; 2) fusion; 3) reverse transcription; 4) integration; 5) replication; 6) assembly; and 7) budding and maturation (Fig. 6). Initial attachment of HIV-1 virions to host cells is mediated by the gp120 subunit of Env that interacts with the host receptor CD4 on the cell surface. CD4 is primarily expressed on the surface of CD4+ T-lymphocytes, a key cell type of the adaptive immune system and the main target cell of HIV-1[30]. CD4 plays an important role in the interaction between CD4+ T-lymphocytes and antigen-presenting cells (APCs) as it binds to the ß2-domain of class II major histocompatibility complex (MHC) molecules to facilitate

interactions between T-cell receptors (TCRs) and antigenic peptides presented on class II MHC proteins[31].

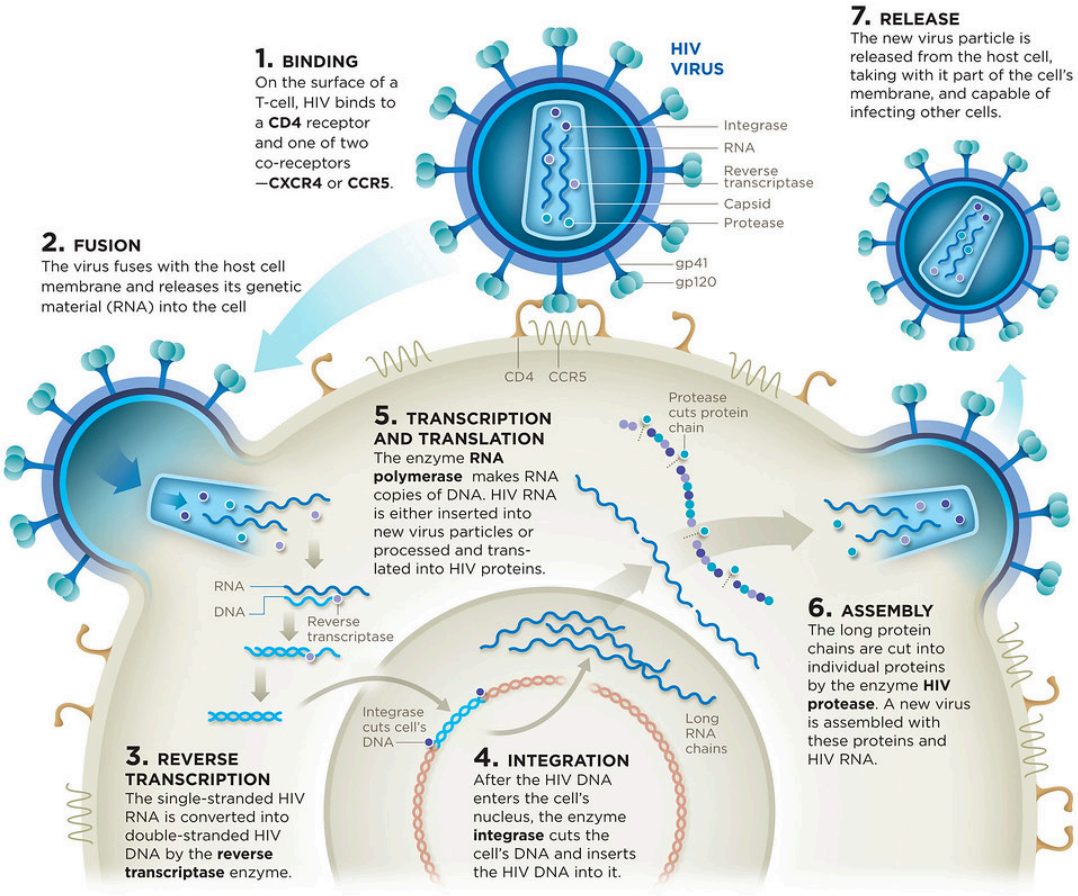

Figure 6. Individual stages of the HIV-1 lifecycle.

During HIV-1 attachment, CD4-binding induces a conformational change in gp120 that allows binding to a second host cell protein, the HIV-1 co-receptor[32]. In early infection, the HIV-1 co-receptor is the chemokine receptor CCR5; as the infection progresses, the viral population can evolve to use a related protein, CXCR4, as a co-receptor[33]. Co-receptor binding results in more stable attachment of HIV-1 virions to host cells and triggers

additional conformational changes in HIV-1 Env that initiate fusion of the lipid membranes of the virus and host cell. Insertion of the N-terminal fusion peptide of the gp41 subunit into the host cell plasma membrane creates a pre-hairpin intermediate[34], and gp120 subunits are shed from Env spikes[35]. Heptad repeat regions 1 and 2 within the gp41 subunits then interact to form a 6-helical bundle, which brings the viral and host cell membranes into close proximity and allows formation of a fusion pore through which the HIV-1 capsid can enter the target cell cytoplasm.

Following cell entry, the HIV-1 capsid containing the RNA genome migrates along microtubules towards the cell nucleus[36]. During this process, the single-stranded positive-sense viral RNA is converted into double-stranded DNA by the HIV-1 enzyme reverse transcriptase[24]. This enzyme performs three sequential biochemical functions: i) RNA-dependent DNA polymerase activity to synthesize the DNA strand complementary to the viral RNA; ii) ribonuclease H activity to degrade the viral RNA template; iii) DNA-dependent DNA polymerase activity to generate the second DNA strand[37]. This process is highly error-prone as reverse transcriptase lacks proofreading ability, which produces many viral variants within infected individuals and enables HIV-1 to escape from the immune system and ART[24].

Uncoating of the HIV-1 capsid releases the synthesized double-stranded DNA inside the cell nucleus[38,39], which is then integrated into the host cell genome, a multi-step process driven by the viral enzyme integrase[40]. The integrated DNA copy of the viral genome remains in an infected cell, resulting in a latent reservoir of cells that cannot be targeted by

the immune system or ART, but which can pass on the viral DNA to daughter cells of the original infected cell, allowing the descendants of the infected cell to produce new HIV virions[41].

The ~9.7 kb HIV-1 genome comprises nine genes that encode for 15 viral proteins[42] (Fig. 7). At the 5' and 3' ends, the genome contains non-coding sequences called long terminal repeats (LTRs), which play important regulatory roles in the HIV-1 lifecycle. For the integrated HIV-1 provirus, the 5' LTR functions as promoter to drive transcription while the 3' LTR contains transcription termination and polyadenylation signals[43]. HIV-1 replication requires the presence of certain host transcription factors, most importantly NF-κB, which is upregulated in activated CD4+ T-cells and interacts with specific sites located in the 5' LTR[44].

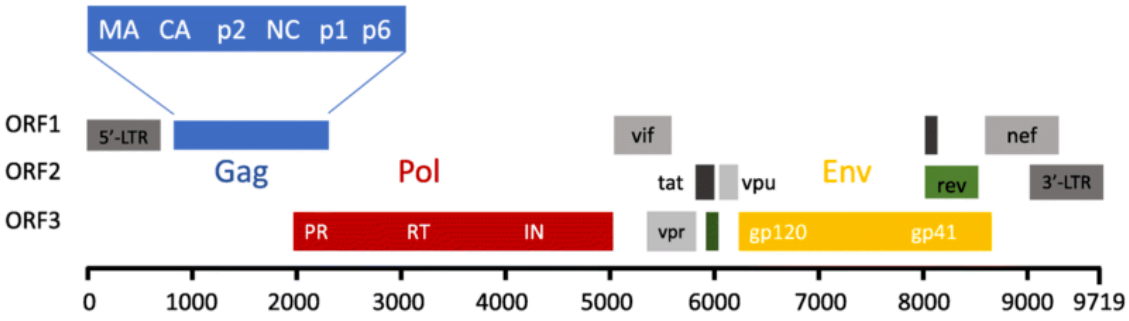

Figure 7. Organization of the HIV-1 genome.

During replication, the integrated proviral DNA is transcribed as a full-length precursor mRNA, which undergoes extensive alternative splicing to generate completely spliced (*tat, rev, nef*), partially spliced (*env, vpu, vpr, vif*), and unspliced (*gag-pol*) mRNA

transcripts[45]. During the early stage of the replication cycle, transcripts are completely spliced and translated into the essential regulatory proteins Tat and Rev. Tat greatly enhances the efficiency of viral transcription by interacting with the trans-activating response element (TAR), an RNA stem loop structure located at the 5' ends of nascent viral transcripts and subsequent recruitment of P-TEFb, which interacts with RNA polymerase II to promote transcriptional elongation[46]. The Rev protein localizes to the nucleus where it interacts with the Rev response element (RRE), a highly structured RNA sequence located within the *env* coding region of partially spliced and unspliced HIV-1 mRNAs[47]. Assembly of the Rev-RRE complex leads to the recruitment of host proteins such as exportin-1 and Ran-GTP, which facilitates the export of these late HIV-1 transcripts into the cytoplasm[48].

Translation of late HIV-1 mRNAs results in expression of the HIV-1 structural polyproteins Gag, Pol, and Env. The unspliced transcripts encode Gag and Pol, but since viral assembly requires more copies of Gag than Pol, HIV-1 has evolved a ribosomal frameshifting mechanism that regulates their translation[49]. An A-U-rich pseudoknot downstream of the Gag termination codon causes the ribosome to slip by one nucleotide into a different reading frame and translation continues to synthesize Gag-Pol[49]. This frameshifting mechanism is inefficient and only occurs during ~5% of translation events resulting in a Gag to Gag-Pol ratio of ~20:1[50]. Some copies of the unspliced RNA get packaged as viral genomes into assembling HIV-1 virions[49].

The viral spike glycoprotein Env is encoded by partially spliced transcripts and is initially translated into gp160, which forms a homotrimer and subsequently gets

proteolytically cleaved by the cellular protease furin into the surface-exposed gp120 and membrane-anchored gp41 components[51]. The gp120 and gp41 subunits remain non-covalently attached to form a trimer of heterodimers. As Env is the sole protein exposed on the surface of the virus, HIV-1 has evolved a number of strategies to prevent effective targeting of Env by humoral immune responses. First, Env gets heavily glycosylated within the Golgi apparatus with N-linked glycans comprising ~50% of the total molecular mass of Env spikes[52]. This dense array of N-linked glycans serves as a shield to prevent access of antibodies that recognize neutralizing and conserved epitopes, which contributes to the immunodominance of autologous and non-neutralizing epitopes, a major obstacle for HIV-1 vaccine design efforts[53]. Another immune evasion mechanism employed by HIV-1 is the comparatively low density of Env spikes on the viral surface, as the large inter-spike distances impede antibodies from simultaneously using both antigen-binding fragments (Fabs) to bivalently bind to Env spikes[54,55]. To achieve low spike density on virions, HIV-1 Env surface expression is tightly regulated during viral replication through degradation of frequently misfolded gp160 precursor proteins in the endoplasmic reticulum[56] and rapid endocytosis of Env proteins at the plasma membrane[57]. In combination with the rapid mutation rate of HIV-1, these characteristics of the Env protein facilitate viral immune evasion and represent a roadblock to the development of an effective HIV-1 vaccine.

In addition to the regulatory and structural proteins, four accessory proteins (Nef, Vif, Vpr, Vpu) are produced during HIV-1 replication. Nef is translated from completely spliced transcripts during the early stage of the lifecycle and promotes viral replication and pathogenicity by modulating the expression of a wide range of cellular target proteins,

including the downregulation class I MHC molecules from the cell surface, another immune evasion mechanism that prevents cytotoxic CD8+ T-cells from attacking infected cells[58]. Nef also downregulates CD4, which ensures incorporation of Env into budding virions and efficient release of infectious HIV-1 particles from the plasma membrane[59]. The main function of the accessory proteins Vif and Vpu is to antagonize the cellular restriction factors apolipoprotein B editing complex 3G/F (APOBEC3G/F) and Tetherin, respectively. APOBEC3G/F are cytidine deaminases that interfere with reverse transcription of the HIV-1 RNA in multiple ways, most notably by introducing an excessive number of mutations to render viral genomes non-functional[60]. Vif counteracts this effect by interacting with APOBEC3G/F, which induces ubiquitination and proteasomal degradation[61]. Tetherin is a dimeric type II transmembrane protein that inhibits the release of budding HIV-1 particles by inserting its C-terminal glycophosphatidylinositol (GPI) anchor into the viral envelope thereby physically tethering virions to the cell surface[62]. Vpu induces downregulation of tetherin from the cell surface[63] and works synergistically with the Env and Nef proteins to downregulate CD4 through distinct and independent mechanisms[59]. The final accessory protein, Vpr, gets incorporated into virions and facilitates nuclear import of the viral pre-integration complex[64]. Vpr also induces cell cycle arrest to block proliferation of infected cells and enhances HIV-1 protein expression[64].

During the late phase of the replication cycle, HIV-1 assembly is initiated by the uncleaved Gag polyprotein, which contains matrix (MA), capsid (CA), nucleocapsid (NC), and p6 domains[65]. The N-terminal MA domain gets myristoylated, which enables Gag to localize at the cytoplasmic side of the plasma membrane[66]. The MA domain also interacts

with the cytoplasmic tail of the Env protein to ensure incorporation of Env spikes into the assembling HIV-1 virion[67]. Gag multimerization is driven by the CA domain, and the NC domain recruits the HIV-1 RNA genome into assembling virions by interacting with the Psi packaging signal[65]. The C-terminal p6 domain of Gag interacts with host proteins from the endosomal sorting complexes required for transport (ESCRT) machinery to promote budding of newly-assembled virions from the plasma membrane[68].

Released virions are initially immature and a number of biochemical and structural maturation steps are required for production of infectious HIV-1 particles. HIV-1 maturation of the Gag and Gag-Pol precursor polyproteins is initiated through Gag-Pol dimerization, which enables the intramolecular HIV-1 protease to self-cleave Gag-Pol[69]. The released protease then continues to process the Gag and Gag-Pol precursor proteins to liberate the structural proteins MA, CA, NC, and p6, as well as the viral enzymes reverse transcriptase and integrase[70]. This proteolytic cleavage cascade results in a number of morphological changes, including the generation of a conical capsid core that is needed for viral infectivity[28]. Mature HIV-1 virions are then able to disseminate and infect new host cells to initiate the next replication cycle, produce large amounts of viral progeny, and drive the clinical progression of the disease.

HIV-1 transmission, pathogenesis, and clinical progression

HIV-1 can be transmitted through direct contact with bodily fluids of an infected individual such as blood, semen, rectal and vaginal fluids, as well as breast milk. Most infectious events occur during vaginal or anal sexual intercourse, during which the virus has to cross the genital or rectal epithelium to establish an infection[71]. The risk of HIV-1 transmission is highest for the rectal epithelium (0.3 – 5%) compared to the female (0.05 – 0.5%) and male genital epithelium (0.04 – 0.14%)[72]. It has been suggested that HIV-1 is able to traverse the mucosal epithelium through micro-tears that arise during sexual intercourse[73]. At mucosal entry sites, HIV-1 frequently encounters dendritic cells (DCs) that capture the virus through interactions between the heavily glycosylated HIV-1 gp120 and the DC-specific heparan sulfate proteoglycan Syndecan or DC-specific intercellular adhesion molecule-grabbing nonintegrin (DC-SIGN)[74]. Although DCs themselves are poorly infected by HIV-1, they can transport captured virions to secondary lymphoid tissues and facilitate trans-infection of a large number of CD4+ T-cells through the formation of immunological synapses, thereby contributing to the rapid spread of the infection[74].

Another common route of transmission is through sharing of contaminated injection equipment between intravenous drug users[75]. Vertical HIV-1 transmission from an infected mother to her child can occur during pregnancy, birth, and breastfeeding[76]. Importantly, the risk of sexual and vertical HIV-1 transmission is extremely low if the infected sexual partner or child-bearing mother is effectively treated with ART and has consistently undetectable viral loads[77]. Other prevention strategies against sexual transmission include the use of

condoms[78] and pre-exposure prophylaxis (PrEP), a once-daily medicine that contains an anti-retroviral drug combination that can be prescribed for uninfected high-risk individuals[79].

During the acute stage of HIV-1 infection, the virus multiplies and spreads rapidly throughout the body leading to high viral loads and substantial declines in CD4+ T-cell counts in the peripheral blood[80] (Fig. 8). Individuals may experience flu-like symptoms such as fever, headache, and rash, but the severity of symptoms varies considerably from person-to-person. Standard HIV-1 diagnostic tests that measure the body's antibody response against the virus cannot reliably detect HIV-1 infection in the initial 1-3 months. This greatly increases the risk of HIV-1 transmission during this window period as plasma viral loads are very high and newly-infected individuals may falsely believe to be HIV-1-negative.

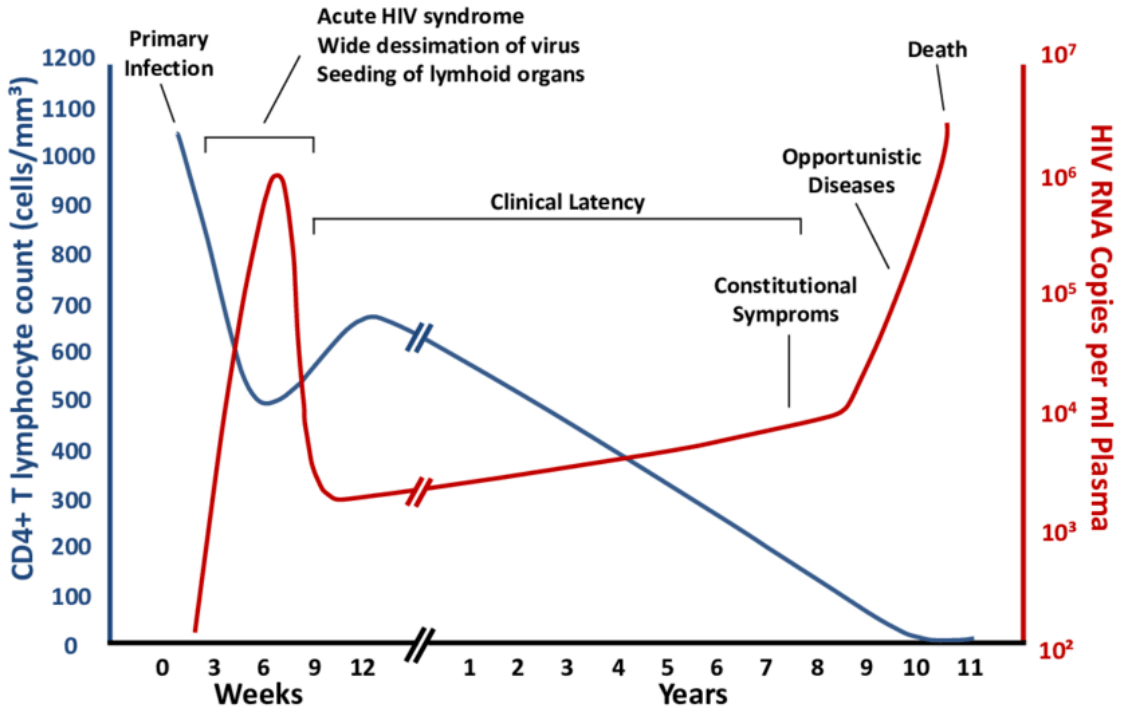

Figure 8. Clinical progression of HIV-1/AIDS.

In response to the acute infection, the body mounts an immune response to temporarily halt the clinical progression of the disease. During the chronic stage of the infection, HIV-1 can establish a latent infection characterized by very low or undetectable replication and plasma viral loads (Fig. 8). This phase can last 8-12 years[81], during which patients may be asymptomatic or experience only mild HIV-1-related symptoms. CD4+ T-cell counts initially recover towards normal levels, although they often don't return to pre-infection levels. As the immune system fails to clear the infection, HIV-1 continues to replicate resulting in a gradual decline of CD4+ T-cell counts and onset of early symptoms such as thrush, weight loss, and fatigue[82]. Viral adaptation to use CXCR4 instead of CCR5 as co-receptor often occurs during the latent stage of infection and is associated with rapid T-cell depletion and accelerated disease progression[83]. Once CD4+ T-cell levels drop below 200 cells/mm^3, patients develop AIDS, and their weakened immune system becomes unable to fight off AIDS-related malignancies and opportunistic infections, including tuberculosis, PCP, and cytomegalovirus infection[84]. The median time from infection to death is 8-10 years in untreated patients[85].

Treatment of HIV-1/AIDS

Highly-active ART (HAART), the only current treatment for HIV-1 infection, significantly prolongs the life expectancy of infected individuals with average lifespans being only seven years lower than for uninfected people[86]. HAART is a cocktail of small molecule-based anti-retroviral drugs that inhibit viral enzymes involved in key steps of the

HIV-1 lifecycle, including reverse transcriptase (e.g., tenofovir, efavirenz), protease (e.g., indinavir), and integrase (e.g., raltegravir)[87]. Additional drugs target the viral entry step by blocking the co-receptor CCR5 (e.g., maraviroc) or by disrupting the HIV-1 molecular fusion machinery (e.g., enfuvirtide)[88]. Because of HIV-1's rapid mutation rate, HAART is only effective when given as a combination of 3-4 drugs from at least two different drug classes[89], each of which is associated with significant side effects. For example, HIV-1 reverse transcriptase inhibitors can cross-react to inhibit host cell mitochondrial DNA polymerases, resulting in lipodystrophy (body fat redistribution), chronic renal insufficiency, and/or liver failure[90].

Although the viral load is typically reduced to undetectable levels during HAART treatment, HIV-1 levels rebound within weeks of HAART treatment cessation because complete eradication of HIV-1 from the body is prevented by latent viral reservoirs, thus necessitating daily and lifelong treatment. The side effect profile and complex medication regimens associated with HAART often cause poor treatment adherence[91]. Lack of compliance is a major obstacle to the success of HAART as it enables HIV-1 to replicate and mutate, which leads to drug resistance and treatment failure[92]. HAART regimens can be adjusted by switching drugs if the prescribed treatment plan fails to suppress viral loads or if patients experience serious adverse drug reactions. Patient management therefore includes frequent monitoring of viral loads, CD4+ T-cell counts, and drug resistance, to ensure effective control of the infection. The average annual cost of HIV-1 care, including HAART, doctor visits, and regular blood testing, has been estimated to be $12,000-$20,000 per patient[93]. Although great progress has been made to facilitate global supply of medications

and almost 70% of infected individuals have access to HAART worldwide[12], the cost of lifelong treatment remains a roadblock to controlling the HIV-1 epidemic.

A promising alternative to HAART for the treatment of HIV-1 infection are broadly neutralizing antibodies (bNAbs) that are being evaluated in clinical trials. Some infected individuals develop bNAbs over the course of natural HIV-1 infection[94], which can be isolated by single-B-cell antibody cloning. While the majority of antibodies produced during infection are strain-specific or non-neutralizing, bNAbs have broad neutralizing activity against a large number of HIV-1 strains as they recognize highly conserved epitopes on HIV-1 Env proteins such as the CD4-binding site (CD4-bs), the V3-glycan patch, the V2 loop at the Env trimer apex, the membrane-proximal external region (MPER), and the subunit interface region between the gp120 and gp41 subunits[95]. Vaccines designed to elicit bNAbs are being tested in pre-clinical[96-100] and clinical studies, but there are significant challenges as most bNAbs exhibit unusual characteristics such as long complementarity determining regions (CDRs) to penetrate HIV-1 Env's glycan shield and a high frequency of somatic hypermutation as a result of continuous antibody-virus co-evolution[101,102].

However, passive transfer of monoclonal bNAbs is a promising treatment strategy against HIV-1 and has several advantages over HAART. While most small molecule-based HAART medications need to be taken daily, bNAbs have long half-lives of up to two months in vivo[103] and might require only 3-6 administrations per year. bNAbs have excellent safety profiles and cause fewer side effects than HAART. Moreover, bNAbs bound to HIV-1 Env proteins expressed on the cell surface could engage the host immune system to kill infected

cells[103]. Clinical studies in humans have shown that bNAbs can transiently suppress viremia and delay viral rebound in the absence of HAART[104-107]. Similar to multi-drug HAART regimens, multiple bNAbs targeting different epitopes will need to be administered in combination to achieve persistent suppression of viral replication to prevent the rapid emergence of resistant HIV-1 variants[107,108]. In addition, pre-screening of patients will be necessary as many infected individuals already harbored viruses that were resistant to bNAbs prior to the start of the study[103]. Despite less frequent administrations, combination bNAb therapy could be more expensive than HAART as the production cost for therapeutic antibodies is higher than for small-molecule drugs, and bNAbs need to be injected by healthcare professionals. Given these advantages and challenges, it will be interesting to see how bNAbs could be optimally integrated into the management of HIV-1 patients and the global fight to control this epidemic.

Barriers and strategies for the development of an HIV-1 cure

HAART effectively controls viral replication, but it is not curative and necessitates lifelong treatment. Hence the development of a cure against HIV-1 infection could have an enormous impact on the HIV-1/AIDS epidemic. Patients would be able to permanently stop HAART, significantly improving their physical and mental health. As a result of the reduced treatment cost and duration, curing HIV-1 infection with a single intervention would permit the treatment of more people living with HIV-1. The spread of HIV could be contained more effectively, and the disease may eventually be eradicated.

Among all infected individuals worldwide there are only two well-documented examples of an HIV-1 cure: the "Berlin"[109] and "London" patients[110]. Both individuals were diagnosed with advanced-stage blood cancers and needed allogeneic hematopoietic stem cell (HSC) transplants to treat the malignancies. In both cases, HSCs were isolated from a donor homozygous for a naturally-occurring deletion in the gene encoding the HIV-1 coreceptor CCR5 that prevents HIV-1 entry[111]. Stable HIV-1 remission was achieved in both patients as the virus remained undetectable in the absence of HAART. Although not possible as a general method for an HIV-1 cure because of the dangers associated with hematopoietic stem cell transplants, these cases suggest that a cure for HIV-1 infection is possible.

HIV-1 cure research focuses on the development of two types of cure approaches: a "sterilizing cure" and a "functional cure"[112] (Fig. 9). A sterilizing cure would completely eradicate HIV-1 from the body, which is difficult to achieve due to the presence of long-lived latently infected cells that harbor replication-competent HIV-1 genomes[113]. The dominant sterilizing cure approach is called "shock and kill", which aims to reactivate HIV-1 from its latent state (shock) to make infected cells visible to the immune system and conventional therapeutics (kill)[114]. Latent HIV-1 can be induced to replicate by latency-reversing agents (LRAs) such as vorinostat, I-BET 151, and the immune modulatory anti-CTLA4 antibody, a combination that has been shown to activate ART-resistant reservoirs in HIV-1-infected humanized mice[115]. However, it remains a challenge to reactivate all latent HIV-1 proviruses with conventional LRAs[116], and the non-specific nature of these drugs increases the susceptibility of CD4+ T-cells to HIV-1 infection[117] and causes suppression of cytotoxic T-lymphocytes[118]. Moreover, this approach could potentially have dangerous consequences as

reactivated HIV-1 could rapidly mutate to become resistant to immune responses and therapeutics. A study performed in non-human primates (NHPs) further suggested that shock and kill strategies could lead to harmful brain inflammation[119] as brain cells such as microglial cells frequently harbor latent HIV-1[120].

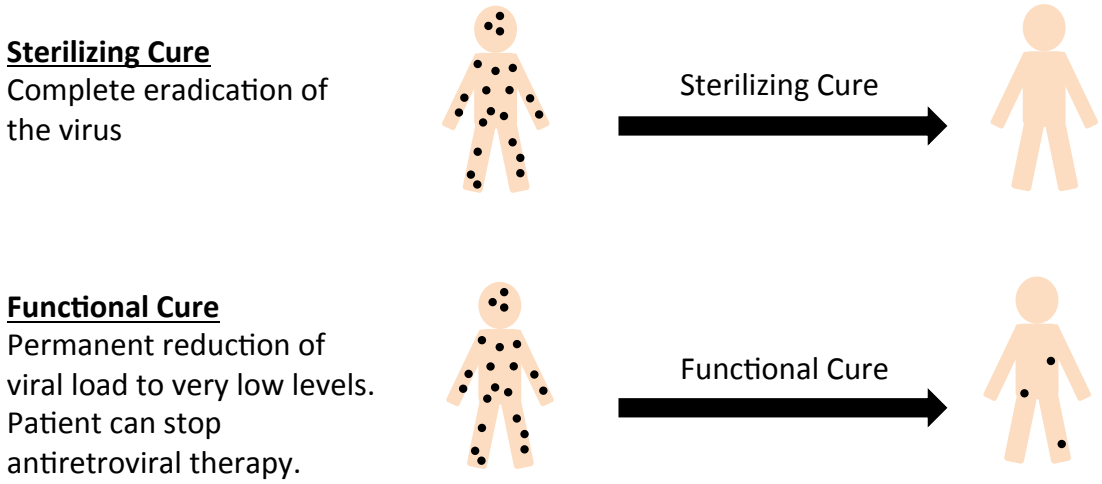

Figure 9. Comparison of sterilizing and functional cure approaches for HIV-1 infection.

Due to the challenges associated with achieving complete eradication of the HIV-1 latent reservoir, recent research has focused on designing a functional cure, which has been defined as a therapeutic strategy that enables long-term suppression of HIV-1 replication and remission of symptoms in the absence of HAART[121]. Thus, a functional cure would not completely eradicate HIV-1 from the body, but permanently reduce viral replication to undetectable levels. Three factors are important for the design of a successful functional cure strategy: i) the therapeutic intervention needs to have a permanent effect (e.g., gene therapy); ii) HIV-1 cannot develop resistance against the therapeutic strategy; iii) the therapeutic intervention does not cause adverse reactions or permanent damage to the patient.

Various strategies are being investigated for the development of a functional cure. A rare subset of infected people known as "elite controllers" naturally control HIV-1 infection in the absence of treatment[122] and these individuals have been studied intensely to gain insight about the viral control mechanisms. Most studies concluded that long-term viral control is achieved through T-cell-mediated immune responses, which may be influenced by genetic factors such as the presence of certain class I MHC alleles[123] or viral factors such as low levels of HIV-1 diversity[124]. As the underlying mechanisms appear highly complex and many elite controllers lose their ability to control viremia over the course of infection[122], it might be difficult to design therapeutic interventions that replicate these rare cases to achieve a functional cure.

Building on the examples of the Berlin and London patients, other researchers aim to develop ex vivo gene editing strategies to modify the CCR5 co-receptor gene in CD34+ HSCs[125]. However, it will be difficult to achieve uniform modification of all HSCs in the absence of total body irradiation and conditioning chemotherapy, which would enable HIV-1 to continue to replicate in unmodified cells and eventually evolve to use CXCR4 as co-receptor[126]. Another functional cure approach is called "block and lock", which aims to block HIV-1 transcription and introduce epigenetic modifications to lock the viral promoter in a super-latent state to permanently silence HIV-1 proviruses[127]. While block and lock might be safer and more specific than the shock and kill approach, a major limitation for both strategies is the need for efficient delivery of therapeutic agents to all latently-infected cells[127].

Gene transfer using adeno-associated virus (AAV)-based vectors that encode bNAbs or bNAb-like reagents has also shown promise for the development of a functional cure. This strategy has been demonstrated to produce stable bNAb serum concentrations and protection against viral challenges in vivo following a single intramuscular (IM) AAV injection[128-130]. The functional cure of a single NHP infected with a simian-human immunodeficiency virus (SHIV) has recently been reported after AAV-mediated delivery of the bNAbs 3BNC117 and 10-1074[131]. However, the effectiveness of this approach is limited by anti-drug antibody (ADA) responses that are frequently observed against the expressed bNAbs[131,132]. In addition, multiple bNAbs would need to be delivered in combination to prevent the emergence of resistant HIV-1 variants, and the slow onset of bNAb expression after AAV delivery provides a window opportunity for HIV-1 to replicate and rapidly acquire escape mutations.

Thesis overview

The work presented here describes a new therapeutic direction for the development of a functional cure against HIV-1. This approach is based on the hypothesis that HIV-1 would be unable to escape from a nanoparticle (NP)-based decoy therapeutic that presents clusters of CD4 receptors because it would mimic viral target cells more accurately than soluble CD4-based inhibitors and permit high-avidity interactions with trimeric HIV-1 Env proteins. Chapter 2 describes the initial design and extensive in vitro evaluation of CD4-NPs demonstrating that CD4-NPs are >10,000-fold more potent than soluble CD4 (sCD4) and

prevent viral escape in vitro. Chapter 3 discusses the development of AAV-based delivery strategies for various self-assembling CD4-NP designs and summarizes the results from ongoing in vivo experiments in mice and NHPs. Chapter 4 describes the in vitro production of engineered red blood cells (RBCs) that express viral receptors as an alternative decoy approach against HIV-1.

The work on CD4-NP designs presented in Chapter 3 also led to the invention and development of the EBR NP technology, which modifies any type of membrane protein to self-assemble into enveloped virus-like nanoparticles without the need for additional proteins. EBR NP assembly is induced by inserting a short amino acid sequence into the cytoplasmic tail of the membrane protein, which was designed to recruit host proteins from the endosomal sorting complex required for transport (ESCRT) pathway. Chapter 5 describes the mechanism of this technology and its application as a vaccine development platform for the design of NP-based vaccines against Severe Acute Respiratory Syndrome coronavirus 2 (SARS-CoV-2) and other coronaviruses. Future applications for the EBR NP technology are discussed, including the design of hybrid vaccine approaches that combine attributes of mRNA- and protein NP-based vaccines to enhance the potency of mRNA-based rapid-response vaccines and the development of a universal coronavirus vaccine to prevent future pandemics.

Chapter 2

NANOPARTICLES PRESENTING CLUSTERS OF CD4 EXPOSE A UNIVERSAL VULNERABILITY OF HIV-1 BY MIMICKING TARGET CELLS

Abstract

CD4-based decoy approaches against HIV-1 are attractive options for long-term viral control, but initial designs, including soluble CD4 (sCD4) and CD4-Ig, were ineffective. To evaluate a therapeutic that more accurately mimics HIV-1 target cells than monomeric sCD4 and dimeric CD4-Ig, we generated virus-like nanoparticles that present clusters of membrane-associated CD4 (CD4-VLPs) to permit high-avidity binding of trimeric HIV-1 envelope spikes. In neutralization assays, CD4-VLPs were >12,000-fold more potent than sCD4 and CD4-Ig, and >100-fold more potent than the broadly neutralizing antibody (bNAb) 3BNC117, with >12,000-fold improvements against strains poorly neutralized by 3BNC117. CD4-VLPs also neutralized patient-derived viral isolates that were resistant to 3BNC117 and other bNAbs. Intraperitoneal injections of CD4-CCR5-VLP only produced sub-neutralizing plasma concentrations in HIV-1–infected humanized mice, but elicited CD4-binding site mutations that reduced viral fitness. All mutant viruses showed reduced sensitivity to sCD4 and CD4-Ig but remained sensitive to neutralization by CD4-VLPs in vitro. In vitro evolution studies demonstrated that CD4-VLPs effectively controlled HIV-1 replication at neutralizing concentrations and viral escape was not observed. Moreover, CD4-VLPs potently neutralized viral swarms that were completely resistant to CD4-Ig, suggesting that escape pathways that confer resistance against conventional CD4-based inhibitors are ineffective against CD4-VLPs. These findings suggest that therapeutics that mimic HIV-1 target cells could prevent viral escape by exposing a universal vulnerability of HIV-

1: the requirement to bind CD4 on a target cell. We propose that therapeutic and delivery strategies that ensure durable bioavailability need to be developed to translate this concept into a clinically-feasible functional cure therapy.

Adapted from:

Hoffmann, M.A.G., Bar-On, Y., Yang, Z., Gristick, H.B., Gnanapragasam, P.N.P, Vielmetter, J., Nussenzweig, M.C. and Bjorkman, P.J., 2020. Nanoparticles presenting clusters of CD4 expose a universal vulnerability of HIV-1 by mimicking target cells. *Proceedings of the National Academy of Sciences*, *117*(31), pp.18719-18728.

Introduction

Anti-retroviral therapy (ART) prolongs the life expectancy of HIV-1-infected individuals, but is associated with side effects, and multiple drugs need to be given in combination to prevent the development of viral resistance[133]. In addition, treatment must continue for the lifetime of the individual due to the existence of a long-lived latent proviral reservoir. While a "sterilizing" cure remains difficult to achieve due to difficulties associated with identifying and clearing latently-infected cells[113,134], recent research has focused on designing a "functional" cure, i.e., a therapeutic strategy that enables long-term suppression of HIV-1 replication and remission of symptoms in the absence of ART[121].

The development of viral resistance is a major obstacle to achieving a functional cure, since low levels of latent replication-competent viruses persist in the body. Decoy approaches that closely mimic HIV-1 target cells are an attractive option for long-term viral control, as viral resistance through mutation could not develop without concomitant loss of target cell infectivity[135,136]. HIV-1 primarily infects CD4+ T-cells; the gp120 subunit of the viral envelope glycoprotein (Env) initially binds CD4, triggering a conformational change that allows it to interact with a host cell coreceptor protein, the chemokine receptors CCR5 or CXCR4, leading to fusion between the viral and host cell membranes[34].

Initial attempts to design decoys against HIV-1 used a soluble form of CD4 (sCD4) to block the receptor-binding sites on Env, but this strategy was ineffective in patients[137,138]. Subsequent studies revealed that many primary HIV-1 isolates

were relatively insensitive to sCD4 neutralization without apparent loss of viral fitness[139]. In addition, HIV-1 can develop resistance to CD4-based inhibitors by acquiring mutations in the CD4 binding site (CD4bs) on gp120 that lower its affinity for CD4[140-142] (Fig. 1). A potential explanation for the shortcomings of sCD4 therapy is that monomeric sCD4 fails to accurately mimic an HIV-1 target cell, where clusters of CD4 molecules on the membrane could enable Env, a trimeric protein with three CD4bs, to form multiple interactions that tether it to the cell surface[143]. Thus HIV-1 variants could escape from sCD4-mediated inhibition through avidity effects that compensate for a lower intrinsic sCD4 binding affinity by using multivalent interactions, thereby retaining the ability to efficiently infect target cells. Dimeric CD4-immunoglobulin fusion proteins (CD4-Ig)[144] do not overcome this problem, since bivalent binding with both CD4 arms is prevented by the low density of Env spikes on the viral surface and/or the architecture of single Env trimers[54,55,145] (Fig. 1).

To test this hypothesis, we generated HIV-1 Gag-based virus-like nanoparticles that present clusters of CD4 in its natural membrane-associated conformation (CD4-VLPs) (Fig. 1). We demonstrate that CD4-VLPs neutralize HIV-1 with enhanced potency and breadth compared to sCD4, CD4-Ig, and 3BNC117, a broadly neutralizing antibody (bNAb) that targets the CD4bs. We also show that viral escape pathways that confer resistance to sCD4 and CD4-Ig are ineffective against CD4-VLPs, suggesting that therapeutics that mimic HIV-1

target cells could prevent viral escape by exposing a universal vulnerability, the requirement to bind clusters of CD4 on a target cell.

Results

CD4-VLPs potently neutralize HIV-1

CD4-VLPs were generated by transiently co-expressing HIV-1 Gag and CD4 in Expi293 cells. When expressed in human cells, the Gag polyprotein self-assembles into immature core particles that form ~120 nm diameter VLPs by budding through the plasma membrane[146]. CD4-CCR5-VLPs were also generated to investigate if adding a coreceptor would enhance HIV-1 neutralization potency and breadth. VLPs were collected from transfected cell supernatants and concentrated by centrifugal filtration or sucrose cushion ultracentrifugation (Methods). Western blot analysis confirmed that CD4 and CCR5 were present on CD4-VLPs and CD4-CCR5-VLPs, respectively, but not on control VLPs (Fig. 2A). To determine VLP concentrations, we converted p24 measurements from enzyme-linked immunosorbent assays (ELISAs) against the Gag p24 capsid protein into VLP concentrations by assuming that each VLP contains 2,000 copies of Gag[147,148] (Methods). Typical VLP concentrations in transfected supernatants were ~10^{10} VLPs/mL, which could be concentrated to ~10^{11} VLPs/mL. To estimate the number of CD4 molecules per VLP, we combined supernatants from five independent CD4-VLP productions and purified CD4-VLPs using sucrose cushion ultracentrifugation and size exclusion chromatography (SEC) (Fig. S1A-B). Quantitative Western blot

analysis showed that purified CD4-VLPs contained the Gag-EGFP fusion protein and CD4 at a molar ratio of ~14:1 (Fig. S2A-C), suggesting that CD4-VLPs incorporated an average of 140 +/- 48 molecules of CD4. Cryo-electron tomography (cryo-ET) imaging of purified CD4-VLPs revealed spherical particles of ~120 nm diameter with discernable internal layers of immature Gag (Fig. 2B; Movie S1). Although membrane-bound CD4 molecules are too small to be visualized by cryo-ET, their presence on a number of CD4-VLPs, but not control VLPs, was confirmed by densities for bound soluble Env trimers (Fig. 2B; Movie S1). However, since there is no specific mechanism for packaging CD4 and CCR5 into HIV-1 Gag-based VLPs, CD4-VLPs that contained little or no CD4 were also observed.

The ability of CD4-VLPs to inhibit HIV-1 infection of target cells was evaluated using pseudovirus-based TZM-bl neutralization assays[149]. CD4-VLPs and CD4-CCR5-VLPs neutralized the HIV-1 strain YU2 at half maximal inhibitory concentrations (IC_{50}s) of 0.012 μg p24/mL and 0.006 μg p24/mL, equivalent to 1.5 x 10^8 and 0.8 x 10^8 VLPs/mL, respectively (Fig. 2C). Control VLPs showed no neutralization at concentrations up to 1.5 x 10^{10} VLPs/mL. Neutralization activity was independent of the VLP purification method and similar for different batches of CD4-VLPs (Fig. S3). A concentration of 2.1 x 10^{10} CD4 molecules/mL (0.0017 μg/mL) (calculated assuming that each CD4-VLP displays 140 copies of CD4) was required to achieve 50% neutralization. The comparable neutralization profiles of CD4-VLPs and CD4-CCR5-VLPs suggested that the presence of CD4 on VLPs

was sufficient for potent HIV-1 neutralization in the absence of CCR5. Extracellular vesicles (EVs) naturally secreted by eukaryotic cells[150] did not contribute to the neutralization activity of CD4-VLPs, as supernatants from cells transfected with CD4 in the absence of Gag had no effect (Fig. S4A-B).

CD4-VLPs neutralize HIV-1 with enhanced potency and breadth compared to sCD4, CD4-Ig, and a CD4bs bNAb

To investigate whether CD4 multimerization enhances the potency and breadth of CD4-based inhibitors, the neutralization activity of CD4-VLPs was compared to monovalent sCD4, bivalent CD4-Ig, and to 3BNC117 IgG, a CD4bs bNAb that has been evaluated in human clinical trials[104,107]. Potency and breadth were compared by quantifying the number of CD4 molecules (CD4-VLPs, sCD4, CD4-Ig) or antigen-binding fragments (Fabs) (3BNC117) required to neutralize a panel of 12 HIV-1 Env reference strains representing the global HIV-1 epidemic[151].

CD4-VLPs neutralized all 12 strains with a geometric mean IC_{50} of 1.3 x 10^8 VLPs/mL (Table S1). CD4-CCR5-VLPs did not show an overall enhanced potency compared to CD4-VLPs (geometric mean IC_{50} = 1.2 x 10^8 VLPs/mL). Assuming ~140 copies of CD4 per VLP (Fig. S2A-C), neutralization was achieved at a geometric mean IC_{50} of 1.9 x 10^{10} CD4 molecules/mL (Fig. 3A; Table S1). sCD4 and CD4-Ig neutralized only nine (sCD4) or seven (CD4-Ig) of 12 strains with geometric mean IC_{50} values of 10.0 and 27.7 μg/mL, respectively, equivalent

to 2.3 x 10^{14} and 3.3 x 10^{14} CD4 molecules/mL (Fig. 3A; Table S2). These results demonstrated that CD4-mediated neutralization of HIV-1 is >12,000-fold more potent for multivalent CD4, likely due to high avidity interactions between clustered CD4 receptors and HIV-1 Env.

CD4-VLPs were also more potent and broad than 3BNC117, which neutralized 11 of 12 strains with a geometric mean IC_{50} of 0.31 μg/mL (2.5 x 10^{12} Fabs per mL) (Fig. 3A; Table S2). Hence the geometric mean IC_{50} of CD4 molecules on CD4-VLPs was >100-fold lower compared to the required concentration of 3BNC117 Fabs, and >12,000-fold lower for the X1632, CH119, and BJOX2000 strains that are relatively insensitive to 3BNC117. Interestingly, there was only a 15-fold difference between the highest and lowest IC_{50}s against the 12 strains for CD4-VLPs compared to a 4,500-fold difference for 3BNC117, highlighting the excellent neutralization breadth of CD4-VLPs.

The neutralization activity of CD4-VLPs was also evaluated against primary isolates obtained from two previously-described HIV-1–infected patients[152]. These isolates were poorly neutralized by bNAbs that target various epitopes on Env, including the CD4bs, V1V2, the membrane-proximal external region, and the gp120-gp41 interface (IC_{50} values > 1 μg/mL) (Fig. 3B; Table S3). However, both isolates were potently neutralized by CD4-VLPs at concentrations similar to IC_{50}s determined against the HIV-1 strains in the 12-strain panel. Comparing the numbers of CD4 and Fab molecules required for 50% neutralization revealed that CD4-VLPs were 500–11,000-fold more potent than the CD4bs bNAb

3BNC117. Similar differences in potency were also observed when comparing CD4-VLPs to bNAbs targeting epitopes other than the CD4bs. These results demonstrated that primary HIV-1 isolates that are resistant to multiple bNAbs can be potently neutralized by a therapeutic that mimics HIV-1 target cells.

CD4-CCR5-VLP treatment in HIV-1–infected hu-mice elicits CD4bs mutations in HIV-1 Env despite poor bioavailability

We investigated the ability of CD4-CCR5-VLPs to suppress HIV-1 replication and prevent viral escape in vivo in HIV-1_{YU2}–infected humanized mice (hu-mice). CD4-CCR5-VLPs were selected for in vivo experiments to prevent the potential emergence of CD4-independent HIV-1 escape variants[153-155]. To determine an optimal administration regimen, initial half-life studies were performed in uninfected hu-mice. 7.6 x 10^9 CD4-CCR5-VLPs (610 ng of p24) were intraperitoneally (IP) injected into five hu-mice. Blood samples were taken from one animal per time point after 20 min, 1 hour, 2 hours, 4 hours, and 6 hours, and plasma CD4-CCR5-VLP concentrations were measured by p24 ELISA. CD4-CCR5-VLP concentrations were either slightly above or below the detection limit of 1.5 ng p24/mL (1.9 x 10^7 VLPs/mL) at all time points. A peak concentration of 8.5 x 10^7 VLPs/mL was measured 1 hour post-injection. Incomplete diffusion across the peritoneal membrane into the hepatic portal vein and rapid hepatic clearance[156] likely contributed to the poor bioavailability of CD4-CCR5-VLPs administered IP. These studies showed that IP administrations of CD4-CCR5-VLPs

reached only sub-neutralizing plasma concentrations as peak levels were lower than in vitro neutralization IC_{50} values against HIV-1_{YU2} (Table S1).

To achieve maximal plasma concentrations for experiments in HIV-1_{YU2}-infected mice, 6 x 10^9 control or CD4-CCR5-VLPs were IP injected twice daily for 10 days. This regimen failed to maintain detectable plasma VLP concentrations, as control VLPs and CD4-CCR5-VLPs were undetectable 6 hours post-injection on day 6 of treatment. The efficacy of CD4-CCR5-VLP treatment was compared with twice weekly IP injections of 1 mg of 10-1074, a V3-glycan patch bNAb being evaluated in human clinical trials [105]. While 10-1074 treatment achieved robust reductions in viral loads in all treated animals, control and CD4-CCR5-VLPs had no effect on viral loads (Fig. 4A).

To investigate whether intermittent sub-neutralizing CD4-CCR5-VLP plasma concentrations exerted selective pressure on HIV-1 in vivo, the circulating plasma viruses of two HIV-1–infected control VLP-treated animals and three CD4-CCR5-VLP-treated animals were analyzed by single-genome sequencing on day 10 after treatment cessation. Four recurring mutations (G366E, G458D/S, E466K, and G471R) were observed in the gp120 subunits of the HIV-1_{YU2} Envs obtained from CD4-CCR5-VLP-treated hu-mice, which were rare or absent from sequences derived from control VLP-treated animals (Fig. 4B). All individual mutations occurred in at least two animals and were mutually exclusive, except for one gp120 sequence, which contained both a G458D and a G471R mutation. Together, these variants accounted for 61.5% of the *env* genes sequenced from CD4-CCR5-VLP-

treated hu-mice, indicating that these mutations provided a selective advantage in the presence of intermittent sub-neutralizing CD4-CCR5-VLP plasma concentrations. Interestingly, in one CD4-CCR5-VLP–treated mouse, these mutations were found in 75% of the viruses (Fig. S5).

The substitutions mapped to residues in close proximity to the CD4bs in the gp120 subunit of Env (Fig. 4C), suggesting that the mutations reduced the ability of Env to bind CD4, thereby potentially allowing escape from CD4-based reagents. Indeed, the G366E[157], G458D[158], and G471R[142] mutations have been reported to confer partial resistance against CD4-based inhibitors. No recurrent mutations were found near the coreceptor-binding site, indicating that selective pressure was primarily exerted by CD4 on the CD4-CCR5-VLPs. All mutated residues are highly conserved among HIV-1 Env sequences, whereas the substitutions in the variants are rare (Fig. 4D), suggesting that these mutations could compromise viral fitness.

HIV-1_{YU2} variants are less infectious and not resistant to CD4-VLPs

Surface plasmon resonance (SPR) studies were performed to determine if the recurring mutations in *env* sequences from HIV-1-infected and CD4-CCR5-VLP-treated animals affected the CD4 binding affinity of HIV-1_{YU2} gp120. Potential avidity effects were avoided by injecting monomeric gp120 proteins ($YU2_{wt}$ gp120 and each YU2 gp120 variant) over immobilized CD4-Ig (Fig. S6A). The $YU2_{G366E}$ gp120 mutant was excluded from the SPR analysis, as gel

electrophoresis showed that this protein was unstable and migrated as multiple species (Fig. S6B).

Changes in CD4 binding were most evident for $YU2_{G458D}$ gp120, which dissociated 11-fold faster than $YU2_{wt}$ gp120 (Fig. 5A; Table S4). Weaker binding of this mutant was expected, as the Gly in $YU2_{wt}$ gp120 directly interacts with CD4, whereas the substituted Asp introduced a negative charge and potential steric clashes at this position (Fig. 4C). Changes in the CD4 binding affinity for the $YU2_{E466K}$ and $YU2_{G471R}$ gp120 mutants were less pronounced, since residues at both positions do not directly interact with CD4 (Fig. 4C). However, both substitutions introduced positive charges that could destabilize the CD4bs. Although SPR measurements were not possible for $YU2_{G366E}$ gp120, the substitution introduces a larger side chain and a negative charge into a residue that directly contacts CD4, thus it seems likely that $YU2_{G366E}$ gp120 binds CD4 more weakly than $YU2_{wt}$ gp120.

To ascertain if the changes in CD4 binding affinity directly impacted the ability of HIV-1 to infect target cells, we performed in vitro infection assays using HIV-1_{YU2} pseudoviruses carrying the observed mutations in gp120. Equivalent amounts of p24 (40 pg) were added to target cells for $YU2_{wt}$ and the YU2 variant pseudoviruses, and luciferase expression was monitored in CD4+/CCR5+ TZM-bl cells as a measure of HIV-1 infectivity. Infection was higher for the wild-type YU2 virus than for the variants (Fig. 5B); three of the mutant viruses ($YU2_{G366E}$, $YU2_{E466K}$, and $YU2_{G471R}$) were 3.8–6.6-fold less infectious than $YU2_{wt}$, while a 24-

fold reduction in viral entry fitness was observed for the $YU2_{G458D}$ variant. The decreased infectivity of the mutant viruses could be related to changes affecting their binding to CD4, in particular for the $YU2_{G458D}$ variant.

In vitro neutralization assays were performed to determine if the mutations confer resistance to CD4-VLPs and CD4-CCR5-VLPs. All mutant viruses were ~30-fold less sensitive than $YU2_{wt}$ to sCD4 and CD4-Ig (Fig. 5C; Table S5). Surprisingly, the mutant viruses were neutralized by CD4-VLPs and CD4-CCR5-VLPs at equivalent concentrations to those required for neutralization of the wild-type virus. This suggests that the mutations provided a selective advantage when exposed to short-lived, sub-neutralizing concentrations of CD4-CCR5-VLPs, but did not decrease viral sensitivity to neutralizing CD4-VLP or CD4-CCR5-VLP concentrations. This demonstrates that CD4bs mutations that enable viral escape against conventional CD4-based inhibitors would not confer resistance to CD4-VLPs.

To investigate if HIV-1 is able to escape when exposed to neutralizing CD4-VLP concentrations, we performed in vitro evolution experiments. Replication-competent $HIV\text{-}1_{YU2}$ was propagated on the Rev-A3R5 CD4+ T-cell reporter line[159] for 21 days to generate a diversified viral population. Infection rates were maintained at ~10% of infected cells by transferring the viral supernatant onto fresh target cells every three days. To compare the ability of CD4-Ig and CD4-VLPs to suppress viral replication, the viral swarm was distributed into multiple wells and exposed to their respective IC_{80}s and IC_{95}s for one hour before fresh target cells

were added. This cycle was repeated every 3 days and a total of 6 cycles were completed. On day 3, HIV-1-induced GFP expression in Rev-A3R5 cells was measured by flow cytometry, which demonstrated that both inhibitors suppressed infection rates effectively (Fig. 6A). After 4 cycles (day 12), infection rates increased to >4% in the presence of 17.5 μg/mL CD4-Ig (IC_{80}) for all replicates, which was set as a threshold to indicate viral escape. CD4-Ig concentrations were doubled to 35 μg/mL for the next cycle to assess if the viral swarms were still sensitive to higher inhibitor concentrations. No signs of viral escape were observed for all other conditions at this point. After cycles 5 and 6 (days 15 and 18), infection rates also increased in the presence of 22.5 μg/mL CD4-Ig (IC_{95}), and viral escape was observed for 2 of 3 replicates (Fig. 6A). Interestingly, infection rates for CD4-Ig (IC_{80}) remained above 4% for 2 of 3 replicates despite increasing the concentration to 70 μg/mL after cycle 5. Infection rates remained low for CD4-VLPs at both concentrations, suggesting that a therapeutic that presents clusters of CD4 is more effective at controlling HIV-1 replication and preventing viral escape than traditional CD4-based inhibitors.

A modified version of a recently published in vitro evolution protocol[160] was used to evaluate if HIV-1 can escape when intermittently exposed to increasing CD4-VLP concentrations. As above, the diversified HIV-1_{YU2} swarm was exposed to CD4-Ig and CD4-VLPs at starting concentrations of 17.5 μg/mL and $5x10^8$ VLPs/mL, respectively, for one hour before adding fresh target cells. After 3 days, infection rates were assessed under a fluorescent microscope and the cycle was

repeated in the absence of inhibitor to enable HIV-1 replication and ensure sufficient viral titers for the next selection cycle. This six-day on/off cycle was repeated 15 times (90 days), and inhibitor concentrations were gradually increased to final concentrations of 280 μg/mL of CD4-Ig and $1.6x10^{10}$ CD4-VLPs/mL. To evaluate if the selected viral swarms were resistant to the inhibitors, in vitro neutralization assays were performed. The diversified HIV-1_{YU2} control swarm that was continuously passaged in the absence of any inhibitor remained similarly sensitive as $YU2_{wt}$ to CD4-Ig (IC_{50} = 0.91 μg/mL) and CD4-VLPs (IC_{50} = 0.02 μg p24/mL) (Fig. 6B). However, the HIV-1_{YU2} swarm that was intermittently exposed to increasing CD4-Ig concentrations was completely resistant to CD4-Ig (IC_{50} > 100 μg/mL). In contrast, the viral swarm that was passaged in the presence of CD4-VLPs remained as sensitive to CD4-VLPs as the control swarm (IC_{50} = 0.014 μg p24/mL) (Fig. 6B). Importantly, CD4-VLPs also potently neutralized the CD4-Ig-resistant swarm (IC_{50} = 0.009 μg p24/mL), which confirmed that escape pathways against conventional CD4-based inhibitors are ineffective against CD4-VLPs. These results demonstrate that decoy therapeutics designed to present clusters of CD4 have the potential to effectively control HIV-1 replication and prevent viral escape.

Discussion

Here we show that virus-like nanoparticles that mimic HIV-1 target cells by presenting an array of CD4 molecules neutralize HIV-1 with enhanced potency and

breadth compared to conventional CD4-based inhibitors and bNAbs. In vivo studies in HIV-1_{YU2}-infected hu-mice showed that intermittent sub-neutralizing CD4-CCR5-VLP plasma concentrations induced recurring CD4bs mutations in Env that reduced viral fitness and neutralization sensitivity to sCD4 and CD4-Ig in vitro, but all mutant viruses remained as sensitive as wild-type virus to CD4-VLPs at neutralizing concentrations. In vitro evolution studies demonstrated that CD4-VLPs effectively controlled HIV-1 replication and viral escape was not observed. These results provide an explanation for the lack of efficacy of conventional CD4-based inhibitors and motivate the development of therapeutic strategies that more accurately mimic HIV-1 target cells to prevent viral escape and provide sustained suppression of HIV-1.

The enhanced neutralization potency and breadth of CD4-VLPs implies that membrane-associated display of multiple CD4 molecules is a more accurate mimic of the HIV-1 target cell than are monovalent or bivalent CD4-based inhibitors. Cell surface CD4 receptors co-localize in nanoclusters that contain ~4-15 molecules of CD4[161,162], which would facilitate multivalent binding to HIV-1 Envs. Because Env spikes are trimeric, each Env can bind up to three CD4 receptors and multiple Envs may be engaged during the cell entry process[163,164], leading to avidity effects. By comparison to soluble CD4-based therapeutics such as sCD4 and CD4-Ig, CD4-VLPs required >12,000-fold fewer copies of CD4 to neutralize a diverse panel of HIV-1 strains. This suggests that multiple CD4-Env interactions between CD4-VLPs and HIV-1 virions were formed, making it nearly impossible for HIV-1 to

dissociate from CD4-VLPs, thereby minimizing the number of VLPs required to neutralize HIV-1. Cryo-ET imaging of CD4-VLPs is consistent with distinct CD4 nanoclusters on a single VLP being involved in neutralizing multiple virions simultaneously. Moreover, a single HIV-1 virion could be completely neutralized by two to four CD4-VLPs, as bound VLPs would sterically hinder the virus from interacting with target cells. The relatively large sizes of CD4-VLPs likely also prevented enhancement of HIV-1 infection of target cells in vitro, which has been observed for sCD4 at low concentrations[165].

Twice-daily IP injections of large doses of CD4-CCR5-VLPs only produced intermittent sub-neutralizing plasma concentrations in hu-mice, likely due to rapid clearance by hepatic sinusoidal endothelial cells that have been shown to clear nanoparticles at a rate of up to 10^8 particles/min[156]. As for conventional CD4-based inhibitors, interactions with class II major histocompatibility complex (MHC) proteins presented on antigen-presenting cells (APCs) could shorten the half-life of CD4-CCR5-VLPs. Although human APCs have been shown to be generated in the hu-mouse model used in this study[166,167], the bioavailabilities of control VLPs and CD4-CCR5-VLPs were similarly poor, suggesting that low VLP concentrations were not related to binding to human class II MHC-expressing cells. Despite poor bioavailability, intermittent sub-neutralizing CD4-CCR5-VLP concentrations elicited recurrent mutations in the CD4bs in circulating viruses. In vitro neutralization assays showed that YU2 viruses with these mutations were as sensitive to CD4-VLPs and CD4-CCR5-VLPs as the wild-type YU2 virus. We

postulate that the mutations provided an advantage in the presence of short-lived sub-neutralizing CD4-CCR5-VLP concentrations, but do not confer resistance to neutralizing concentrations of CD4-VLPs and CD4-CCR5-VLPs. It is possible that the mutations protected the virus during short periods immediately after injections when there were relatively high plasma CD4-CCR5-VLP concentrations and/or protected against constant exposure to low CD4-CCR5-VLP concentrations. In contrast, all mutant viruses were 30-fold less sensitive to sCD4 and CD4-Ig. For three of the four mutations, this loss of neutralization sensitivity was accompanied by only a 4-7-fold reduction in infectivity. These results confirmed that the ability of Env to bind multiple CD4 receptors on the target cell with avidity provides an escape route for HIV-1 against sCD4 and CD4-Ig, as the virus is able to tolerate CD4bs mutations that lower the intrinsic binding affinity for monomeric sCD4 or bivalent CD4-Ig without considerable fitness cost.

The in vitro evolution experiments showed that CD4-VLPs effectively suppressed viral replication at neutralizing concentrations, and intermittent exposure to increasing CD4-VLP concentrations failed to select resistant viral swarms. This evolution strategy has been shown to generate viral populations completely resistant to CD4-Ig and the CD4bs bNAb NIH45-46[160], and a modest loss in viral sensitivity was also observed for the potent antibody-like inhibitor eCD4-Ig, a fusion of CD4-Ig and a CCR5-mimetic sulfopeptide, which protected rhesus macaques from simian-human immunodeficiency virus (SHIV) challenge following delivery using an adeno-associated virus (AAV) vector[130]. Similar to

eCD4-Ig, viral swarms resistant to CD4-Ig remained sensitive to CD4-VLPs, demonstrating that escape pathways that are effective against conventional CD4-based inhibitors do not enable HIV-1 to escape against therapeutics that more accurately mimic HIV-1 target cells. Overall, our results suggest that effective viral escape against CD4-VLPs is difficult as the neutralization sensitivity to the therapeutic and the ability to infect target cells decrease concomitantly, thus progressively forcing HIV-1 to become less infectious.

CD4-VLPs were >100-fold more potent against a globally-representative virus panel than the CD4bs bNAb 3BNC117 when comparing the required numbers of CD4 molecules versus IgG Fabs. Importantly, CD4-VLPs were >12,000-fold more potent against three viral strains that were poorly neutralized by 3BNC117 and also potently neutralized two clinical viral isolates that were partially or completely resistant to 3BNC117 and other bNAbs. Therapeutics that present multiple copies of CD4 tethered to a surface have two potential advantages over bNAbs that could promote greater neutralization breadth and resistance to viral escape: (i) Anti-Env IgGs (and CD4-Ig) are unlikely to utilize avidity effects to bind HIV-1 Env because the low spike density on the viral surface and the distribution of epitopes on the Env trimer result in primarily monovalent binding that is vulnerable to escape through mutation of HIV-1 Env[54,55]. (ii) Although HIV-1 can mutate to become resistant to any single antibody[135], it must retain the ability to interact with its receptor in order to infect cells.

In summary, our results demonstrate that nanoparticles that mimic HIV-1 target cells by presenting multiple copies of membrane-associated CD4 neutralize HIV-1 with enhanced potency, breadth, and resistance to viral escape as compared with conventional CD4-based inhibitors and CD4bs bNAbs. We therefore postulate that therapeutics that mimic viral target cells could prevent escape and permanently control HIV-1 infection by exposing a universal vulnerability, the requirement to bind clusters of CD4 on a target cell, which is potentially inherent to all HIV-1 strains and variants. Since direct injections of CD4-VLPs failed to achieve therapeutic concentrations in vivo, alternative therapeutic and/or delivery strategies that ensure durable bioavailability and minimize the requirement for repeated administrations need to be developed to translate this concept into a clinically-feasible functional cure therapy.

Methods and Materials

VLP production

VLPs were produced by transiently transfecting Expi293 cells (Life Technologies) grown in Expi293 expression media (Life Technologies) on an orbital shaker at 37°C and 8% CO_2. Cells were transfected with a plasmid vector expressing Rev-independent HIV-1 Gag-Pol (pHDM-Hgpm2 plasmid; PlasmID Repository, Harvard Medical School) or a Gag-EGFP fusion protein (HIV-1 HXB2 Gag-EGFP expression vector; NIH AIDS Reagent Program). To generate CD4-VLPs and CD4-CCR5-VLPs, cells were co-transfected with a second plasmid (cDNA sequences of CD4 and CCR5 were subcloned into the pHAGE-CMV-IRES-ZsGreen plasmid; PlasmID Repository, Harvard Medical School) encoding CD4 alone or CD4 and CCR5 at a DNA ratio of 4:1 Gag-Pol:CD4-(CCR5). Control VLPs were generated by expression of HIV-1 Gag-Pol alone. Expi293 cells were also transfected with CD4 in the absence of Gag-Pol to make CD4-positive EVs. 48-72 hours post-transfection, cells were centrifuged at 350 x g for 8 min, and supernatants were collected and passed through a 0.45-μm syringe filter.

VLP purification

For in vitro neutralization experiments, VLPs were concentrated and buffer-exchanged into TZM-bl cell culture medium in Amicon Ultra-15 centrifugal filter units with a 100 kDa molecular weight cut-off (Millipore). For initial experiments,

VLPs were isolated by ultracentrifugation at 28,000 rpm (96,000 x g) for 2 hours at 4°C using a SW32 Ti rotor and a Beckman L8-80M ultracentrifuge (Beckman Coulter) on a 20% w/v sucrose cushion. The supernatant was carefully aspirated and the pellet was re-suspended in 500-µL culture medium at 4°C overnight.

For quantitative Western blot analysis and cryo-ET imaging studies, 50 mL of filtered supernatant (combined from 5 independent CD4-VLP productions) were concentrated and buffer-exchanged into 500 µL PBS by sucrose cushion ultracentrifugation as described above, centrifuged at 10,000 x g for 15 min, passed through a 0.45-µm syringe filter, and further purified by SEC on a Superose 6 10/300 column (GE Healthcare) equilibrated with 20 mM $NaHPO_4$ (pH 7.4), 150 mM NaCl. Fractions were collected and loaded onto 4-20% polyacrylamide gels (Bio-Rad) and stained with InstantBlue protein stain (Expedeon).

For in vivo experiments, control and CD4-CCR5-VLPs were concentrated from 1,000 mL to 5 mL in Slide-A-Lyzer dialysis cassettes (Thermo Fisher Scientific), which were immersed in a 40% w/v PEG (20 kDa) in ultrapure water concentrating solution (Thermo Fisher Scientific) and buffer-exchanged into PBS.

VLP quantification

VLP concentrations were quantified using the lentivirus-associated p24 ELISA kit (Cell Biolabs). To ensure accurate quantification of VLPs for in vitro neutralization studies, we used Gag-Pol instead of Gag-EGFP for generating VLPs

because detection of the Gag-encoded capsid protein p24 is less efficient for immature Gag than for mature Gag that has been processed by the HIV-1 protease encoded within Pol after budding[168]. VLP concentrations were calculated using the following equation in accordance with the manufacturer's directions: 1 ng p24 = 1.25 x 10^7 VLPs[169,170], which assumes that each VLP contains 2,000 molecules of p24[147,148].

In vitro neutralization assays

The ability of VLPs to neutralize HIV-1 was evaluated using a pseudovirus-based TZM-bl assay[149]. Pseudoviruses with Envs from $YU2_{wt}$, YU variants, and strains from a 12-strain global HIV-1 panel[151] were generated in HEK293T cells as described[171]. Serial dilutions of control VLPs, CD4-VLPs, and CD4-CCR5-VLPs were incubated with pseudovirus for 1 hour at 37°C. TZM-bl cells (NIH AIDS Reagents Program) that express a Tat-inducible luciferase reporter gene were added, and luminescence was measured after 48 hours. The HIV-1 neutralization activity of CD4-VLPs was compared with sCD4, CD4-Ig, and the CD4bs bNAb 3BNC117. Neutralization assays were also performed against primary virus isolates obtained from the latent reservoirs of two HIV-1–infected patients who received repeated infusions of 3BNC117[152]. Viruses were isolated from PBMCs by a quantitative and qualitative viral outgrowth assay (Q^2VOA) as previously described[172].

The number of CD4 molecules/mL required to achieve 50% neutralization was calculated by multiplying the VLP concentration (derived from p24 ELISA) at the IC_{50} (derived from an in vitro neutralization assay) by the average number of CD4 copies per VLP (derived from quantitative Western blot analysis). For sCD4 D1D2 (26 kDa), CD4-Ig (100 kDa), and 3BNC117 (150 kDa), the numbers of CD4 molecules/mL (sCD4, CD4-Ig) or Fab molecules/mL (3BNC117) were calculated by converting the measured IC_{50}s (in μg/mL) to molar concentrations. The respective numbers of inhibitor molecules were then derived from molar IC_{50} concentrations using Avogadro's number. The numbers of inhibitor molecules (CD4 or Fab) were then multiplied by a factor of one (sCD4) or two (CD4-Ig, 3BNC117) depending on whether the inhibitor molecule contained one or two CD4/Fab copies. IC_{50}s calculated from independent assays generally agreed to within 2-4-fold (Fig. S3).

In vivo studies

Studies in hu-mice were performed in accordance with the recommendations in the *Guide for the Care and Use of Laboratory Animals* of the National Institutes of Health. The protocol was reviewed and approved by the Rockefeller University Institutional Animal Care and Use Committee (IACUC), and experiments were designed in accordance with established guidelines at the Rockefeller University (protocol number 13618-H).

Hu-mice were generated as previously described[108]. Briefly, human CD34+ hematopoietic stem cells were obtained from human fetal livers (Human Fetal Tissue Repository, NY) and injected intrahepatically into irradiated non-obese diabetic $Rag1^{-/-}$ $IL2rg^{null}$ (NOD.Cg-Rag1tm1Mom Il2rgtm1Wjl/SzJ) mice (Jackson Laboratory). Half-life studies for VLPs were performed in uninfected hu-mice. CD4-CCR5-VLPs (610 ng of p24) were intraperitoneally (IP) injected into five hu-mice and a single blood sample was taken from each animal after 20 min, 1 hour, 2 hours, 4 hours, or 6 hours. Plasma CD4-CCR5-VLP concentrations were measured by lentivirus-associated p24 ELISA (Cell Biolabs).

For treatment experiments, hu-mice were infected with HIV-1_{YU2} and viral plasma loads were measured by qRT-PCR 10 days post-infection as described[108]. Infected hu-mice were distributed into 4 treatment groups, which received either no treatment (Group I), twice daily IP injections of 480 ng p24 of control VLPs (Group II), CD4-CCR5-VLPs (Group III), or twice weekly administrations of 1 mg of the bNAb 10-1074 (Group IV). Treatments were continued for a total of 10 days and viral plasma loads were measured on days 3, 6, and 10 by qRT-PCR as described[108].

Viral fitness assay

To evaluate the ability of HIV-1_{YU2} Env mutants to enter and infect target cells, a previously-described infection assay[173,174] was used with minor modifications. 40 pg p24 of $YU2_{wt}$ or mutant YU2 pseudoviruses (quantified by lentivirus-associated p24 ELISA; Cell Biolabs) were added to TZM-bl reporter

cells in the presence of 30 μg/mL DEAE-Dextran. After 48 hours incubation at 37°C, cells were lysed and luminescence was measured after addition of Britelite plus (PerkinElmer). The average luminescence between 8 replicates was calculated for $YU2_{wt}$ and each YU2 variant, and the experiment was repeated three times with different pseudovirus batches. The viral entry fitness of the YU2 mutant viruses was calculated as a function of the reduction in average luminescence compared to the $YU2_{wt}$.

In vitro evolution assays

Replication-competent HIV-1_{NL4-3} carrying the HIV-1_{YU2} envelope[175] was passaged on Rev-A3R5 CD4+ T-cells[159] (Cube Biosystems) for 21 days to diversify the viral population. Rev-A3R5 cells were maintained in RPMI-1640 media supplemented with 10% FBS, 1% Pen-Strep, 1% L-Glutamine, 1 mg/mL Geneticin, and 1 μg/mL Puromycin at 37°C and 5% CO_2. To test if CD4-VLPs can suppress viral replication, 30 μL of viral supernatant was added to multiple wells on a 48-well plate. Previously determined IC_{80}s and IC_{95}s of CD4-Ig (17.5 and 22.5 μg/mL) and CD4-VLPs ($5x10^8$ and $1.25x10^9$ VLPs/mL) or no inhibitor were added to the wells in triplicates in the presence of 5 μg/mL DEAE-Dextran and media was added for a final volume of 500 μL. After one hour of incubation at 37°C, $5x10^4$ Rev-A3R5 cells were added and plates were incubated for 16 hours at 37°C. The next day, cells were centrifuged at 350 x g for 8 min, supernatants were removed, and cells were re-suspended in 500-μL fresh media. After 48 hours, infection rates were

quantified by measuring HIV-1-induced GFP expression in Rev-A3R5 cells by flow cytometry (MACSQuant, Miltenyi Biotec). For the second cycle, 350 µL of viral supernatants for each condition were transferred into fresh 48-well plates, and inhibitors, dextran-DEAE, and cells were added as for cycle 1. A total of six cycles were performed, and infection rates were determined after cycles 4-6. Infection rates in the absence of inhibitor were maintained at ~10% infected cells, and to account for variations between cycles, infection rates were normalized to a viral control infection of 10%. Viral escape was defined as >4% infected cells (60% neutralization), and inhibitor concentrations were increased 2-fold for replicates that surpassed this threshold for next cycle.

A modified version of a previously described in vitro evolution protocol[160] was used to evaluate if HIV-1 can escape from CD4-VLPs when intermittently exposed to increasing inhibitor concentrations. 10-20 µL of viral supernatant was added to multiple wells on a 96-well plate and CD4-Ig and CD4-VLPs were added at starting concentrations of 17.5 µg/mL and $5x10^8$ VLPs/mL, respectively, in the presence of 5 µg/mL DEAE-Dextran, and media was added for a final volume of 200 µL. After one-hour incubation at 37°C, $2.5x10^4$ cells were added and plates were incubated at 37°C. After 8 hours, cells were centrifuged, supernatants were removed, and cells were re-suspended in 200 µL fresh media. After 64 hours, infection rates were assessed using a fluorescent microscope (AX10, Zeiss). The second cycle was performed in the absence of inhibitor to enable HIV-1 replication and ensure sufficient viral titers for the next selection cycle. This six-day on/off

cycle was repeated 15 times (90 days), and inhibitor concentrations were doubled every 2-4 cycles to final concentrations of 280 μg/mL of CD4-Ig and $1.6x10^{10}$ CD4-VLPs/mL. To maintain infections at higher inhibitor concentrations, up to 150 μL of viral supernatants were passaged and repeated cycles in the absence of inhibitor needed to be performed. After the final cycle, viral supernatants for each condition (no inhibitor, CD4-Ig, CD4-VLPs) were collected and TZMbl assays were performed as described above.

Statistical analysis

Concentrations at which half-maximal neutralization was observed (IC_{50} values) were calculated using software in HIV Antibody Database[176]. The levels of conservation of the mutated residues and the respective substitutions observed in *env* sequences obtained from HIV-1–infected and CD4-CCR5-VLP–treated hu-mice were determined through filtered web alignment of HIV-1 sequences in the Los Alamos National Laboratory HIV Database (http://www.hiv.lanl.gov/).

Acknowledgements

We thank the Caltech Protein Expression Center in the Beckman Institute, Y.E. Lee, and T. Luong for expression of VLPs and proteins; J.R. Keeffe for reagents; M.G. Murphy for help with figures; C. Kieffer and A.P. West for helpful discussion and advice; J.C.C. Lorenzi for providing primary viral isolates; T.

Eisenreich and L. Nogueira for help with hu-mouse experiments; J.A. Pai for bioinformatic analyses; and the NIH AIDS Reagent Program for reagents. Cryo-electron tomography was performed in the Beckman Institute Resource Center for Transmission Electron Microscopy at Caltech. **Funding:** This work was supported by the Bill and Melinda Gates Foundation grant OPP1202246, and by a generous gift from Kairos Ventures. **Author Contributions:** M.A.G.H., Y.B.-O., J.V., M.C.N., and P.J.B. designed the research, M.A.G.H., Y.B.-O., Z.Y., and H.B.G. performed the research, M.A.G.H., Y.B.-O., Z.Y., H.B.G., and P.J.B. analyzed data, and M.A.G.H. and P.J.B. wrote the manuscript. **Competing interests:** The authors declare no competing interests. **Data and materials availability:** All data associated with this study are available in the main text or the supplementary materials.

Supplementary material

Supplementary materials and methods

Fig. S1. Purification of CD4-VLPs for quantitative Western blot analysis and cryo-ET.

Fig. S2. Quantitative Western blot analysis.

Fig. S3. Comparison of neutralization by different CD4-VLP batches.

Fig. S4. Neutralization activity requires Gag and CD4.

Fig. S5. CD4-CCR5-VLP treatment selects mutations in HIV-1_{YU2}-infected humanized mice.

Fig. S6. SPR binding analysis of YU2 gp120 mutants.

Table S1. IC_{50}s for CD4-VLPs and CD4-CCR5-VLPs against a panel of HIV-1 strains.

Table S2. IC_{50}s for sCD4, CD4-Ig, and 3BNC117 against a panel of HIV-1 strains.

Table S3. IC_{50}s for CD4-VLPs and various bNAbs against HIV-1 isolates obtained from infected individuals.

Table S4. K_D, k_a, k_d values for binding of YU2 gp120 variants to CD4-Ig.

Table S5. IC_{50}s for CD4-VLPs, CD4-CCR5-VLPs, sCD4, and CD4-Ig against $YU2_{wt}$ and YU2 mutant pseudoviruses.

Movie S1. Tomographic reconstruction of CD4-VLPs bound to BG505 SOSIP.664.

Figures

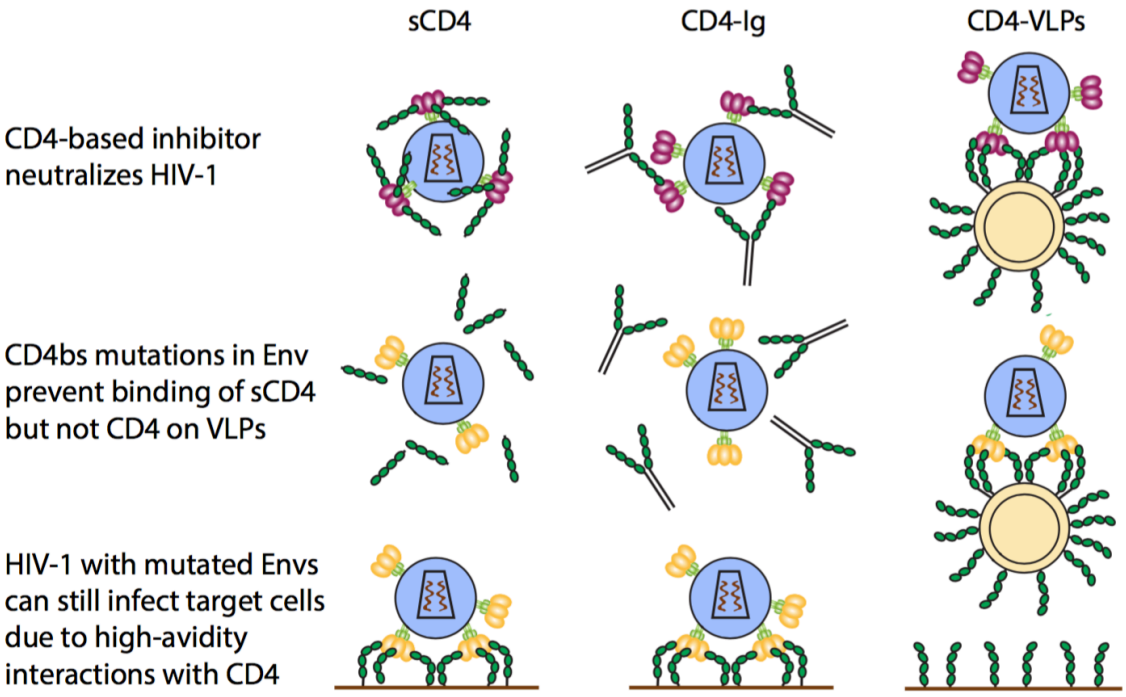

Figure 1. CD4-VLPs can overcome HIV-1 Env mutations that prevent neutralization by soluble CD4-based inhibitors. Schematic comparison of responses of soluble CD4-based inhibitors and CD4-VLPs to Env mutations. Monovalent sCD4 and bivalent CD4-Ig neutralize sCD4-sensitive strains (purple Env trimers, row 1), but mutations in the CD4bs that lower the affinity of Env for sCD4 (yellow Env trimers, row 2) render other strains resistant to soluble CD4-based inhibitors while maintaining the ability to infect CD4+ target cells via avidity effects through binding to multiple CD4 receptors tethered to the host cell membrane (row 3). CD4-VLPs can neutralize viral strains that are resistant to soluble CD4-based

inhibitors through high-avidity binding to multiple CD4 receptors tethered to the VLP membrane.

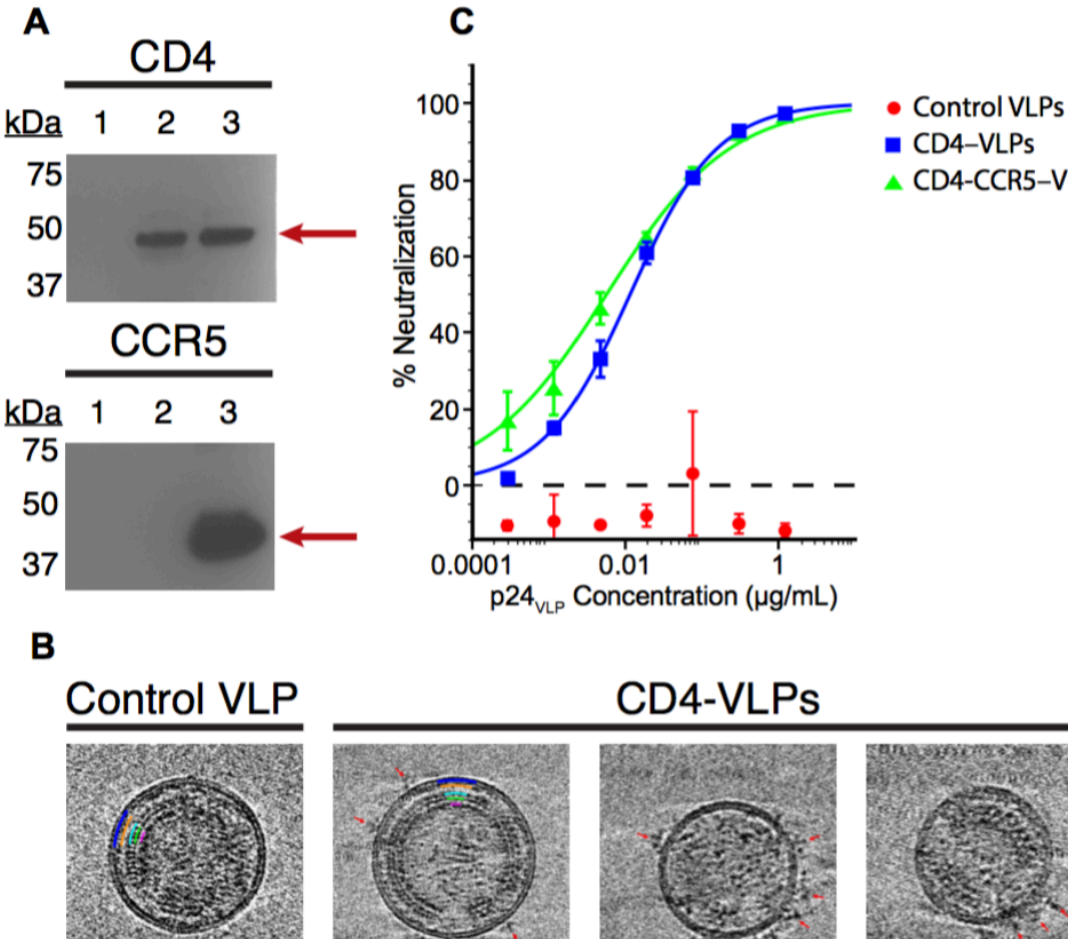

Figure 2. VLPs incorporate CD4 and CCR5 and neutralize HIV-1. (**A**) Western blot analysis to detect CD4 (left) and CCR5 (right) in supernatants containing HIV-1 Gag-derived VLPs from Expi293 cells transfected with Gag alone (control VLPs; lane 1), Gag and CD4 (CD4-VLPs; lane 2), Gag, CD4, and CCR5 (CD4-CCR5-VLPs; lane 3). (**B**) Tomographic slices (10.9 nm) from cryo-ET analysis of control VLPs (left panel) or CD4-VLPs (right three panels) incubated with a soluble native-like Env trimer (BG505 SOSIP.664). Scale bar = 20 nm. Red arrows indicate densities for bound Env trimers. Approximate positions of immature Gag shell layers

are highlighted on the left two panels. Note the hexagonal lattice in the capsid layer of Gag. See also Video 1. (**C**) In vitro neutralization assay against HIV-1_{YU2} pseudovirus comparing control VLPs, CD4-VLPs, and CD4-CCR5-VLPs. The neutralization activity of VLPs determined in terms of concentrations of the Gag p24 capsid protein. Data points are presented as the mean and standard deviation of duplicate measurements.

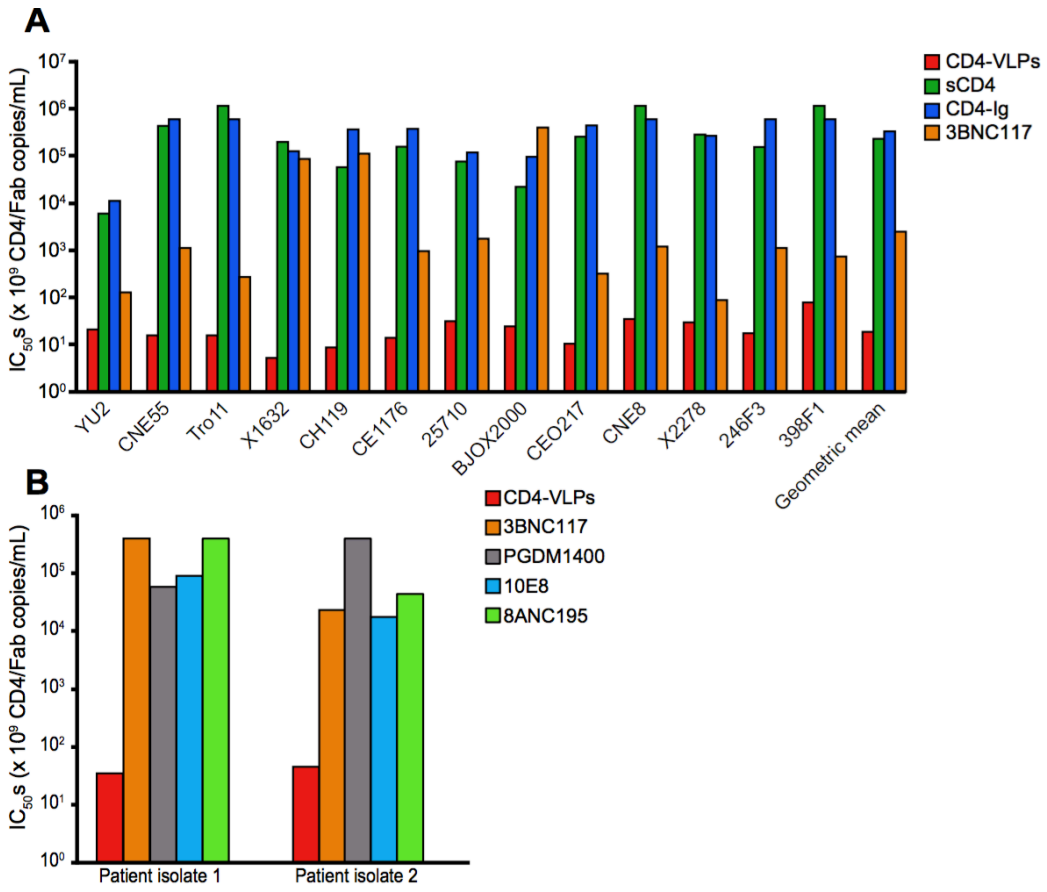

Figure 3. CD4-VLPs neutralize HIV-1 with enhanced potency and breadth compared to sCD4, CD4-Ig, and 3BNC117. (**A**) In vitro neutralization of HIV-1_{YU2} and a panel of 12 HIV-1 Env reference strains[151]. IC_{50}s against each strain and the geometric mean IC_{50} are presented in CD4 copies per mL for CD4-VLPs, sCD4, and CD4-Ig, and in Fab copies per mL for 3BNC117 (see Table S1 and S2). IC_{50}s of 50 μg/mL were used for strains that were not neutralized at 50 μg/mL by sCD4, CD4-Ig, and 3BNC117 for the geometric mean IC_{50} calculations. (**B**) In vitro neutralization of two HIV-1 patient isolates that exhibited resistance against multiple bNAbs[152]. IC_{50}s are presented in CD4 copies per mL for CD4-VLPs, and in Fab copies per mL

for 3BNC117 (CD4bs bNAb), PGDM1400 (V1V2 bNAb), 10E8 (membrane-proximal external region bNAb), and 8ANC195 (gp120-gp41 interface bNAb) (Table S3).

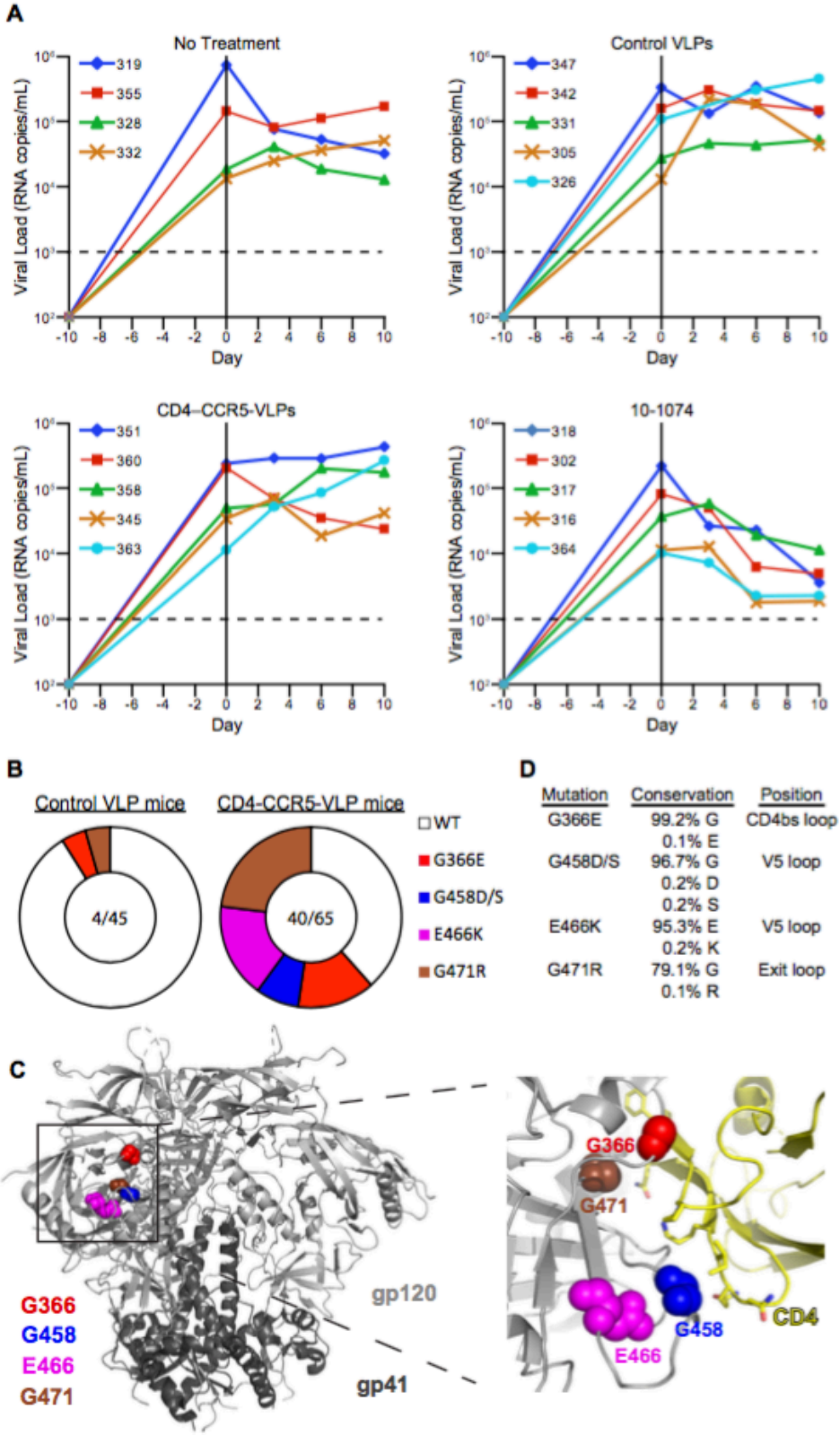
A
No Treatment
319
355
328
332
Control VLPs
347
342
331
305
326
CD4–CCR5-VLPs
351
360
358
345
363
10-1074
318
302
317
316
364
Viral Load (RNA copies/mL)
Day
B
Control VLP mice
CD4-CCR5-VLP mice
4/45
40/65
WT
G366E
G458D/S
E466K
G471R
C
G366
G458
E466
G471
gp120
gp41
CD4
D
Mutation
Conservation
Position
G366E
99.2% G
0.1% E
CD4bs loop
G458D/S
96.7% G
0.2% D
0.2% S
V5 loop
E466K
95.3% E
0.2% K
V5 loop
G471R
79.1% G
0.1% R
Exit loop

Figure 4. CD4-CCR5-VLP treatment in HIV-1_{YU2}-infected hu-mice elicits CD4bs mutations in gp120. (A) Viral loads (RNA copies/mL) measured over time (days) in HIV-1_{YU2}-infected hu-mice. Each line represents measurements for a single hu-mouse (identified by different numbers). The dotted line indicates the detection limit. Hu-mice were infected 10 days prior to initiation of treatment: either no treatment, twice daily IP injections of control VLPs (6 x 10^9 control VLPs per injection), twice daily IP injections of CD4-CCR5-VLPs (6 x 10^9 VLPs per injection), or twice weekly IP injections of the 10-1074 bNAb (1 mg per injection) for 10 days. (**B**) Pie charts showing the frequency of recurrent mutations in the gp120 subunits of the HIV-1_{YU2} *env* genes of plasma viruses obtained from control VLP-treated and CD4-CCR5-VLP-treated hu-mice. The slices are proportional to the number of sequences that contained the indicated substitutions. White slices represent the number of sequences that lacked any recurrent mutations. The numbers in the center indicate the total number of sequences that contained recurrent mutations over the total number of sequences analyzed. (**C**) Left: Cartoon diagram of Env trimer structure (PDB 5T3Z) with locations of residues that were mutated highlighted as colored surfaces. Right: Close-up of the gp120-CD4 binding interface highlighting the proximity of the mutated residues to the CD4bs. (**D**) Levels of conservation of each mutated residue and its respective substitution (http://www.hiv.lanl.gov/).

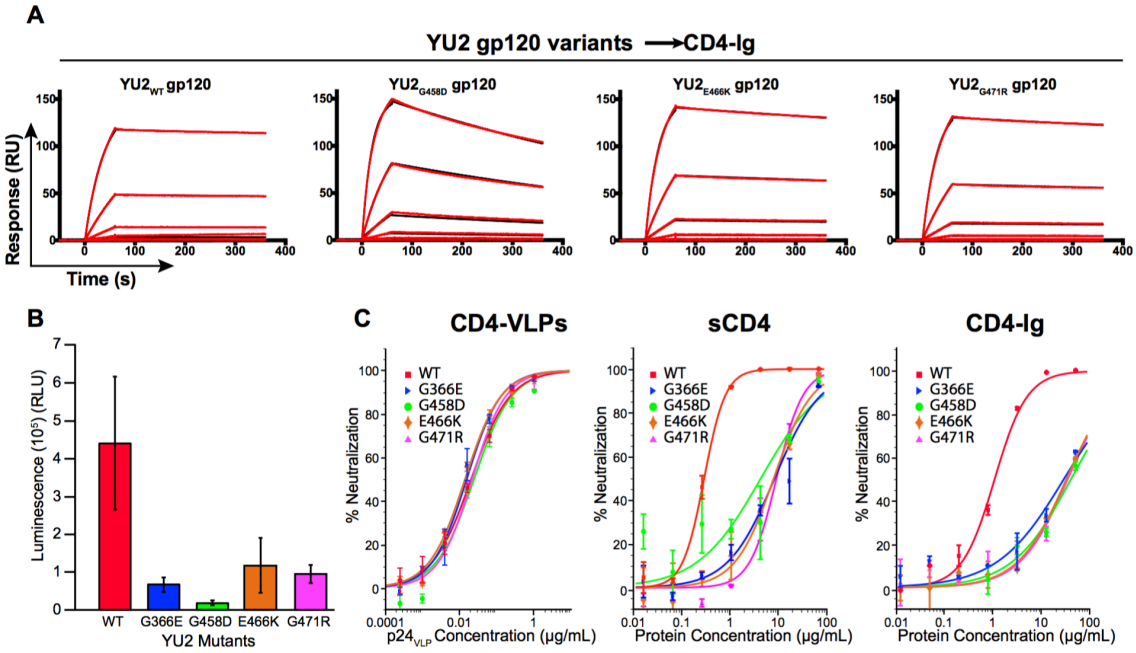

Figure 5. HIV-1$_{YU2}$ variants have lower affinity for CD4, are less infectious, and not resistant to CD4-VLPs. (**A**) SPR binding assays of CD4-Ig with YU2$_{wt}$ and YU2 variant gp120 proteins. Representative sensograms (red) and fits (black) for binding of YU2$_{wt}$, YU2$_{G458D}$, YU2$_{E466K}$, and YU2$_{G471R}$ gp120 proteins to CD4-Ig captured on a protein A biosensor chip (Fig. S6A). The YU2$_{G366E}$ gp120 mutant was excluded from the SPR analysis, as this protein was unstable (Fig. S6B). YU2 gp120 proteins were flowed over the chip as a 4-fold dilution series with a top concentration of 250 nM. K_D, k_a, k_d values are presented in Table S4. (**B**) Infectivity assay comparing the ability of WT and variant HIV-1$_{YU2}$ pseudoviruses to enter and infect target cells. YU2$_{wt}$ or mutant viruses (40 pg p24) were added to TZM-bl cells and luminescence was measured after 48 hours. Columns and error bars represent the mean and standard deviations for measurements from three separate experiments using 8 replicates per experiment. (**C**) Overlay of neutralization curves for CD4-

VLPs, sCD4, and CD4-Ig against $YU2_{wt}$ and the indicated YU2 mutant pseudoviruses. Inhibitor concentrations are shown as p24 concentrations for CD4-VLPs (see Fig. 2C and Methods) and protein concentrations for sCD4 and CD4-Ig. Data points are presented as the mean and standard deviation of duplicate measurements. IC_{50}s for CD4-VLPs, CD4-CCR5-VLPs, sCD4, and CD4-Ig against $YU2_{wt}$ and YU2 mutant pseudoviruses are presented in Table S5.

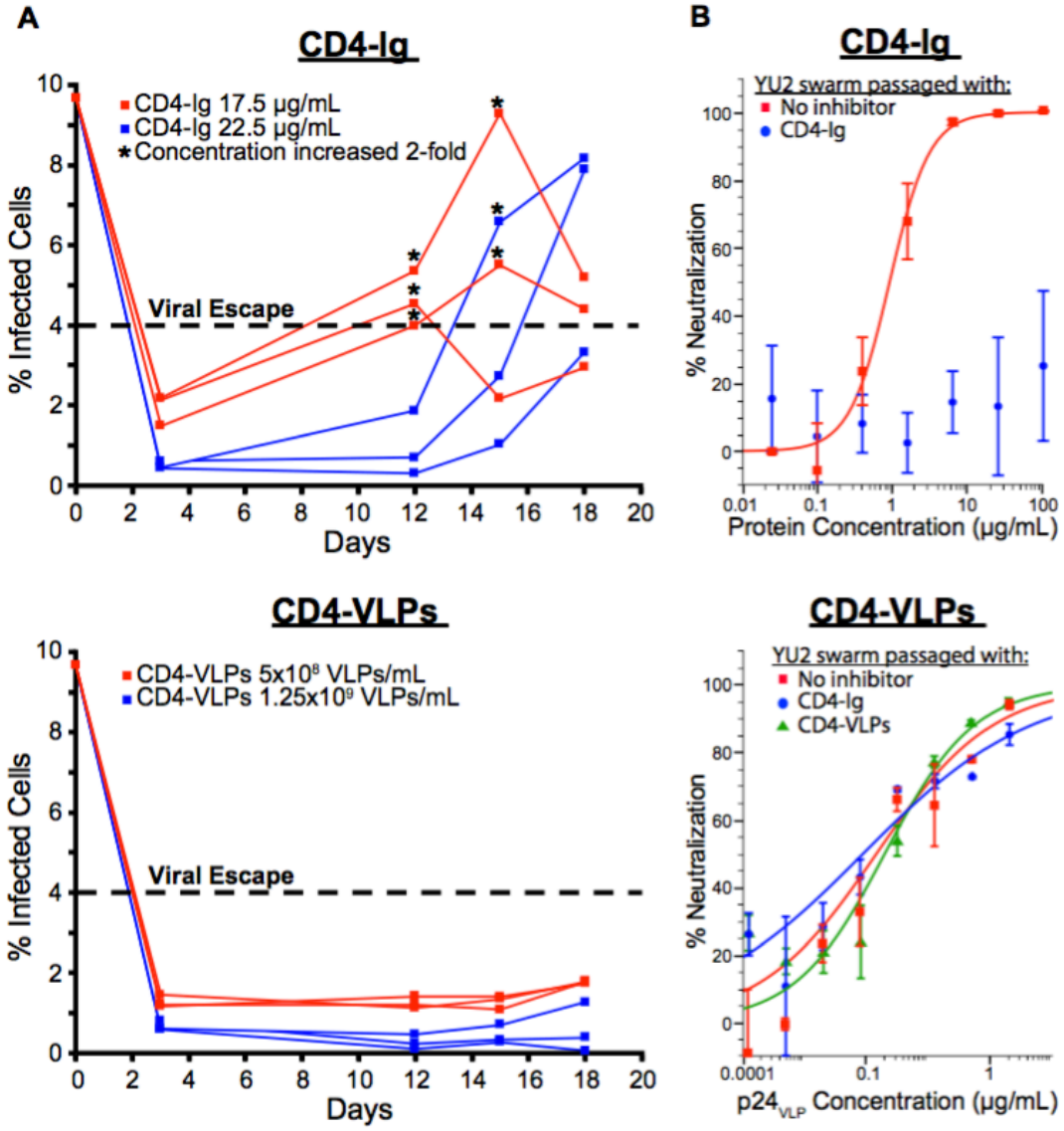

Figure 6. CD4-VLPs suppress HIV-1 replication and prevent viral escape in vitro (**A**) In vitro evolution experiment comparing the ability of CD4-Ig and CD4-VLPs to suppress HIV-1 replication. Prior to the experiment, a diversified viral swarm had been generated by passaging replication-competent HIV-1_{YU2} on Rev-A3R5 CD4+ T-cells for 21 days. On day 0, the viral supernatant was distributed into multiple wells and IC_{80}s (red) and IC_{95}s (blue) of CD4-Ig (top) or CD4-VLPs

(bottom) were added. After one hour, fresh Rev-A3R5 cells were added and infection rates were determined by measuring HIV-1-induced GFP expression by flow cytometry after 72 hours. This cycle was repeated every 3 days and a total of 6 cycles were completed. Infection rates >4% were set as a threshold to indicate viral escape (dashed line), and inhibitor concentrations were doubled (*) for replicates that surpassed this threshold for the next cycle. (**B**) In vitro neutralization assays for CD4-Ig (top) and CD4-VLPs (bottom) against HIV-1_{YU2} swarms that had been extensively passaged in the presence of no inhibitor (red), CD4-Ig (blue), or CD4-VLPs (green) (see Methods). Inhibitor concentrations are shown as protein concentrations for CD4-Ig and p24 concentrations for CD4-VLPs (see Fig. 2C and Methods). Data points are presented as the mean and standard deviation of duplicate measurements.

Supplementary materials

Materials and methods

Protein expression

6 x His-tagged $YU2_{wt}$ and mutant gp120 proteins were expressed by transient transfection using pTT5 expression vectors (NRC Biotechnology Research Institute) in HEK293-6E cells (National Research Council of Canada). The cells were grown in FreeStyle 293 expression media (Gibco) on an orbital shaker at 37°C and 8% CO_2. gp120 proteins were purified from cell supernatants by Ni-NTA affinity chromatography (GE Healthcare) followed by size exclusion chromatography (SEC) using a Superdex 200 30/200 column (GE Healthcare). sCD4 (D1-D2 and D1-D4 constructs), CD4-Ig, HIV-1 bNAbs, control IgGs, and a soluble native-like BG505 SOSIP.664 Env trimer[177] were expressed and purified from transfected cell supernatants as described[178,179]. Proteins were stored at 4°C in 20 mM Tris, pH 8.0, and 150 mM sodium chloride (TBS buffer).

Western blot analysis

The presence of CD4 and CCR5 on VLPs was confirmed by Western blots. Briefly, total protein concentrations for all samples were measured using the Pierce BCA protein assay kit (Thermo Fisher Scientific). 1 μg of total protein was separated by SDS-PAGE and transferred to nitrocellulose membranes (0.2 μm) (GE Healthcare). The following antibodies were used for detecting CD4 and CCR5:

rabbit anti-CD4 (ab133616; Abcam) at 1:10,000, rat anti-CCR5 (ab111300; Abcam) at 1:2,000, HRP-conjugated mouse anti-rabbit IgG (211-032-171; Jackson ImmunoResearch) at 1:1,000, and HRP-conjugated mouse anti-rat IgG (3065-05; Southern Biotech) at 1:1,000. Protein bands were visualized using ECL Prime Western Blotting Detection Reagent (GE Healthcare).

The number of CD4 molecules displayed on the surface of CD4-VLPs was estimated by quantitative Western blot analysis. Various dilutions of SEC-purified CD4-VLPs and known amounts of purified Gag p55 (Abcam) and sCD4 D1-D4 were separated by gel electrophoresis and transferred to nitrocellulose membranes (GE Healthcare). Gag-EGFP was detected using a polyclonal rabbit anti-p17/p55 antibody (ab63195; Abcam) and HRP-conjugated mouse anti-rabbit IgG (211-032-171; Jackson ImmunoResearch) at dilutions of 1:2,500 and 1:1,000, respectively. CD4 was detected as described above. Band intensities of the Gag and sCD4 standards and CD4-VLP sample dilutions were measured using ImageJ to estimate the concentrations of Gag-EGFP and CD4. The number of CD4 copies per VLP was derived from the molar Gag-EGFP (84 kDa) to CD4 (48 kDa) ratio, assuming that each VLP contains 2,000 copies of Gag-EGFP[147,148]. The average number of CD4 copies per VLP was calculated using results from six quantitative Western blot replicate experiments.

Cryo-ET

SEC-purified CD4-VLPs were incubated with 10 μg/mL BG505 SOSIP.664 for 4 hours at room temperature. CD4-VLP/BG505 SOSIP.664 complexes were then re-purified over SEC. Cryo-EM grids containing CD4-VLP/BG505 SOSIP.664 complexes were prepared using a Mark IV Vitrobot (ThermoFisher Scientific) operated at 21°C and 100% humidity. 2.5 μL of sample was mixed with 1 μL of 10 nm colloidal gold beads (Sigma-Aldrich) and applied to 200 mesh Quantifoil R2/1 grids, blotted for 3.5 s, and then plunge-frozen in liquid ethane surrounded by liquid nitrogen.

Cryo-grids were loaded into a 300kV Titan Krios transmission electron microscope (ThermoFisher Scientific) equipped with a Gatan energy filter (slit width 20 eV) operating at a nominal 42,000x magnification. Tilt series were recorded on a K3 direct electron detector (Gatan) in counting mode with a pixel size of 2.176 Å•pixel^{-1} using SerialEM software[180]. The defocus range was -2 to -5 μm with a total dose of ~80 $e^-/Å^2$ per tilt series. Tilt-series images were collected from -60° to 60° at 3° intervals using dose-symmetric tilt scheme[181]. Images were aligned and reconstructed using IMOD software[182].

Surface plasmon resonance binding experiments

SPR experiments were performed using a Biacore T200 instrument (GE Healthcare). Protein A was immobilized on a CM5 chip by primary amine

chemistry (Biacore manual), and 10 nM CD4-Ig or a non-HIV-1 binding IgG (mG053) was injected for 60 seconds at a flow rate of 10 μl/min as described[183], resulting in attachment of 250-300 resonance units (RUs) of an Fc-containing protein. 1 μM human Fc was injected for 60 seconds at a flow rate of 10 μl/min to block remaining protein A sites, followed by a concentration series of YU2 gp120 variants (a total of six 4-fold dilutions starting from a top concentration of 250 nM) for a contact time of 60 seconds and a dissociation time of 300 sec at a flow rate of 30 μl/min. Binding reactions were allowed to reach equilibrium, and K_Ds were calculated from the ratio of association and dissociation rates ($K_D = k_d/k_a$). Kinetic constants were derived using Biacore T200 Evaluation Software v3.2 by simultaneously fitting the association and dissociation phases of all curves in each data set using a 1:1 binding. Flow cells were regenerated with 1 M guanidine HCl and/or 10 mM glycine pH 2.0 at a flow rate of 90 μl/min.

Single genome sequencing of HIV-1 *env*

HIV-1 *env* sequences from 2 hu-mice treated with control VLPs and 3 hu-mice treated with CD4-CCR5-VLPs were obtained as previously described[184]. For single genome sequencing of viruses, HIV-1 RNA was extracted from 200 uL plasma samples collected on day 10 of VLP treatment from each mouse (QIAGEN MinElute Virus Spin Kit), and cDNA was generated by reverse transcription (SuperScript III Reverse Transcriptase). Samples were treated with RNaseH to remove residual RNA for 20 min at 37°C. cDNA samples were diluted and

amplified by two cycles of nested PCR with previously-described gp160-specific primers[185]. PCR products with the expected size of HIV-1 *env* and amplification efficiencies of <30% were selected for library preparation using the Illumina Nextera DNA Sample Preparation Kit. Sequencing was performed as described[172].

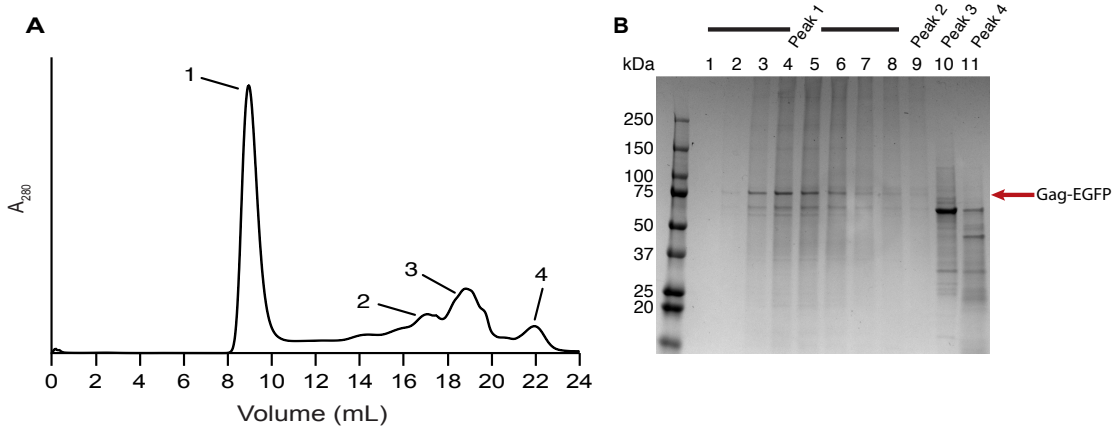

Figure S1. Purification of CD4-VLPs for quantitative Western blot analysis and cryo-ET. (**A**) Size exclusion chromatogram of CD4-VLPs following purification by sucrose cushion ultracentrifugation. (**B**) SDS-PAGE analysis of fractions corresponding to peaks 1 (lanes 1-8), 2 (lane 9), 3 (lane 10), and 4 (lane 11). Gag-EGFP-containing fractions corresponding to lanes 3-6 were selected for quantitative Western blot analysis and cryo-ET imaging.

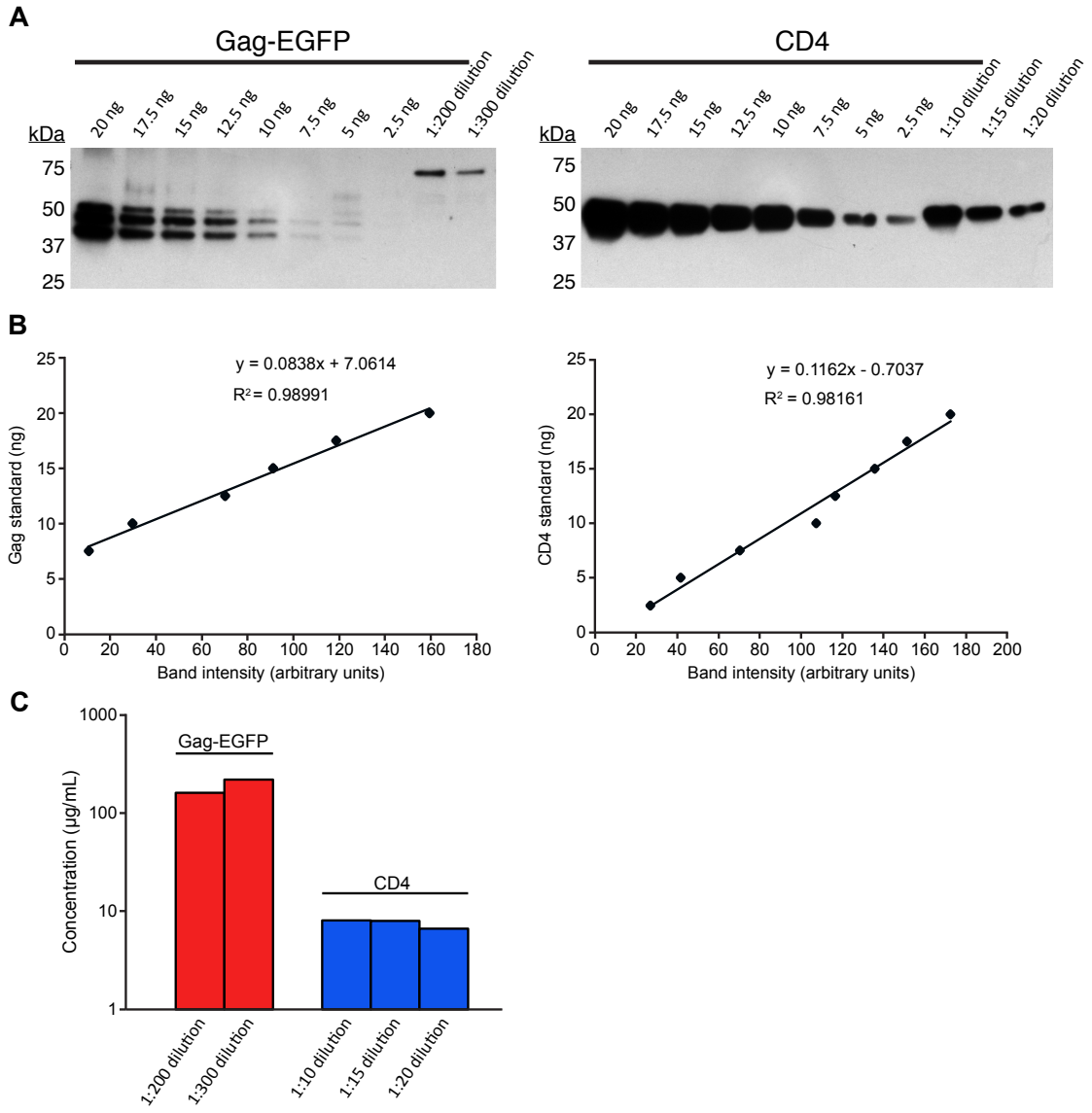

Figure S2. Quantitative Western blot analysis. Supernatants from five independent CD4-VLP productions were combined and purified (Fig. S1). Representative Gag and CD4 blots from six quantitative Western blot replicate experiments are shown, from which an average of 140 +/- 48 CD4 copies per VLP was calculated (results ranged from 60-190 CD4 copies per VLP). (**A**) Western blots showing decreasing amounts of Gag (55 kDa) and sCD4 (43 kDa) standards,

respectively (lanes 1-8). Two degradation bands were present for Gag standards, which result from proteolytic removal of p6 (49 kDa) and p7 (42 kDa). Various dilutions of the SEC-purified CD4-VLPs (Fig. S1) were included to determine the concentrations of Gag-EGFP (84 kDa) and CD4 (48 kDa). (**B**) Standard curves corresponding to measured band intensities for Gag (left) and sCD4 (right) standards using linear regression analysis. Band intensities were measured using ImageJ, and all three bands were included for the Gag standard. Linear regression equations and correlation coefficients are displayed. (**C**) Gag-EGFP and CD4 concentrations determined for each sample dilution using the linear regression equations from (B).

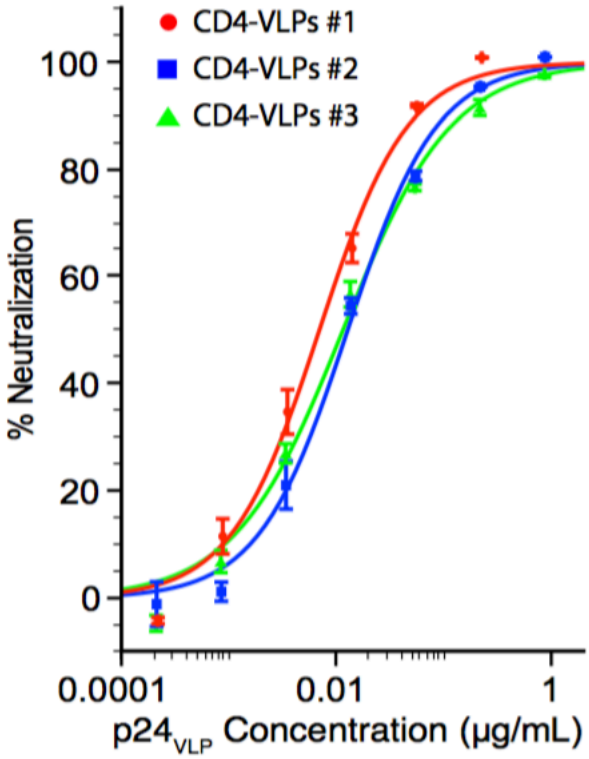

Figure S3. Comparison of neutralization by different CD4-VLP batches. Neutralization curves for three different CD4-VLP batches against HIV-1_{YU2}. Data points are presented as the mean and standard deviation of duplicate measurements.

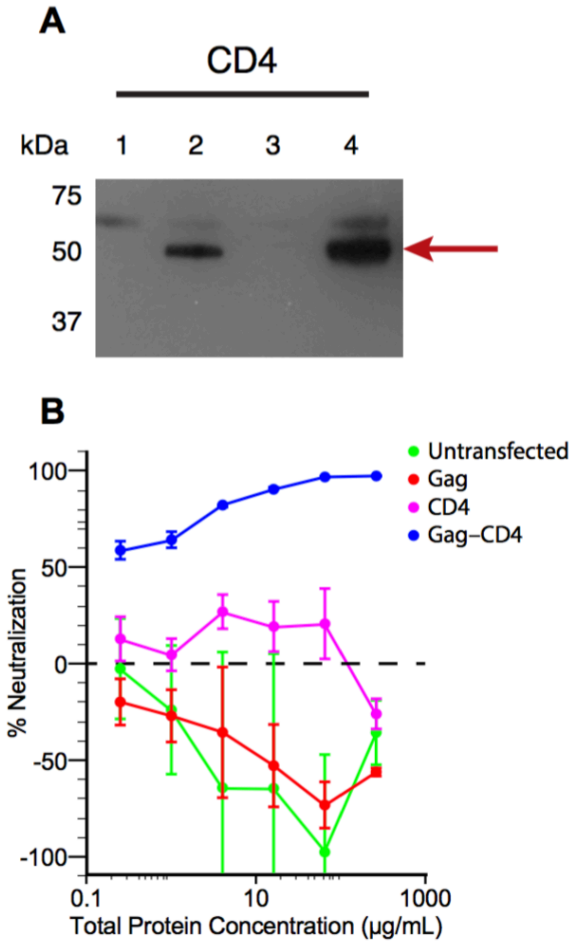

Figure S4. Neutralization activity requires Gag and CD4. (**A**) Western blot analysis comparing relative CD4 levels in concentrated supernatants containing extracellular veciscles (EVs) only (Lane 1, untransfected control cells, and Lane 2, transfected cells expressing CD4) or EVs and VLPs (Lane 3, transfected cells expressing Gag, and Lane 4, transfected cells expressing Gag and CD4). (**B**) In vitro neutralization assay against HIV-1_{YU2} pseudovirus comparing the neutralization activity of EVs and VLPs. Equivalent total protein concentrations were used for concentrated supernatants collected from transfected Expi293 cells under the following conditions: untransfected cells (EVs only), cells expressing Gag (EVs and

VLPs, no CD4), cells expressing CD4 (CD4-positive EVs), and cells expressing Gag and CD4 (CD4-positive EVs and CD4-VLPs). Data points are presented as the mean and standard deviation of duplicate measurements.

	IC_{50}					
HIV Strain	**CD4-VLPs (µg p24/mL)**	**CD4-VLPs (VLPs/mL)**	**CD4-VLPs (CD4 copies/mL)**	**CD4-CCR5-VLPs (µg p24/mL)**	**CD4-CCR5-VLPs (VLPs/mL)**	**CD4-CCR5-VLPs (CD4 copies/mL)**
YU2	0.012	1.5×10^8	2.1×10^{10}	0.006	0.8×10^8	1.1×10^{10}
CNE55	0.009	1.1×10^8	1.6×10^{10}	0.008	1.0×10^8	1.4×10^{10}
Tro11	0.009	1.1×10^8	1.6×10^{10}	0.010	1.3×10^8	1.8×10^{10}
X1632	0.003	0.4×10^8	0.5×10^{10}	0.003	0.4×10^8	0.5×10^{10}
CH119	0.005	0.6×10^8	0.9×10^{10}	0.004	0.5×10^8	0.7×10^{10}
CE1176	0.008	1.0×10^8	1.4×10^{10}	0.007	0.9×10^8	1.2×10^{10}
25710	0.018	2.3×10^8	3.2×10^{10}	0.021	2.6×10^8	3.7×10^{10}
BJOX2000	0.014	1.8×10^8	2.5×10^{10}	0.012	1.5×10^8	2.1×10^{10}
CEO217	0.006	0.8×10^8	1.1×10^{10}	0.005	0.6×10^8	0.9×10^{10}
CNE8	0.020	2.5×10^8	3.5×10^{10}	0.028	3.5×10^8	4.9×10^{10}
X2278	0.017	2.1×10^8	3.0×10^{10}	0.018	2.3×10^8	3.2×10^{10}
246F3	0.010	1.3×10^8	1.8×10^{10}	0.011	1.4×10^8	1.9×10^{10}
398F1	0.045	5.6×10^8	7.9×10^{10}	0.013	1.6×10^8	2.3×10^{10}
Geometric mean	**0.011**	**1.3×10^8**	**1.9×10^{10}**	**0.010**	**1.2×10^8**	**1.7×10^{10}**

Table S1. IC_{50}s for CD4-VLPs and CD4-CCR5-VLPs against a panel of HIV-1 strains. In vitro neutralization of HIV-1_{YU2} and a global panel of 12 HIV-1 Env reference strains[151]. IC_{50}s against each strain and the geometric mean IC_{50}s for CD4-VLPs and CD4-CCR5-VLPs are presented in µg of p24/mL. IC_{50} VLP concentrations were derived from p24 concentrations using the following equation: 1 ng p24 = 1.25×10^7 VLPs[169,170], which assumes that each VLP contains 2,000 copies of p24[147,148]. Since each VLP displays an average of ~140 copies of CD4 (Fig. S2), IC_{50} concentrations of VLP-associated CD4 molecules were calculated by multiplying the number of VLPs by 140.

HIV Strain	IC_{50}					
	sCD4 (µg/mL)	sCD4 (CD4 copies/mL)	CD4-Ig (µg/mL)	CD4-Ig (CD4 copies/mL)	3BNC117 (µg/mL)	3BNC117 (Fab copies/mL)
YU2	0.26	6.0×10^{12}	0.93	1.1×10^{13}	0.016	1.3×10^{11}
CNE55	18.8	4.4×10^{14}	>50	6.0×10^{14}	0.14	1.1×10^{12}
Tro11	>50	1.2×10^{15}	>50	6.0×10^{14}	0.034	2.7×10^{11}
X1632	8.6	2.0×10^{14}	10.5	1.3×10^{14}	10.8	8.7×10^{13}
CH119	2.5	5.8×10^{13}	30.4	3.7×10^{14}	14.0	1.1×10^{14}
CE1176	6.8	1.6×10^{14}	31.3	3.8×10^{14}	0.12	9.6×10^{11}
25710	3.3	7.6×10^{13}	9.9	1.2×10^{14}	0.22	1.8×10^{12}
BJOX2000	0.96	2.2×10^{13}	8.0	9.6×10^{13}	>50	4.0×10^{14}
CEO217	11.1	2.6×10^{14}	37.0	4.5×10^{14}	0.04	3.2×10^{11}
CNE8	>50	1.2×10^{15}	>50	6.0×10^{14}	0.15	1.2×10^{12}
X2278	12.3	2.8×10^{14}	22.3	2.7×10^{14}	0.011	8.8×10^{10}
246F3	6.7	1.6×10^{14}	>50	6.0×10^{14}	0.14	1.1×10^{12}
398F1	>50	1.2×10^{15}	>50	6.0×10^{14}	0.092	7.4×10^{11}
Geometric mean	**10.0**	**2.3×10^{14}**	**27.7**	**3.3×10^{14}**	**0.31**	**2.5×10^{12}**

µg/mL	0.01 – 0.1	0.1 – 1	1 - 10	10 - 50	> 50

Table S2. IC_{50}s for sCD4, CD4-Ig, and 3BNC117 against a panel of HIV-1 strains. In vitro neutralization of HIV-1_{YU2} and a global panel of 12 HIV-1 Env reference strains[151] by sCD4, CD4-Ig, and 3BNC117. IC_{50}s against each strain and geometric mean IC_{50}s are shown in µg/mL. Colors indicate IC_{50} ranges. IC_{50}s are also presented in CD4 copies/mL for sCD4 D1D2 (26 kDa) and CD4-Ig (100 kDa), and Fab copies/mL for 3BNC117 (150 kDa). Concentrations of CD4/Fab copies were derived by converting IC_{50}s into molar concentrations and then calculating the respective numbers of inhibitor molecules. The numbers of inhibitor molecules were then multiplied by a factor of one (sCD4) or two (CD4-Ig, 3BNC117) depending on whether a single inhibitor molecule contains one or two CD4/Fab copies.

	IC_{50}				
Patient Isolate	**CD4-VLPs (VLPs/mL)**	**3BNC117 (µg/mL) CD4bs**	**PGDM1400 (µg/mL) V1V2**	**10E8 (µg/mL) MPER**	**8ANC195 (µg/mL) gp120-gp41 interface**
601 Wk23 MQ19	2.5×10^8	>50	7.3	11.3	>50
605 Wk23 MK10	3.3×10^8	2.9	>50	2.2	5.5

µg/mL	0.01 – 0.1	0.1 – 1	1 - 10	10 - 50	> 50

Table S3. IC_{50}s for CD4-VLPs and various bNAbs against HIV-1 isolates obtained from infected individuals. IC_{50}s are shown in VLPs/mL for CD4-VLPs and in µg/mL for the HIV-1 bNAbs 3BNC117, PGDM1400, 10E8, and 8ANC195. Epitopes on HIV-1 Env are listed for each bNAb[186]. CD4bs = CD4 binding site and MPER = membrane-proximal external region. The colors indicate different IC_{50} ranges for bNAbs.

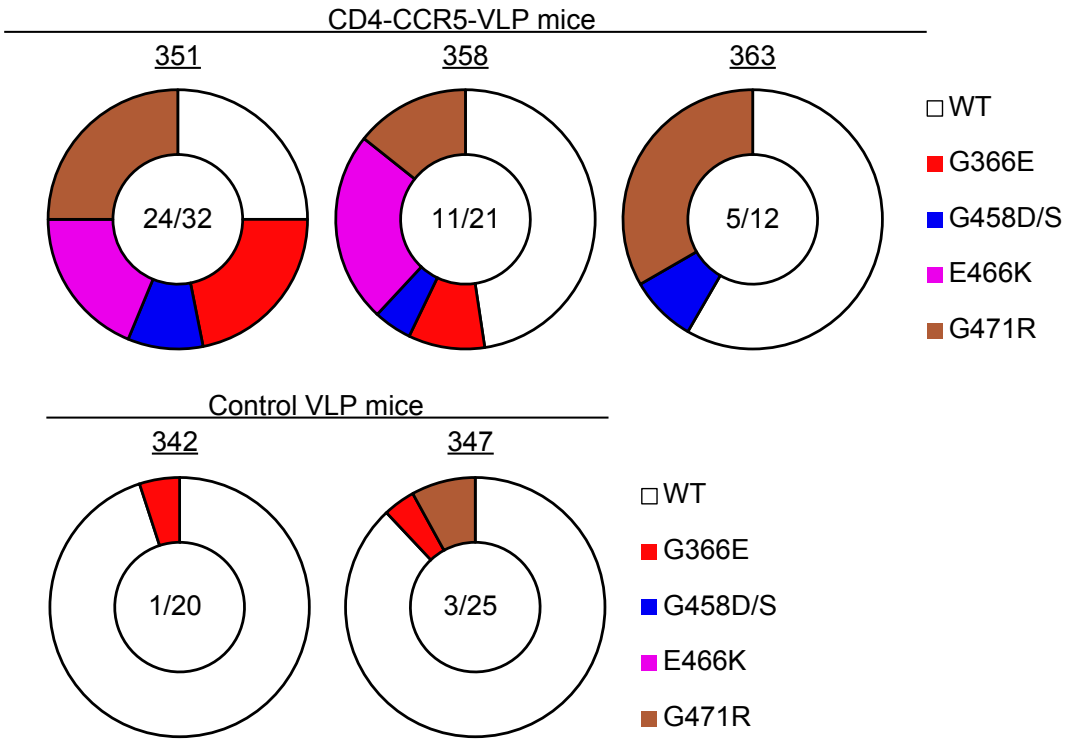

Fig. S5. CD4-CCR5-VLP treatment selects mutations in HIV-1_{YU2}-infected humanized mice. Pie charts showing the frequency of recurrent HIV-1_{YU2} *env* mutations obtained from individual CD4-CCR5-VLP-treated (#351, #358, #363) and control-VLP-treated hu-mice (#342, #347). The slices are proportional to the number of sequences that contained the indicated substitutions. White slices represent the number of sequences that lacked any recurrent mutations. The numbers in the center denote the total number of sequences that contained recurrent mutations over the total number of sequences obtained for each animal.

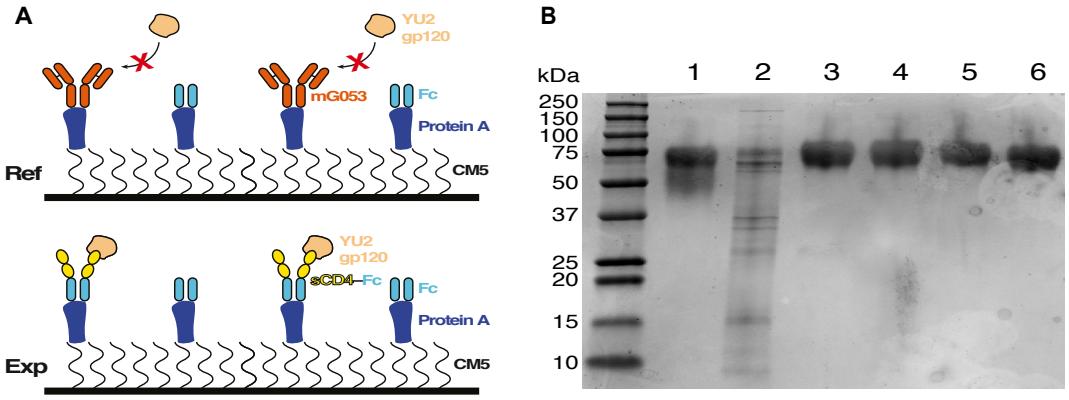

Fig. S6. SPR binding analysis of YU2 gp120 mutants. (**A**) Schematic showing the experimental setup for SPR binding assays. A non-HIV-1-binding IgG mG053 (reference) or CD4-Ig (experiment) were immobilized on protein A-coated CM5 biosensor chips followed by injection of a concentration series of monomeric YU2 gp120. (**B**) SDS-PAGE analysis of expressed $YU2_{wt}$ (lane 1), $YU2_{G366E}$ (lane 2), $YU2_{D457E}$ (lane 3), $YU2_{G458D}$ (lane 4), $YU2_{E466K}$ (lane 5), and $YU2_{G471R}$ (lane 6) gp120 proteins.

Analyte	Capture protein	k_a (10^5 $M^{-1}s^{-1}$)	k_d ($10^{-4}s^{-1}$)	K_D (nM)
$YU2_{WT}$ gp120	CD4-Ig	1.1	1.1	1.0
$YU2_{G458D}$ gp120	CD4-Ig	2.0	12.1	6.0
$YU2_{E466K}$ gp120	CD4-Ig	1.6	2.7	1.7
$YU2_{G471R}$ gp120	CD4-Ig	1.4	2.1	1.6
$YU2_{G366E}$ gp120	ND	ND	ND	ND

Table S4. K_D, k_a, k_d values for binding of YU2 gp120 variants to CD4-Ig. Results from SPR binding assays of CD4-Ig with $YU2_{wt}$ and YU2 variant gp120 proteins (see Fig. 5A).

HIV Strain	IC_{50}							
	CD4-VLPs (VLPs/mL)	Fold Change	CD4-CCR5-VLPs (VLPs/mL)	Fold Change	sCD4 (µg/mL)	Fold Change	CD4-Ig (µg/mL)	Fold Change
YU2	2.5×10^8		2.3×10^8		0.29		1.07	
$YU2_{G366E}$	1.9×10^8	0.8	2.0×10^8	0.9	8.3	28.6	28.5	26.6
$YU2_{G458D}$	3.0×10^8	1.2	3.5×10^8	1.6	4.3	14.8	40.0	37.4
$YU2_{E466K}$	1.8×10^8	0.7	2.8×10^8	1.2	7.9	27.2	32.2	30.1
$YU2_{G471R}$	2.6×10^8	1.1	2.5×10^8	1.1	9.0	31.0	34.2	32.0

µg/mL	0.01 – 0.1	0.1 – 1	1 - 10	10 - 50

Table S5. IC_{50}s for CD4-VLPs, CD4-CCR5-VLPs, sCD4, and CD4-Ig against $YU2_{wt}$ and YU2 mutant pseudoviruses. IC_{50}s are shown in VLPs/mL for CD4-VLPs and CD4-CCR5-VLPs and in µg/mL for sCD4 and CD4-Ig. The fold change was calculated by dividing a YU2 variant IC_{50} by the $YU2_{wt}$ IC_{50}. The colors indicate IC_{50} ranges for sCD4 and CD4-Ig.

Chapter 3

AAV-MEDIATED DELIVERY OF NANOPARTICLE DECOYS TO FUNCTIONALLY CURE HIV-1

Abstract

Despite almost 40 years of intensive research, there is still no curative treatment for HIV-1/AIDS. While a sterilizing cure is difficult to achieve due to the presence of long-lived latent reservoirs, a functional cure has been defined as a therapeutic strategy that enables long-term control of HIV-1 replication and remission of symptoms in the absence of HAART. As the virus is not completely eradicated from the body, a functional cure strategy against HIV-1 needs to have a persistent therapeutic effect and prevent viral escape. We recently demonstrated that nanoparticle-based decoys that present clusters of the HIV-1 receptor CD4 (CD4-NPs) are >10,000-fold more potent than soluble CD4-based inhibitors and effectively control HIV-1 replication in vitro. To achieve stable and therapeutic serum concentrations of CD4-NPs in non-human primates (NHPs), the HIV-1 gag and human CD4 genes were co-delivered by AAV-mediated gene transfer. However, this approach only resulted in transient CD4-NP serum concentrations due to CD8+ T-cell responses against Gag. To prevent transgene-directed immune responses, we designed "humanized" CD4-NP constructs by fusing the extracellular domain of CD4 to the respective N-termini of the human Arc and human Ferritin light chain proteins that both self-assemble into non-enveloped protein NPs. CD4-Arc and CD4-Ferritin NPs potently neutralized HIV-1 in vitro, and AAV-mediated delivery of CD4-Ferritin NPs produced stable serum concentrations of 0.7 – 2 μg/mL in mice for 8 weeks. Serum concentrations were ~200 – 700-fold higher than the IC_{50} determined by in vitro neutralization assay for

CD4-Ferritin NPs suggesting these concentrations could effectively suppress HIV-1 replication in vivo. This approach is now being evaluated in viral challenge studies in NHPs.

Introduction

Despite almost 40 years of intensive research, there is still no curative treatment for HIV-1/AIDS. There are two definitions for a cure against HIV-1: a sterilizing and a functional cure[112]. A sterilizing cure would require complete eradication of the virus from the body, which is difficult to achieve because HIV-1 establishes a long-lived latent reservoir by integrating into the host cell genome[113]. A functional cure has been defined as a therapeutic strategy that enables long-term control of HIV-1 replication and remission of symptoms in the absence of HAART[121]. Thus, the virus would not get completely eliminated from the body, but viral replication would be permanently reduced to undetectable levels. Three factors are important for the design of a successful functional cure strategy: the therapeutic intervention needs to i) have a persistent effect; ii) prevent the development of viral resistance; iii) and not cause adverse reactions or permanent damage to the patient.

A persistent therapeutic effect could be achieved in multiple ways. For instance, host cells could be genetically modified to become resistant to HIV-1 infection through knockdown or mutation of the CCR5 co-receptor and/or expression of protein- or nucleic acid-based therapeutics[126]. However, uniform modification of all host cells is difficult to achieve, which would allow HIV-1 to continue to infect unmodified cells and eventually evolve to use CXCR4 as co-receptor[126] and acquire mutations that lead to resistance against the expressed therapeutics. Long-term suppression of viral replication could also be achieved

through epigenetic modifications to lock the viral promoter in a latent state to permanently silence integrated HIV-1 proviruses[127]. However, the need for efficient delivery of therapeutic agents to all latently-infected cells represents a major drawback for this "block and lock" approach[127].

Continuous expression of broadly neutralizing antibodies (bNAbs) or bNAb-like reagents through adeno-associated virus (AAV)-mediated gene transfer is an alternative approach to achieve a persistent therapeutic effect. This strategy has been shown to produce stable serum concentrations following a single intramuscular (IM) AAV injection in vivo, which resulted in protection against repeated viral challenges[128-130]. A recent study reported the functional cure of a single NHP infected with a simian-human immunodeficiency virus (SHIV) after AAV-mediated delivery of the bNAbs 3BNC117 and 10-1074[131]. However, the effectiveness of this approach is limited by anti-drug antibody (ADA) responses that are frequently observed against the expressed bNAbs[131,132]. In addition, multiple bNAbs would need to be delivered in combination to prevent the emergence of resistant HIV-1 variants, and the slow onset of bNAb expression after AAV delivery provides a window of opportunity for HIV-1 to replicate and rapidly acquire escape mutations.

We have recently proposed that HIV-1 would not be able to develop resistance against a nanoparticle-based decoy that presents clusters of the CD4 receptor (CD4-NPs) due to the formation of high-avidity interactions with trimeric HIV-1 Env spikes on virions[187]. We generated CD4-NPs by co-expressing HIV-1 Gag and CD4, and demonstrated that CD4-NPs were >10,000-fold more potent

than conventional CD4-based inhibitors such as soluble CD4 (sCD4) and CD4-Ig and >100-fold more potent than various bNAbs against a diverse panel of HIV-1 strains in vitro[187]. Moreover, CD-NPs effectively suppressed viral replication and prevented viral escape in vitro[187]. While CD4-NPs have the potential to permanently control HIV-1 infection in vivo, the half-life of NP-based therapeutics is short due to rapid hepatic clearance[156]. As for conventional CD4-based inhibitors, interactions with class II major histocompatibility complex (MHC) proteins presented on antigen-presenting cells (APCs) could further shorten the half-life of CD4-NPs. Thus, to translate this concept into a clinically-feasible functional cure for HIV-1 infection, a delivery strategy to ensure durable bioavailability and minimize the requirement for repeated administrations needs to be developed.

Here we explored whether stable therapeutic CD4-NP serum concentrations could be achieved through AAV-based gene transfer to skeletal muscle, which has previously been shown to produce sustained therapeutic concentrations of hormone-based therapeutics with short half-lives[188-190]. AAV-mediated co-delivery of the HIV-1 Gag and CD4 genes only resulted in transient CD4-NP serum concentrations in non-human primates (NHPs) due to CD8+ T-cell responses against Gag. To prevent transgene-directed immune responses, we designed "humanized" CD4-NP constructs by fusing the extracellular domain of CD4 to the N-termini of the human Arc[191] and Ferritin[192] proteins that self-assemble into non-enveloped protein NPs. CD4-Arc and CD4-Ferritin NPs potently neutralized HIV-1 in vitro and AAV-mediated delivery of CD4-Ferritin NPs produced stable serum

concentrations of >1 μg/mL in mice, which is ~1,000-fold higher than in vitro IC_{50} values, suggesting these concentrations could be therapeutic. This approach is now being evaluated in challenge studies in NHPs.

Results

AAV-mediated co-delivery of gag and CD4 only produces transient CD4-NP serum concentrations in NHPs

To achieve stable serum concentrations in vivo, the HIV-1 gag and human CD4 genes required for continuous CD4-NP production were inserted into an AAV vector backbone plasmid under the control of a ubiquitous CASI promoter (Fig. 1a). The gag and CD4 genes were separated by a P2A peptide that induces ribosomal skipping and co-translational cleavage to ensure efficient expression of both transgenes[193]. To assemble AAV-Gag-CD4 vectors, the capsid from serotype AAV9 was used, which has been shown to efficiently transduce skeletal muscle cells[194]. Transgene expression and CD4-NP production was initially assessed by in vitro transduction of HEK-293T cells. 10^6 cells were seeded in 6-well plates, and $2x10^{10}$ vector copies of the AAV9-Gag-CD4 vector were added after 24 hours. CD4 expression on the surface of transduced cells was measured by flow cytometry after 72 hours. To quantify CD4-NP production, supernatants were harvested and analyzed by enzyme-linked immunosorbent assay (ELISA) against the p24 subunit of Gag as previously described[187].

CD4 expression (Fig. 1b) and CD4-NP production (Fig. 1c) was poor for the initial AAV9-Gag-CD4 vector design. To investigate if codon-optimization could improve AAV-mediated transgene expression, we generated the AAV9-Gag_{Opt}-$CD4_{Opt}$ vector. CD4 expression was markedly higher for the codon-optimized vector (Fig. 1b) and CD4-NP production increased 35-fold (Fig. 1c). The CD4-NPs expressed by the transduced cells were similarly potent to CD4-NPs that were generated by DNA plasmid transfections, and effectively neutralized the HIV-1 strain YU2 (HIV-1_{YU2}) in vitro (Fig. 1d).

To evaluate if AAV-mediated delivery could produce stable CD4-NP serum concentrations in pigtailed macaques, AAV9 vectors encoding the codon-optimized HIV-1 gag and pigtailed macaque CD4 (pgtCD4) genes were generated. 10^{13} vector copies were injected intramuscularly (IM) into the quadriceps muscle of 3 macaques that had been pre-screened for serum reactivity against AAV9. pgtCD4-NP serum concentrations were quantified by p24 ELISA in weekly intervals for a period of 6 weeks. pgtCD4-NP serum concentrations of 4-8x10^8 NPs/mL were detected in all 3 animals 10 and 17 days post-injection (Fig. 2a). In the following weeks, pgtCD4-NP serum concentrations dropped and became undetectable (detection limit = 5 x 10^7 NPs/mL). While no T-cell-mediated immune responses were observed against the AAV9 capsid protein, CD4+ and CD8+ T-lymphocyte responses were detected against the Gag protein in all animals, which likely caused the drop in pgtCD4-NP expression (Fig. 2b-e). In addition, the measured pgtCD4-NP serum concentrations were ~50-100-fold higher than IC_{50}s

obtained from in vitro neutralization assays against the simian-human immunodeficiency virus (SHIV) strain 1157ipEL-p, but serum samples from days 10 and 17 post-injection did not show enhanced in vitro neutralization activity compared to control serum (data not shown). The lack of neutralization activity suggests that pgtCD4 expression was relatively low in AAV-transduced skeletal muscle cells leading to inefficient incorporation of pgtCD4 into budding pgtCD4-NPs and reduced potency.

CD4-Arc and CD4-Ferritin NPs potently neutralize HIV-1 in vitro

AAV-mediated co-delivery of the gag and CD4 genes for continuous production of CD4-NPs in vivo had three disadvantages: i) HIV-1 Gag is a viral protein and induced T-cell responses in vivo that limited transgene expression; ii) CD4-NP production requires co-expression of two proteins resulting in lower expression levels, especially for CD4, which was positioned downstream of the 2A peptide; iii) NP assembly is exclusively driven by Gag and there is no specific interaction between Gag and CD4 that ensures efficient CD4 incorporation into NPs. Hence low AAV-mediated CD4 expression leads to inefficient incorporation of CD4 and reduced CD4-NP potency.

To address these issues, we designed optimized CD4-NP constructs by fusing the extracellular domain of CD4 (residues 1-396) to the N-termini of the human Arc[191] and Ferritin[192] proteins that self-assemble into non-enveloped protein NPs. In contrast to Gag-based CD4-NPs, CD4-Arc and CD4-Ferritin NPs should

not induce immune responses as Arc and Ferritin are both human proteins. Moreover, CD4-Arc and CD4-Ferritin NP assembly only requires expression of a single fusion protein and CD4 gets directly incorporated into the NP. To evaluate their neutralization potency, 10-mL cultures of Expi293 cells were transfected with DNA plasmids encoding the CD4-Arc and CD4-Ferritin fusion constructs. After 72 hours, supernatants were harvested, spun down to remove cell debris, and filtered. CD4-Arc and CD4-Ferritin NPs were then purified by ultracentrifugation on a 20% sucrose cushion and re-suspended in 200 μL PBS overnight.

In vitro neutralization assays were performed to compare the neutralization activity of the purified CD4-Arc and CD4-Ferritin NPs to Gag-based CD4-NPs that were expressed and purified in parallel. Equal dilutions for all purified samples were tested against the HIV-1_{YU2} pseudovirus. Gag-based CD4-NPs achieved 50% inhibition of HIV-1_{YU2} infection at an inhibitory dilution (ID_{50}) of 139 (Fig. 3a). Interestingly, CD4-Arc NPs (ID_{50} = 2,414) and CD4-Ferritin NPs (ID_{50} = 326) were 17- and 2-fold more potent than Gag-based CD4-NPs, respectively. CD4 concentrations were quantified by ELISA to determine IC_{50}s for CD4-Arc NPs (IC_{50} = 0.0004 μg/mL) and CD4-Ferritin NPs (IC_{50} = 0.003 μg/mL), which were ~40- and ~6-fold more potent than 3BNC117, a bNAb that targets the CD4-binding site (CD4bs)[187], respectively.

To verify that CD4-Arc NPs and CD4-Ferritin NPs are able to form multivalent interactions with trimeric HIV-1 Env spikes on virions, neutralization was evaluated against a mutant HIV-1_{YU2} Env G471R pseudovirus that was

resistant to monomeric soluble CD4, but was sensitive to Gag-based CD4-NPs[187]. Only ~2-fold reductions in neutralization potency were observed for Gag-based CD4-NPs (ID_{50} = 72), CD4-Arc NPs (ID_{50} = 1,400), and CD4-Ferritin NPs (ID_{50} = 135), respectively, indicating that all three CD4-NP designs could prevent viral escape through the formation of high-avidity interactions with HIV-1 Env spikes (Fig. 3b).

AAV-mediated delivery of CD4-Ferritin NPs produces stable serum concentrations in mice

AAV vectors encoding murine versions of CD4-Arc (muCD4-Arc) and CD4-Ferritin (muCD4-Ferritin) were generated to investigate whether AAV-mediated gene transfer of these fusion constructs could produce stable muCD4-NP serum concentrations in mice. The capsid from serotype AAV8 was used for this experiment as AAV8 has been shown to efficiently transduce mouse skeletal muscle[128] and induce immune tolerance against transgenes[195]. Mice received a single IM injection of 10^{11} vector copies of AAV8-muCD4-Arc or AAV8-muCD4-Ferritin, and muCD4 serum concentrations were measured by ELISA in biweekly intervals.

While muCD4 concentrations were undetectable in baseline serum samples taken prior to AAV administration (detection limit = 0.1 ng/mL), muCD4 serum concentrations were detected in all mice 14 days post-injection (Fig. 4). For the AAV8-muCD4-Arc group, muCD4 concentrations were relatively low ranging

from 3.5 – 6.8 ng/mL. muCD4 concentrations were markedly higher for mice that received the AAV8-muCD4-Ferritin vector ranging from 844 – 1,558 ng/mL. These serum muCD4 concentrations were 281 – 519-fold higher than the IC_{50} determined by in vitro neutralization assay for CD4-Ferritin NPs (Fig. 3a) suggesting that these concentrations could effectively suppress HIV-1 replication in vivo. After 6 weeks, muCD4 serum concentrations increased for mice that received AAV8-muCD4-Arc with peak concentrations of 23.6 – 27.8 ng/mL (Fig. 4), which is 59 – 70-fold higher than the in vitro IC_{50} measured for CD4-Arc NPs (Fig. 3a). For the AAV8-muCD4-Ferritin group, muCD4 serum concentrations were maintained between 600 – 2,000 ng/mL for all animals over 8 weeks (Fig. 4). This experiment is ongoing and serum concentrations will be monitored for an additional 8 weeks.

Discussion

Our results demonstrate that AAV-mediated delivery of muCD4-Arc and muCD4-Ferritin produces potentially therapeutic muCD4-NP serum concentrations in vivo. Importantly, serum concentrations were stable over 8 weeks and highly consistent for all mice in each group. This suggests that AAV-mediated gene transfer and continuous expression of muCD4-Arc and muCD4-Ferritin did not elicit transgene-specific immune responses as observed for co-expression of HIV-1 Gag and CD4. In addition, no adverse effects were observed. The neutralization activity of mouse serum samples could not be evaluated as muCD4

does not bind to HIV-1 Env[196]. Thus, additional in vivo studies in NHPs are underway to fully assess the therapeutic potential of this approach. Future in vivo experiments will also investigate whether CD4-Arc and CD4-Ferritin NP concentrations could be increased through a second AAV administration using the capsid of the AAV1 serotype, a strategy that has been shown to increase serum concentrations of a therapeutic antibody by >4-fold in NHPs[195].

CD4-NPs have several advantages over bNAbs for AAV-based gene transfer approaches to functionally cure HIV-1 infection. CD4-Arc and CD4-Ferritin NPs are 10 – 100-fold more potent than bNAbs and will likely control HIV-1 replication at lower serum concentrations. While AAV-mediated delivery of multiple bNAbs will be necessary to prevent rapid emergence of resistant HIV-1 variants, continuous CD4-NP production only requires delivery and expression of a single fusion construct and has the potential to prevent viral escape and permanently control HIV-1 infection. Finally, the CD4-Arc and CD4-Ferritin constructs are based on endogenous proteins and do not present foreign epitopes that could be targeted by host antibodies. Thus, AAV delivery of CD4-Arc and CD4-Ferritin NPs should not elicit transgene-specific ADA responses as commonly observed for bNAbs, which could ensure stable expression levels and consistent therapeutic effects for a large number of patients.

Methods

CD4-NP production

The CD4-Arc and CD4-Ferritin constructs were designed by fusing the cDNA sequence of the extracellular domain of human CD4 (residues 1-396) to the N-termini of the human Arc and human Ferritin light chain proteins. Both fusion constructs were subcloned into the pHAGE-CMV-IRES-ZsGreen plasmid (PlasmID Repository, Harvard Medical School). HIV-1 Gag-based CD4-NPs, CD4-Arc NPs, and CD4-Ferritin NPs were produced as previously described[187] by transiently transfecting Expi293 cells (Life Technologies) grown in Expi293 expression media (Life Technologies) on an orbital shaker at 37°C and 8% CO_2. 48-72 hours post-transfection, cells were centrifuged at 350 x g for 8 min, and supernatants were collected and passed through a 0.45-μm syringe filter. CD4-NPs were purified by ultracentrifugation at 50,000 rpm (135,000 x g) for 2 hours at 4°C using a TLA-100.3 rotor and a Beckman Optima TLX ultracentrifuge (Beckman Coulter) on a 20% w/v sucrose cushion. The supernatants were carefully aspirated, and pellets were re-suspended in 200 μL culture medium at 4°C overnight. On the following day, samples were centrifuged at 10,000 x g for 10 min to remove cell debris. HIV-1 Gag-based CD4-NPs were quantified using the lentivirus-associated p24 ELISA kit (Cell Biolabs) as previously described[187]. CD4-Arc and CD4-Ferritin NPs were quantified using a human CD4 ELISA kit (Invitrogen).

In vitro neutralization assays

The ability of CD4-NPs to neutralize HIV-1 was evaluated using a pseudovirus-based TZM-bl assay[149]. Pseudoviruses with Envs from $YU2_{wt}$ and the $YU2_{G471R}$ mutant were generated in HEK293T cells as described[171]. Serial dilutions of purified Gag-based CD4-NPs, CD4-Arc NPs, and CD4-Ferritin NPs were incubated with pseudovirus for 1 hour at 37°C. TZM-bl cells (NIH AIDS Reagents Program) that express a Tat-inducible luciferase reporter gene were added, and luminescence was measured after 48 hours.

In vitro evaluation of AAV vectors

The HIV-1 gag and human CD4 cDNA sequences were subcloned into a previously described AAV2 backbone plasmid that contained a CASI promoter and an SV40 polyadenylation signal[128] to generate AAV-Gag-CD4. The gag and CD4 genes were separated by a P2A peptide. Codon optimization of transgene cDNA sequences was performed using the GeneArt GeneOptimizer software (Thermo Fisher Scientific) to generate AAV-Gag_{Opt}-$CD4_{Opt}$. HEK293T cells were co-transfected with the AAV backbone plasmids, an AAV helper plasmid, and a plasmid encoding the AAV9 rep and cap proteins. After 72 hours, supernatants containing AAV9-Gag-CD4 or AAV9-Gag_{Opt}-$CD4_{Opt}$ vectors were collected and passed through a 0.45-μm syringe filter. Samples were concentrated in Amicon Ultra-15 centrifugal filter units with a 100 kDa molecular weight cut-off (Millipore)

to a final volume of 500 µL. AAV vectors were quantified by qPCR as previously described[197].

AAV-mediated transgene expression was evaluated by in vitro transduction of HEK293T cells. 10^6 cells were seeded in 6-well plates overnight. After 24 hours, $2x10^{10}$ vector copies of the AAV9-Gag-CD4 and AAV9-Gag_{Opt}-$CD4_{Opt}$ vectors were added. After 72 hours, CD4 expression on the surface of transduced cells was measured by flow cytometry (MACSQuant, Miltenyi Biotec) as previously described[198]. To quantify CD4-NP production, supernatants were harvested and analyzed by p24 ELISA as previously described[187].

AAV vector production for in vivo studies

AAV vectors for in vivo studies were produced by the Caltech CLOVER Center as previously described[197]. For the NHP studies, codon-optimized cDNA sequences for the HIV-1 gag and pgtCD4 genes were subcloned into the AAV2 backbone plasmid to generate AAV-Gag-pgtCD4. For the mouse studies, codon-optimized cDNA sequences for the muCD4-Arc and muCD4-Ferritin fusion constructs were subcloned into the AAV2 backbone plasmid to generate AAV-muCD4-Arc and AAV-muCD4-Ferritin, respectively. The capsid from serotype AAV9 was used for NHP studies and the capsid from serotype AAV8 was used for mouse studies. All AAV vectors were quantified by qPCR as described[197]. The ratio of full-to-empty AAV capsids was inspected by transmission electron microscopy, and samples were assessed for endotoxin levels.

NHP studies

NHP studies were conducted at the Washington National Primate Research Center in collaboration with Hans-Peter Kiem's laboratory at the Fred Hutch Cancer Research Center. All procedures were performed under the supervision of a clinical veterinarian and in accordance with protocols approved by the Institutional Animal Care and Use Committee (IACUC) at the University of Washington. Three pigtailed macaques (*Macaca nemestrina*) received a single IM injection of 10^{13} vector copies of the AAV9-Gag-pgtCD4 vector into the quadriceps muscle (four 0.5-mL injections per animal; two injections per quadriceps muscle). Serum samples were taken on a weekly basis and analyzed by p24 ELISA (Perkin Elmer) according to the manufacturer's guidelines.

To analyze T-cell-mediated immune responses against the gag transgene, peripheral blood mononuclear cells (PBMCs) were isolated from each animal. To stimulate T-cell reponses, PBMCs were incubated in the presence of Gag-based NPs or AAV9 capsids overnight. After 24 hours, gag-specific T-cell responses were analyzed by flow cytometry to detect expression of the early T-cell activation marker CD69.

Mouse studies

AAV delivery of muCD4-Arc and muCD4-Ferritin constructs were performed in wild-type C57BL/6 mice at Covance Laboratories Inc. Studies were

conducted in accordance with the recommendations in the *Guide for the Care and Use of Laboratory Animals* of the National Institutes of Health. The protocol was reviewed and approved by the (IACUC) at Covance Laboratories Inc. Groups of 4 mice received a single IM injection of 10^{11} vector copies of either AAV8-muCD4-Arc or AAV8-muCD4-Ferritin into the quadriceps muscle (two 50-µL injections per animal; one injection per quadriceps muscle).

Serum samples were obtained every 14 days and muCD4 concentrations were measured by ELISA using the following protocol: 96-well plates (Costar) were coated overnight with a polyclonal anti-muCD4 antibody (Thermo Fisher Scientific) at a concentration of 5 µg/mL in sodium bicarbonate buffer (pH 9.6). On the following day, plates were washed using tris-buffered saline with 0.1% Tween20 (TBST) and blocked with 1% bovine serum albumin (BSA) in TBST for 30 min at room temperature (RT). After the blocking step, plates were washed with TBST and recombinant muCD4 standards (Thermo Fisher Scientific) and diluted serum samples were added. After 2 hours incubation at 37ºC, plates were washed three times with TBST and a biotinylated anti-muCD4 monoclonal antibody (clone GK1.5; BioLegend) was added at a dilution of 1:5,000. After 1-hour incubation at RT, plates were washed three times with TBST and streptavidin-HRP (Abcam) was added at a dilution of 1:40,000. After 45 min incubation at RT, plates were washed three times with TBST and 1-step Ultra TMB-ELISA substrate (Thermo Fisher Scientific) was added. After 5-10 min incubation, the reaction was stopped by

adding 1N hydrochloric acid and absorbance was measured at a wavelength of 450 nm using a microplate reader (BioTek Instruments).

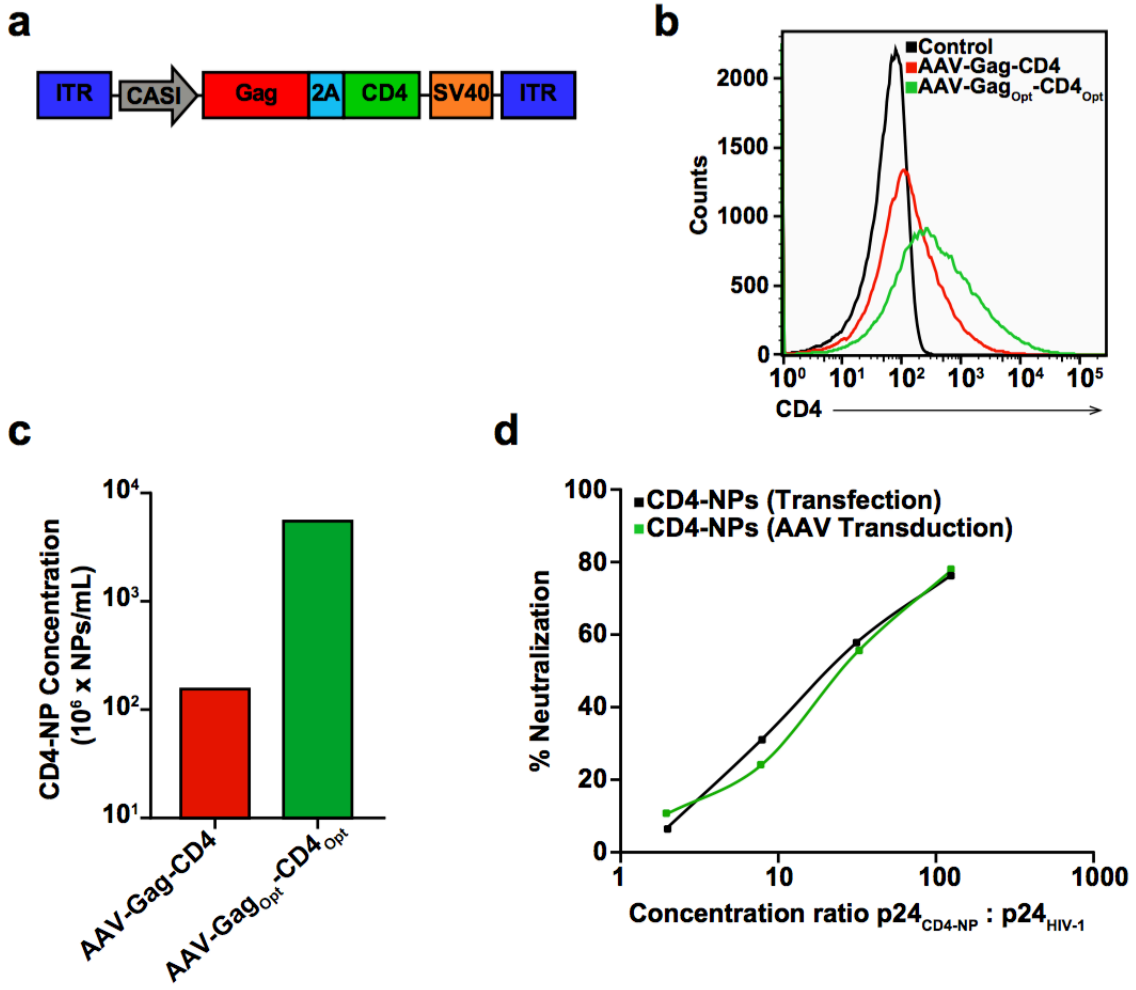

Figure 1. In vitro evaluation of AAV9-Gag$_{Opt}$-CD4$_{Opt}$ vector. a) Schematic presenting the design of the AAV-Gag-CD4 vector. **b)** Flow cytometry analysis to measure CD4 expression on HEK293T cells that were transduced with 2 x 10^{10} vector copies of AAV-Gag-CD4 (red) or AAV-Gag$_{Opt}$-CD4$_{Opt}$ (green). **c)** CD4-NP concentrations in supernatants collected 72 hours post-transduction from HEK293T cells that were transduced with 2 x 10^{10} vector copies of AAV-Gag-CD4 (red) or AAV-Gag$_{Opt}$-CD4$_{Opt}$ (green). **d)** In vitro neutralization assay against HIV-1$_{YU2}$ pseudovirus comparing CD4-NPs that were generated by transient transfection of

Expi293 cells (black) and CD4-NPs produced by the AAV-transduced HEK293T cells (green). The neutralization activity of CD4-NPs was determined in terms of the Gag p24 concentration ratio between CD4-NPs and HIV-1_{YU2} virions.

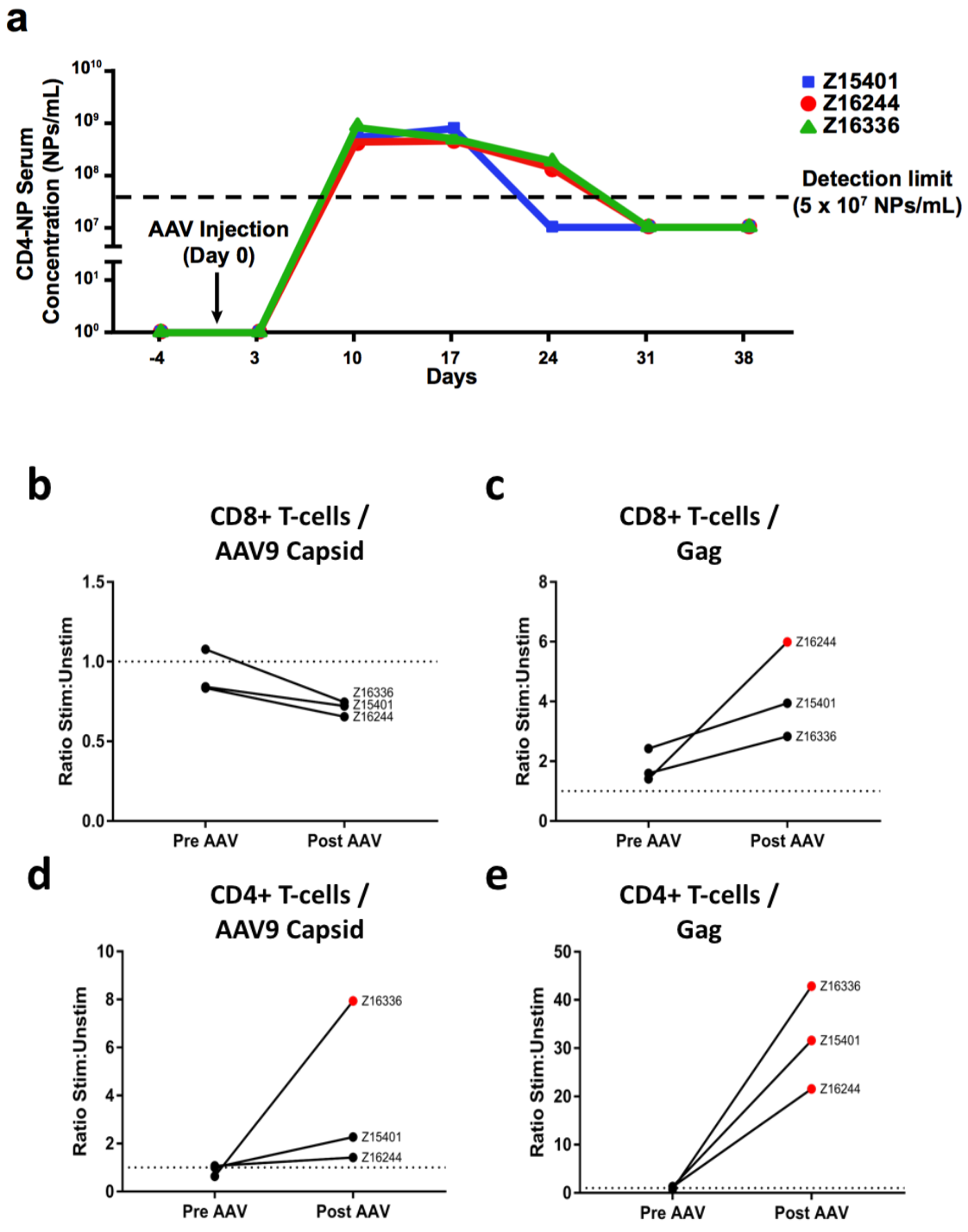

Figure 2. AAV-mediated co-delivery of Gag and pgtCD4 produces transient CD4-NP serum concentrations in NHPs. a) CD4-NP serum concentrations for

three pigtailed macaques following a single IM administration of 10^{13} vector copies of AAV9-Gag-pgtCD4. CD4-NP concentrations were measured by Gag p24 ELISA with a detection limit of 5 x 10^7 NPs/mL. **b – e)** CD8+ and CD4+ T-cell responses against the AAV9 capsid protein and the HIV-1 Gag protein. PBMCs were isolated from animals pre- and post-AAV administration. PBMCs were stimulated by overnight incubation with the AAV9 capsid protein or Gag. After 24 hours, T-cells were analyzed for expression of the early T-cell activation marker CD69 by flow cytometry. Results are presented as ratios of stimulated to unstimulated CD69-positive T-cells and responses are compared for samples taken pre- and post-AAV administration.

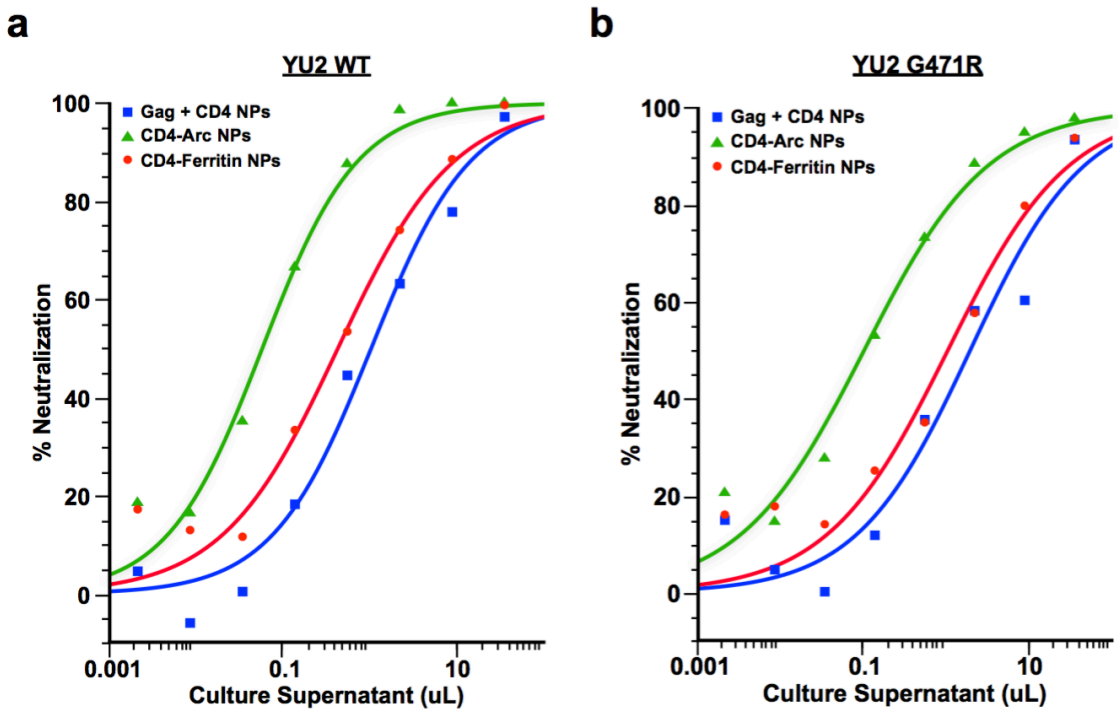

Figure 3. CD4-Arc and CD4-Ferritin NPs potently neutralize HIV-1 in vitro. **a – b)** In vitro neutralization assays against **a)** wild-type HIV-1_{YU2} pseudovirus and **b)** a mutant HIV-1_{YU2} Env G471R pseudovirus comparing Gag + CD4 NPs (blue), CD4-Arc NPs (green), and CD4-Ferritin NPs (red). All CD4-NP samples were expressed and purified from culture supernatants in parallel. Serial dilutions of purified Gag + CD4 NP, CD4-Arc NP, and CD4-Ferritin NP samples were used to determine half-maximal inhibitory dilutions (ID_{50}s).

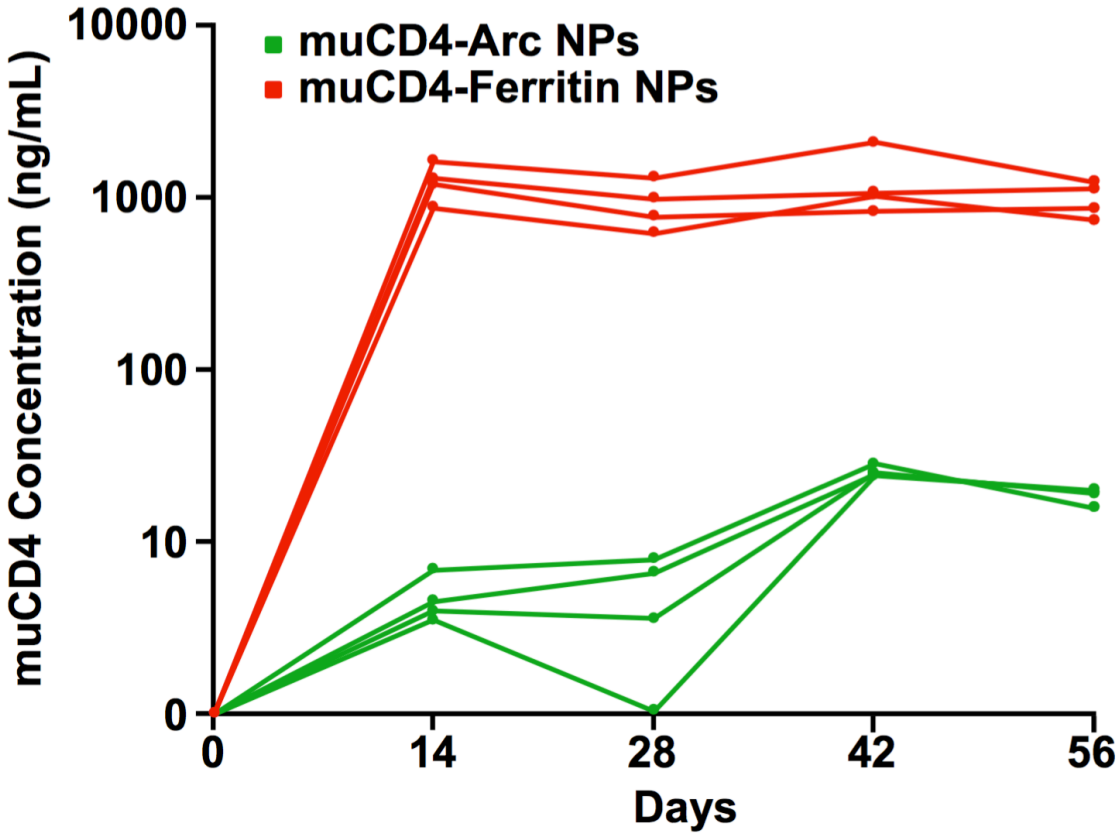

Figure 4. AAV-mediated gene transfer of muCD4-Arc and muCD4-Ferritin produces stable muCD4-NP serum concentrations in mice. muCD4 serum concentrations for groups of four mice that received a single IM injection of 10^{11} vector copies of either AAV8-muCD4-Arc (green) or AAV8-muCD4-Ferritin (red). muCD4 concentrations were measured biweekly by ELISA (detection limit = 0.3 ng/mL).

Chapter 4

IN VITRO CHARACTERIZATION OF ENGINEERED RED BLOOD CELLS AS VIRAL TRAPS AGAINST HIV-1 AND SARS-COV-2

Abstract

Engineered red blood cells (RBCs) expressing viral receptors could be used therapeutically as viral traps as RBCs lack nuclei and other organelles required for viral replication. However, expression of viral receptors on RBCs is difficult to achieve since mature erythrocytes lack the cellular machinery to synthesize proteins. Here we show that the combination of a powerful erythroid-specific expression system and transgene codon optimization yields high expression levels of the HIV-1 receptors CD4 and CCR5, as well as a CD4-glycophorin A (CD4-GpA) fusion protein in erythroid progenitor cells, which efficiently differentiated into enucleated RBCs. HIV-1 efficiently entered RBCs that co-expressed CD4 and CCR5, but viral entry was not required for neutralization as CD4 or CD4-GpA expression in the absence of CCR5 was sufficient to potently neutralize HIV-1 and prevent infection of CD4+ T-cells in vitro due to the formation of high-avidity interactions with trimeric HIV-1 Env spikes on virions. To facilitate continuous large-scale production of RBC viral traps, we generated erythroblast cell lines stably expressing CD4-GpA or ACE2-GpA fusion proteins, which produced potent RBC viral traps against HIV-1 and SARS-CoV-2. Our in vitro results suggest that this approach warrants further investigation as a potential treatment against acute and chronic viral infections.

Adapted from:

Hoffmann, M.A.G., Kieffer, C. and Bjorkman, P.J., 2021. In vitro characterization of engineered red blood cells as viral traps against HIV-1 and SARS-CoV-2. *Molecular Therapy-Methods & Clinical Development*, *21*, pp.161-170.

Introduction

Red blood cells (RBCs) exhibit unique properties that can be exploited for therapeutic applications: they are the most abundant cell type, permeate all tissues, and have a lifespan of 120 days, making them attractive carriers for the delivery of therapeutic cargoes[199,200]. Moreover, RBCs do not express class I major histocompatibility complex molecules[201], thus therapeutic RBCs from type O-negative blood could be universally administered to patients.

Engineered RBCs have been proposed as ideal candidates for the design of viral traps, as they lack nuclei and other organelles required for viral replication[202-205]. Viruses could be lured into attaching to and infecting RBCs that present viral receptors, thereby leading the virus to a dead end and protecting viral target cells from infection. This approach has the potential to prevent viral escape, as viruses must retain the ability to bind their receptors. However, expression of viral receptors on RBCs is difficult to achieve since mature erythrocytes lack the cellular machinery to synthesize proteins. Hence erythroid progenitor cells need to be genetically-engineered to express the viral receptors and then be differentiated into enucleated RBCs. During the erythroid differentiation process, transgene expression is restricted through transcriptional silencing[206], translational control mechanisms[207], and degradation of proteins that are not normally present in RBCs[208].

One strategy to overcome the latter problem is to generate chimeric proteins by fusing the extracellular domain of a non-erythroid protein to a protein that is

abundantly expressed in RBCs, such as glycophorin A (GpA)[209,210]. However, this approach is limited to single-pass transmembrane proteins, prevents localization of viral receptors to their natural membrane subdomains, and might not achieve sufficiently high receptor levels to effectively entrap the virus. In the case of a potential HIV-1 therapeutic, additional strategies are required to generate RBC viral traps as the HIV-1 receptors CD4 and CCR5 co-localize in nanoclusters within lipid rafts[162,211], and CCR5 is a G-protein coupled receptor (GPCR) with seven transmembrane domains.

Here we show that the combination of a powerful erythroid-specific expression system and transgene codon optimization yields high expression levels of the HIV-1 receptors CD4 and CCR5 on enucleated RBCs to generate viral traps that potently inhibit HIV-1 infection in vitro. We then applied these engineering strategies to generate erythroblast cell lines that can continuously produce potent RBC viral traps against HIV-1 and SARS-CoV-2.

Results

Enucleated RBCs express HIV-1 receptors

We used an in vitro differentiation protocol[210] to differentiate human CD34+ hematopoietic stem cells (HSCs) into reticulocytes, an immature form of enucleated RBC that still contains ribosomal RNA (Fig. 1a). At the end of the proliferation phase, erythroid progenitor cells were transduced using lentiviral

vectors carrying CD4 or CCR5 transgenes by spinoculation (Fig. 1a; Fig. S1a). We also evaluated expression of a CD4-glycophorin A (CD4-GpA) fusion protein that contained the extracellular CD4 D1D2 domains fused to the N-terminus of GpA, an abundantly-expressed RBC protein. Three days post-transduction, transgene expression was evaluated by flow cytometry. Expression was low for all transgenes when the CMV promoter or alternative ubiquitous promoters were used (Fig. 1b; Fig. S1b). Surprisingly, CD4-GpA expressed only marginally better than CD4, suggesting that additional strategies are required to achieve robust expression of viral receptors on RBCs.

To evaluate whether transcriptional silencing can be prevented by using an erythroid-specific promoter, transgenes were subcloned into the CCL-βAS3-FB lentiviral vector[212], which contains regulatory elements that support the high expression levels of β-globin during erythroid development (vectors β-CD4, β-CD4-GpA, and β-CCR5) (Fig. S1a). CD4 expression was greatly enhanced by this expression system, CCR5 expression increased to a lesser extent, but CD4-GPA expression was not improved (Fig. 1b).

We hypothesized that the limited availability of ribosomes and transfer RNAs potentially restricts transgene expression in differentiating erythroid cells. Transgene cDNA sequences were codon-optimized to generate β-$CD4_{opt}$, β-CD4-GpA_{opt}, and β-$CCR5_{opt}$. For all transgenes, codon optimization drastically enhanced expression levels (Fig. 1b). These results demonstrated that the combination of a

powerful erythroid-specific promoter and transgene codon optimization yields high expression levels of HIV-1 receptors in erythroid cells.

Genetically-engineered CD4+/CCR5+ erythroid progenitor cells differentiated efficiently into enucleated RBCs (Fig. 1c). After differentiation, almost 90% of cells expressed GpA, of which >80% did not stain for Hoechst nuclear dye, suggesting that the majority of cells were enucleated RBCs (Fig. 1c). May-Grunwald-Giemsa staining confirmed that most cells had lost their nuclei (Fig. 1d). Approximately 1/3 of the enucleated RBCs expressed CD4 and CCR5 on their surface (Fig. 1e) at levels comparable to Rev-A3R5 CD4+ T-cells (Fig. S2). Similar CD4+ T-cell lines have been shown to express ~10^5 copies of CD4 and ~10^3-10^4 copies of CCR5[30], providing a means to estimate receptor copy numbers on engineered RBCs.

HIV-1 enters RBC viral traps

To evaluate the efficacy of RBC viral traps against HIV-1, we generated RBCs that expressed CD4+/-CCR5 or CD4-GpA+/-CCR5 (Fig. 2a) and used the β-lactamase (BlaM) fusion assay[213] to evaluate if HIV-1 can enter RBC viral traps through attachment of HIV-1 Env spikes to the receptors presented on the RBC surface and subsequent fusion of the viral and RBC membranes. RBCs were incubated with a CCR5-tropic HIV-1_{YU2} pseudovirus carrying a BlaM-Vpr fusion protein that enters cells upon infection. When infected cells are exposed to the fluorescence resonance energy transfer (FRET) substrate CCF2-AM, BlaM cleaves

the β-lactam ring in CCF2-AM resulting in a shift of its emission spectrum from green (520 nm) to blue (447 nm)[213]. Whereas viral entry events were ≤0.3% in control RBCs and CD4-RBCs, entry was detected in 6.1% of CD4-CCR5-RBCs suggesting that RBC viral traps that present both receptors can entrap the virus. (Fig. 2b; Fig. S3a). Since only 1/3 of these RBCs expressed both receptors (Fig. 1e), this corresponds to infection of almost 20% of CD4-CCR5-RBCs. CCR5 expression on enucleated RBCs was slightly higher than on nucleated cells; thus it is unlikely that HIV-1 preferentially entered the small number of remaining nucleated cells (Fig. S3b). Higher rates of viral entry were observed for RBCs that co-expressed CD4 and the alternative HIV-1 co-receptor CXCR4 after incubation with a CXCR4-tropic HIV-1 HxBc2 pseudovirus (Fig. 2c; Fig. S4a). However, lower frequencies of viral entry were detected for RBCs that co-expressed the CD4-GpA fusion protein and CCR5 or CXCR4 (Fig. 2b,c), and addition of the CD4 D3D4 domains to CD4-GpA did not improve viral entry efficiency (Fig. S4b). Unlike CD4, GpA does not localize to lipid raft subdomains[214], thus we speculate that these low rates of viral entry resulted from a lack of co-localization between CD4-GpA and the CCR5 and CXCR4 co-receptors.

RBC viral traps potently neutralize HIV-1 in vitro

We assessed the therapeutic potential of RBC viral traps using a modified version of the HIV-1 TZM-bl neutralization assay[149] (Fig. 3a). After incubating RBCs with HIV-1_{YU2} pseudovirus, samples were centrifuged to remove RBCs and

virions that attached to or infected RBCs. Supernatants containing free virions that had not been captured by RBCs were transferred to 96-well plates, and TZM-bl cells were added to measure infectivity. In three independent assays, CD4-GpA-RBCs neutralized HIV-1_{YU2} most potently at an average half-maximal inhibitory concentration (IC_{50}) of $1.9x10^6$ RBCs/mL (Fig. 3b; Table 1). This concentration is equivalent to 0.04% of the RBC concentration of human blood (~$5x10^9$ RBCs/mL), suggesting that it would be feasible to achieve therapeutic concentrations in vivo. CD4-GpA-RBCs were ~3-fold more potent than CD4-RBCs, likely due to higher expression levels (Fig. 2a; Fig.S5). While CCR5 co-expression had no impact on the potency of CD4-GpA-RBCs, co-expression of CCR5 lowered the neutralization activity of CD4-CCR5-RBCs by almost 3-fold in comparison to CD4-RBCs (Fig. 3b; Table 1), implying that HIV-1 infection of RBC viral traps was not required for potent neutralization. CCR5 co-expression slightly lowered CD4 expression levels (Fig. 2a), potentially explaining the observed drop in potency. However, these results do not exclude the possibility that CCR5 expression on RBC viral traps would have beneficial effects in vivo.

We previously showed that virus-like nanoparticles presenting clusters of CD4 (CD4-VLPs) that formed high-avidity interactions with trimeric HIV-1 Env spikes on virions potently neutralized a diverse panel of HIV-1 strains and prevented viral escape in vitro[187]. To confirm that RBC viral traps can also form high-avidity interactions with Env, we evaluated neutralization against a mutant HIV-1_{YU2} Env G471R pseudovirus that was resistant to monomeric soluble CD4,

but was sensitive to CD4-VLPs[187]. CD4-GpA-RBCs potently neutralized the HIV-1_{YU2} G471R pseudovirus (IC_{50} = 1.0x10^7 RBCs/mL) (Fig. 3c), suggesting that RBC viral traps and CD4-VLPs would be similarly effective in preventing viral escape through formation of high-avidity interactions with HIV-1 Env spikes.

RBC viral traps prevent infection of CD4+ T-cells in vitro

The ability of RBC viral traps to protect HIV-1 target cells from infection was evaluated by co-culturing control RBCs or CD4-GpA-RBCs with Rev-A3R5 CD4+ T-cells[159], a reporter cell line that expresses luciferase upon HIV-1 infection (Fig. 4a). RBCs, CD4+ T-cells, and HIV-1 pseudovirus were co-incubated at RBC to T-cell ratios of 2:1 and 5:1 overnight under shaking conditions. The pseudovirus was removed by centrifugation and the cells were re-suspended in Rev-A3R5 CD4+ T-cell media to permit outgrowth of CD4+ T-cells. After 36 hours, luminescence was measured to determine if the presence of RBC viral traps prevented infection of CD4+ T-cells. While control RBCs had no effect, CD4-GpA-RBCs lowered infection rates by 50% and 70%, respectively, demonstrating that RBC viral traps can effectively prevent infection of HIV-1 target cells at RBC:T-cell ratios that are ~1,000-fold lower than typically found in human blood (~5,000:1)[215] (Fig. 4b). Since HIV-1 did not efficiently enter CD4-GpA-RBCs (Fig. 2b), these findings also suggest that high-avidity binding of HIV-1 virions to RBC viral traps is sufficient to prevent attached virions from infecting target cells.

Erythroblast cell lines stably express viral receptors and continuously produce RBC viral traps against HIV-1 and SARS-CoV-2

To generate a renewable and cost-effective source of RBC viral traps, we engineered the immortalized BEL-A erythroblast cell line[216] to stably express high levels of CD4-GpA (Fig. 5a). The BEL-A / CD4-GpA cells efficiently differentiated into enucleated RBCs, as >50% of CD71-expressing cells did not stain for the nuclear marker DRAQ5 (Fig. 5b). After differentiation, CD71+/DRAQ5- RBCs were purified using fluorescence-activated cell sorting (FACS). The majority of RBCs still expressed CD4-GpA (Fig. 5c) and potently neutralized HIV-1_{YU2} in vitro (IC_{50} = $2.1x10^7$ RBCs/mL) (Fig. 5d). Independent replicates of in vitro differentiation of BEL-A / CD4-GpA cells achieved comparable yields of RBC viral traps (Fig. 5b,c; Fig. S6) suggesting that engineered erythroblast cell lines could be used to continuously produce potent RBC viral traps against HIV-1. However, overall production yields would also depend on the quality of the RBCs as the viability of BEL-A cells decreases to ~80% at the end of differentiation[217] and cells could also get damaged during the purification process. To ensure complete removal of nucleated cells for in vivo studies, the RBC viral traps could be further purified using leukoreduction filters and/or gamma irradiation.

To evaluate if RBC viral traps could be effective against other viruses, we generated a BEL-A cell line that continuously produces RBC viral traps against SARS-CoV-2, the virus that caused the ongoing COVID-19 pandemic[218]. BEL-A

cells were transduced to stably express a chimeric ACE2-GpA protein containing the extracellular domain of the SARS-CoV-2 receptor ACE2[218] fused to GpA (Fig. 6a). Differentiation efficiency and transgene expression on sorted CD71+/DRAQ5- RBCs was comparable to the BEL-A / CD4-GpA cell line (Fig. 6b,c). Importantly, lentivirus-based SARS-CoV-2 pseudovirus[219] was highly susceptible to ACE2-GpA-RBC neutralization (IC_{50} = 7x10^5 RBCs/mL) (Fig. 6d) suggesting that RBC viral traps have the potential to be effective anti-viral agents against a range of viruses.

Discussion

In summary, we described engineering strategies that facilitate efficient and continuous production of potent RBC viral traps against HIV-1 and SARS-CoV-2. HIV-1 efficiently entered engineered RBCs expressing HIV-1 receptors, and RBC viral traps potently neutralized the virus in vitro, thus demonstrating the desired properties of a viral trap.

A number of techniques have been developed to attach proteins to the RBC surface for therapeutic applications[220,221], including chemical conjugation[222-225] and affinity targeting to RBC membrane proteins[226-228]. However, genetic manipulation of RBCs has been challenging due to the loss of cellular organelles during erythroid maturation. RBC surface expression of chimeric proteins containing single-domain antibodies (VHHs) fused to RBC membrane proteins GpA and Kell has been achieved through lentiviral transduction of RBC precursor cells followed by in vitro

differentiation into reticulocytes[210]. While shown to be safe and effective in animal models[210,220,221], all of these methods are limited to RBC surface presentation of soluble or single-pass transmembrane proteins, and important properties of membrane proteins such as localization to specific plasma membrane subdomains, ligand-induced conformational changes, and signal transduction activity may not be retained. Moreover, our results showed that fusing the extracellular domain of CD4 to GpA resulted in low surface expression levels in the absence of other optimization steps. However, the combination of an erythroid-specific promoter and transgene codon optimization greatly enhanced CD4-GpA expression and achieved similar expression of wild-type CD4. Importantly, this approach enabled RBC surface expression of the multi-pass transmembrane proteins CCR5 and CXCR4. To the best of our knowledge, this is the first demonstration of robust expression of unmodified non-erythroid transmembrane proteins on the surface of enucleated RBCs. The described engineering strategies could potentially be applied to any type of transmembrane protein and could be widely applicable to genetically engineering therapeutic RBCs.

HIV-1 pseudovirus entered engineered RBCs more efficiently when CCR5 and CXCR4 were co-expressed with wild-type CD4 rather than chimeric CD4-GpA, thus demonstrating that protein modifications that have been used to enhance RBC surface expression[209,210] can affect the functionality of the therapeutic protein. A lack of co-localization of CD4-GpA and co-receptors could be the cause of the low entry rates, as CD4 and CCR5 have been shown to co-localize in lipid raft

microdomains[162,211] and GpA is not typically associated with lipid rafts[214]. It is also possible that substitution of the membrane-proximal extracellular, transmembrane, or cytoplasmic domains of CD4 interfered with the ability of CD4-GpA to initiate the interaction between HIV-1 Env and co-receptors.

Expression of CD4 or the CD4-GpA fusion protein in the absence of CCR5 was sufficient to potently neutralize HIV-1 in vitro due to formation of high-avidity interactions between clusters of CD4 or CD4-GpA on the RBC surface and trimeric HIV-1 Env spikes on virions. RBC viral traps expressing CD4-GpA also reduced HIV-1 infection rates of CD4+ T-cells, suggesting that viral attachment to RBC viral traps effectively prevents HIV-1 virions from infecting target cells. We previously showed that such high-avidity interactions enhanced the potency of CD4-VLPs by >10,000-fold in comparison to conventional CD4-based inhibitors such as soluble CD4 and CD4-Ig, and that HIV-1 was unable to escape against CD4-VLPs in vitro[187]. In contrast to CD4-VLPs that have short in vivo half-lives, RBC viral traps could persist in vivo for months, implying the RBC approach has the potential to provide sustained control of HIV-1 infection. RBC viral traps neutralized HIV-1 in vitro at 2,500-fold lower concentrations than the concentration of total RBCs in human blood and reduced HIV-1 infection of CD4+ T-cells by 70% at an RBC to T-cell ratio of 5:1. Given that RBCs outnumber CD4+ T-cells by ~5,000:1 in the blood[215] and CD4+ T-cell lines are more permissive than natural CD4+ T-cells[229], these results suggest that therapeutic concentrations of RBC viral traps could be achieved in vivo.

Erythroblast cell lines that stably express therapeutic proteins represent a renewable and more cost-effective source for large-scale manufacturing of genetically-engineered RBCs than CD34+ HSCs. BEL-A cell lines that stably expressed CD4-GpA and ACE2-GpA efficiently differentiated into potent RBC viral traps against HIV-1 and the pandemic SARS-CoV-2 virus, respectively, suggesting that RBC viral traps could be effective treatments against a diverse range of viruses. RBC viral traps could become a rapid-response treatment strategy for future viral outbreaks, as erythroblast cell lines could be rapidly developed once a host receptor for a pandemic virus has been identified.

In vivo studies will be required to evaluate the safety and efficacy of RBC viral traps and a number of potential issues need to be addressed. First, it has been shown that reticulocytes generated by in vitro differentiation mature in vivo into biconcave erythrocytes[230], but it needs to be determined if surface expression of viral receptors is affected by this final maturation step in vivo. Second, the half-life of genetically-modified RBCs expressing chimeric VHH-GpA/Kell proteins was comparable to control RBCs following intravenous injection in mice[210], but it is possible that surface expression of viral receptors would shorten the half-life of RBC viral traps. Third, in the case of CD4 presentation on RBCs, unintended interactions with antigen-presenting cells could have negative implications for the immune system. Fourth, surface presentation of antigens on RBCs has been shown to induce antigen-specific immune tolerance[231,232], so it needs to be investigated if attachment of viruses to RBC viral traps has detrimental effects on anti-viral

immune responses. In vivo experiments could address these questions and also elucidate if entrapment of HIV-1 through co-expression of CCR5 has beneficial effects for viral control and if entrapped viruses could still infect macrophages following phagocytosis of RBC viral traps. Finally, the ability of genetically-engineered RBCs to remove circulating viruses and other pathological agents needs to be compared to other approaches such as nanoparticles coated with cellular membrane[233] and RBCs modified through conventional techniques[226,228,234,235].

Methods

In vitro CD34+ HSC differentiation

Human cord blood or mobilized peripheral blood CD34+ HSCs (StemCell Technologies) were differentiated into enucleated RBCs using a modified version of a previously-described protocol[210]. Briefly, CD34+ HSCs were cultured in expansion medium (100 ng/mL rhFlt3, 100 ng/mL rhSCF, 20 ng/mL rhIL-6, 20 ng/mL rhIL-3, and 100 nM dexamethasone in StemSpan II medium) at a density of 10^5 cells/mL for 4 days. Cells were then placed in differentiation 1-2 medium (2% human AB plasma, 3% human AB serum, 3 U/mL heparin, 10 ng/mL rhSCF, 1 ng/mL rhIL-3, and 3 U/mL erythropoietin in StemSpan II medium) at a density of 10^5 cells/mL for 3 days and at 2 x 10^5 cells/mL for an additional 3 days. The cells were then passaged into differentiation 3 medium (2% human AB plasma, 3% human AB serum, 3 U/mL heparin, 10 ng/mL rhSCF, and 1 U/mL erythropoietin in StemSpan II medium) at a density of 2 x 10^5 cells/mL for 4 days. To induce RBC

maturation, cells were cultured in differentiation 4 medium (2% human AB plasma, 3% human AB serum, 3 U/mL heparin, 0.1 U/mL erythropoietin, and 200 μg/mL holo-transferrin in StemSpan II medium) at a density of 10^6 cells/mL for 4 days, and in differentiation 5 medium (2% human AB plasma, 3% human AB serum, 3 U/mL heparin, and 200 μg/mL holo-transferrin in StemSpan II medium) at a density of 5 x 10^6 cells/mL for an additional 3 days. For morphological analysis, cells were spun onto glass slides by cytocentrifugation, stained with May-Grünwald-Giemsa reagents (Sigma-Aldrich), and examined under an LSM800 laser scanning confocal microscope (Zeiss).

Transgenes and codon optimization

Human CD4, CCR5, CXCR4, ACE2, and glycophorin A (GpA) cDNA sequences were obtained from the National Center for Biotechnology Information. The CD4-GpA fusion construct encoded the CD4 signal peptide and D1D2 domains fused to the N-terminus of GpA with a 9-residue linker (Glu-Pro-Lys-Thr-Pro-Lys-Pro-Gln-Pro). The ACE2-GpA fusion protein construct encoded the extracellular domain of human ACE2 (residues 1-614) fused to the N-terminus of GpA with the 9-residue linker. Transgenes were cloned into the lentiviral backbone plasmids pHAGE-IRES-ZsGreen (PlasmID Repository, Harvard Medical School) for expression under ubiquitous promoters (CMV, EF1α, UBC, and CASI promoters) and pCCL-FB^{212} (provided by Dr. Donald Kohn, UCLA) for erythroid-

specific expression. Codon optimization of transgene cDNA sequences was performed using the GeneArt GeneOptimizer software (Thermo Fisher Scientific).

Lentiviral transduction

VSV-G-pseudotyped lentiviral vectors were produced by co-transfecting HEK293T cells with lentiviral backbone plasmids and packaging plasmids (pHDM-Hgpm2, pHDM-tat1b, pRC/CMV-rev1b, pHDM-G) using Fugene HD (Promega) according to the manufacturer's protocol. Supernatants were collected after 48 and 72 hours, and lentiviral vectors were concentrated 50-fold using Lenti-X concentrator solution (Takara) according to the manufacturer's protocol. On day 10 of the differentiation protocol, erythroid progenitor cells were seeded at a density of 10^6 cells/mL in 12-well plates in the presence of 10 μg/mL polybrene. 20 μL of concentrated lentiviral vector was added per well and plates were spun for 1.5 hours at 850 x g at 30°C. Plates were then incubated for 3 hours at 37°C before passaging the transduced cells into differentiation 3 medium. For cells that were co-transduced to express two transgenes, 20 μL of each lentiviral vector was added per well. To generate large numbers of engineered RBCs for neutralization assays, two transductions steps were performed on days 10 and 14 of the differentiation protocol.

Flow cytometry

Transgene expression and RBC maturation efficiency were analyzed by flow cytometry (MACSQuant, Miltenyi Biotec). 2-3 x 10^5 cells were collected for each condition and samples were stained with the following antibodies: APC-conjugated anti-human CD4 (Invitrogen), FITC-conjugated anti-human CD4 (BD Bioscience), FITC-conjugated anti-human CCR5 (BioLegend), PE-conjugated anti-human CXCR4 (Invitrogen), FITC-conjugated anti-human ACE2 (R&D Systems), APC-conjugated anti-CD235ab (BioLegend), and Brilliant Violet 421-conjugated anti-human CD71 (BioLegend). The percentage of enucleated RBCs was measured by double staining cells with APC-conjugated anti-CD235ab and the nuclear stain Hoechst (Thermo Fisher Scientific). Enucleated RBCs were defined as CD235ab+/Hoechst- cells. The percentage of enucleated RBCs that expressed transgenes was measured by triple-staining cells with APC-conjugated anti-human CD4, FITC-conjugated anti-human CCR5, and Hoechst nuclear stain.

β-lactamase fusion assay

The ability of engineered RBCs to be infected by HIV-1 was evaluated using a modified version of the β-lactamase (BlaM) assay[213]. R5-tropic HIV-1_{YU2} and X4-tropic HIV-1_{HxBc2} pseudovirus were produced by co-transfecting a confluent T75 flask of HEK293T cells with the PSG3ΔEnv backbone plasmid (8 μg), the YU2 or HxBc2 Env expression plasmid (4 μg), and a plasmid expressing a BlaM-Vpr fusion protein[236] (4 μg; provided by Dr. Wesley Sundquist, University

of Utah). The supernatant was collected after 72 hours and concentrated by centrifugal filtration. 5 x 10^4 RBCs were seeded in 100 µL differentiation 5 medium in 96-well plates in the presence of 10 µg/mL polybrene. 20 µL of concentrated YU2-BlaM-Vpr or HxBc2-BlaM-Vpr pseudovirus were added and plates were spun at 1,000 x g for 1 hour at 30°C. Plates were then incubated at 37°C overnight. On the next day, freshly prepared 6X CCF2-AM labeling solution was added, and cells were stained for 2 hours at room temperature in the dark. After two washes with PBS, the cells were analyzed by flow cytometry (MACSQuant, Miltenyi Biotec).

HIV-1 neutralization assays

The ability of engineered RBCs to inhibit HIV-1 infection of target cells was tested by using a modified version of the HIV-1 pseudovirus-based TZM-bl assay[149]. Briefly, serial dilutions of control and engineered RBCs were seeded in 400 µL TZM-bl media in 48-well plates and incubated with 0.4 µL HIV-1_{YU2} pseudovirus ($TCID_{50}$ = 3.2 x 10^5 IU/mL) for 4 hours on an orbital shaker (400 rpm) at 37°C in the presence of 10 µg/mL of polybrene. Cells were then spun down at 500 x g for 10 min and 155 µL of the supernatants were transferred to 96-well plates. TZM-bl reporter cells (NIH AIDS Reagents Program) were added, and luminescence was measured after 48 hours.

Rev-A3R5 CD4+ T-cell infection assay

To test whether RBC viral traps can prevent infection of HIV-1 target cells, 10^5 Rev-A3R5 CD4+ T-cells[159] were incubated in 48-well plates with 0.4-μL HIV-1_{YU2} pseudovirus ($TCID_{50}$ = $3.2x10^5$ IU/mL) in 400-μL TZM-bl media in the presence of 10 μg/mL of polybrene. Control RBCs and CD4-GpA-RBCs were added at RBC:CD4+ T-cell ratios of 2:1 ($2x10^5$ RBCs) or 5:1 ($5x10^5$ RBCs), respectively. Cultures were incubated for 12 hours on an orbital shaker (400 rpm) at 37°C overnight. Cells were then spun down at 500 x g for 10 min, virus-containing supernatants were removed, and the cells were re-suspended in 400 μL Rev-A3R5 growth media (RPMI-1640 media supplemented with 10% FBS, 1% Pen-Strep, 1% L-Glutamine, 1 mg/mL Geneticin, and 1 μg/mL Puromycin) to allow outgrowth of CD4+ T-cells. After 36 hours, luminescence was measured for each sample in duplicates and infection rates were calculated as a function of the reduction in average luminescence compared to the control infection of Rev-A3R5 CD4+ T-cells in the absence of RBCs.

SARS-CoV-2 neutralization assays

Lentivirus-based SARS-CoV-2 pseudovirus was generated by transfecting HEK293T cells with a luciferase-expressing lentiviral backbone plasmid, accessory plasmids (pHDM-Hgpm2, pHDM-tat1b, pRC/CMV-rev1b), and a plasmid encoding the SARS-CoV-2 Spike protein with a 21-residue cytoplasmic tail deletion (Wuhan Hu-1 strain; GenBank NC_045512). The neutralization activity of

ACE2-GpA RBCs was measured using a modified version of a recently-reported protocol[219]. 1.25 x 10^4 293T-ACE2 cells (provided by Dr. Jesse Bloom, Fred Hutchinson Cancer Research Center) were seeded per well on poly-L-Lysine-coated 96-well plates (Corning) 18 hours before infection. Serial dilutions of control and ACE2-GpA-RBCs were seeded in 400 µL media (DMEM supplemented with 10% FBS and Pen-Strep) and incubated with 3 µL of lentiviral particles pseudotyped with the SARS-CoV-2 Spike protein ($5.5x10^7$ RLU/mL) for 4 hours on an orbital shaker (400 rpm) at 37°C in the presence of 10 µg/mL of polybrene. The lentiviral backbone of this SARS-CoV-2 pseudovirus system expresses luciferase to enable detection of infected cells. RBCs were spun down at 500 x g for 10 min and 100 µL supernatant was transferred to the 96-well plate with the seeded 293T-ACE2 cells. Luminescence was measured after 48 hours using a plate reader (Tecan).

Generation of stable erythroblast cell lines

Immortalized BEL-A erythroblast cells[216] (provided by Dr. Jan Frayne, University of Bristol) were transduced with VSV-G–pseudotyped lentiviral vectors carrying the CD4-GpA or ACE2-GpA transgenes in the erythroid-specific pCCL-FB expression cassette. To allow positive selection of cells that stably expressed the transgenes, the puromycin-N-acetyltransferase gene was added downstream of the transgene and a P2A cleavage peptide[237]. Stable BEL-A / CD4-GpA and BEL-A / ACE2-GpA cell lines were generated by growing the transduced cells in

expansion media (50 ng/mL rhSCF, 3 U/mL erythropoietin, 1 μM dexamethasone, and 1 μg/mL doxycycline in StemSpan II medium) in the presence of 0.25 μg/mL puromycin for 3-4 weeks. Differentiation of BEL-A cells was initiated as described[216] by transferring the cells into primary media (3% human AB serum, 2% FBS, 3 U/mL heparin, 10 ng/mL rhSCF, 1 ng/mL rhIL-3, 3 U/mL erythropoietin, 200 μg/mL holo-transferrin, and 1 μg/mL doxycycline in StemSpan II medium) for 3-4 days at a density of 2 x 10^5 cells/mL. To induce RBC maturation, cells were moved into tertiary media (3% human AB serum, 2% FBS, 3 U/mL heparin, 3 U/mL erythropoietin, 500 μg/mL holo-transferrin, and 1 U/mL Pen-Strep in StemSpan II medium) for 4 days at a density of 1 x 10^6 cells/mL.

Fluorescence-activated cell sorting (FACS)

Enucleated RBCs were purified by FACS on day 7 of the BEL-A differentiation protocol. Brilliant Violet 421-conjugated anti-human CD71 antibody (BioLegend) and the nuclear stain DRAQ5 (Abcam) were diluted 1:100 and 1:1,000 in PBS+ (PBS supplemented with 2% FBS). Cells were stained at a concentration of 2.5 x 10^7 cells/mL for 30 min at room temperature in the dark. After two washes in PBS+, cells were resuspended in PBS+ at a concentration of 1 x 10^7 cells/mL. Enucleated RBCs were defined as CD71+/DRAQ5- cells and this cell population was purified using a SONY SH800 cell sorter (Sony Biotechnology).

Acknowledgements

We thank N.J. Huang, N. Pishesha, and H.F. Lodish for helpful discussion, advice, and reagents; P.N.P., Gnanapragasam and L.M. Kakutani for producing SARS-CoV-2 pseudovirus and setting up the SARS-CoV-2 pseudovirus neutralization assay in our laboratory; G.L. Chadwick, R. Galimidi, and A. Moradian (formerly Caltech Proteome Exploration Laboratory) for helpful discussions and reagents; G. Spigolon for guidance with light microscopy performed at the Beckman Institute Biological Imaging Facility; Z. Romero-Garcia and D.B. Kohn for the pCCL-AS3-FB plasmid; J. Voetteler and W.I. Sundquist for the CCF2-AM reagent; J.D. Bloom for 293T-ACE2 cells and plasmids for generating SARS-CoV-2 pseudovirus; and the NIH AIDS Reagent Program for reagents. BEL-A2 cell lines were created by Professor Jan Frayne, Professor David Anstee, and Dr. Kongtana Trakarnsanga with funding from the Wellcome Trust (grant numbers 087430/Z/08 and 102610), NHS Blood and Transplant and Department of Health (England) and were kindly provided by J. Frayne. This work was supported by the Bill and Melinda Gates Foundation grant OPP1202246, the DeLogi Trust (facilitated by Caltech), and by a generous gift from Kairos Ventures (facilitated by Caltech).

Author Contributions: M.A.G.H. and P.J.B. designed the research, M.A.G.H. and C.K. performed the research, M.A.G.H. and P.J.B. analyzed data, and M.A.G.H. and P.J.B. wrote the manuscript.

Competing interests: The authors declare no competing interests.

Supplementary information

Fig. S1. Lentiviral vector constructs for engineering RBCs.

Fig. S2. Comparison of HIV-1 receptor expression levels on CD4-CCR5-RBCs and CD4+ T-cells.

Fig. S3. BlaM assay reproducibly shows that HIV-1 enters RBC viral traps.

Fig. S4. Engineered RBCs express CD4 and CXCR4 and can be infected by X4-tropic HIV-1.

Fig. S5. Comparison of expression levels between CD4-RBCs and CD4-GpA-RBCs.

Fig. S6. In vitro differentiation of BEL-A / CD4-GpA cells consistently produces RBC viral traps.

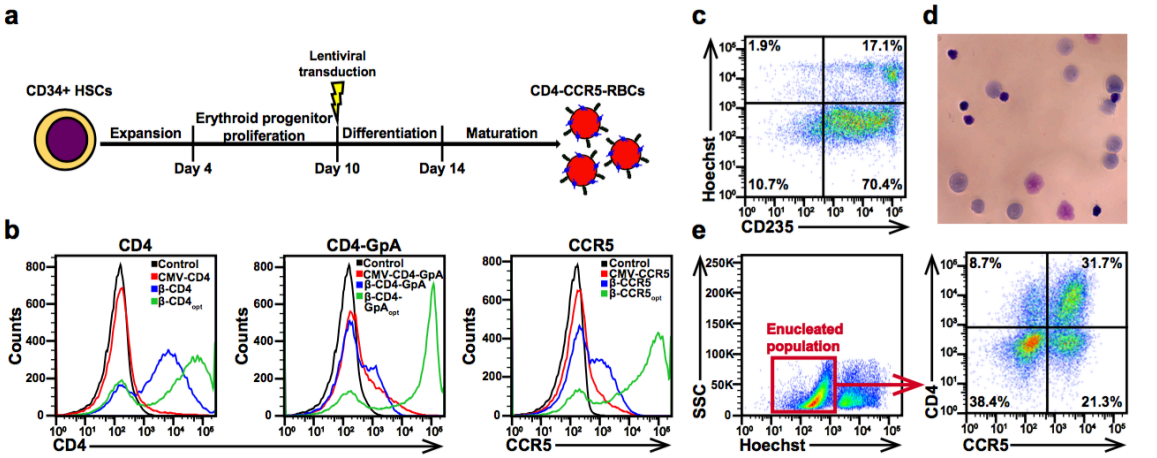

Figure 1. Engineered RBCs express HIV-1 receptors. a) Schematic illustrating the workflow for generating enucleated RBCs expressing HIV-1 receptors. **b)** Flow cytometry analysis of CD4, CD4-GpA, and CCR5 expression on day 13 of differentiation comparing the CMV promoter (red), the β-globin promoter (blue), and the β-globin promoter in combination with codon optimization (green). **c**) Quantification of enucleated CD4-CCR5-RBCs by flow cytometry. Enucleated RBCs expressed CD235 and did not stain for the nuclear dye Hoechst. **d**) Image of CD4-CCR5-RBCs after May-Grunwald-Giemsa staining (magnification x63). **e**) CD4 and CCR5 expression on enucleated (Hoechst-negative) RBCs.

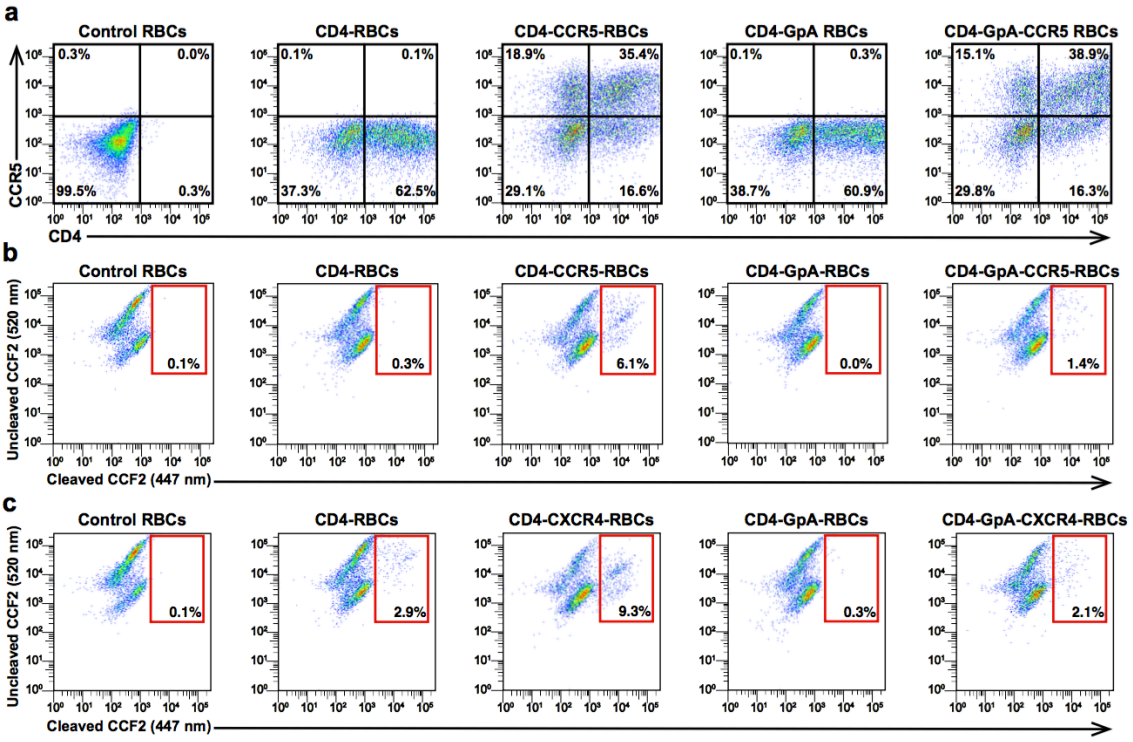

Figure 2. HIV-1 efficiently enters RBC viral traps. **a**) Flow cytometry measurement of CD4 and CCR5 expression at the end of differentiation for control RBCs, CD4-RBCs, CD4-CCR5-RBCs, CD4-GpA-RBCs, and CD4-GpA-CCR5-RBCs. **b-c**, Flow cytometry analysis of HIV-1 infection of engineered RBCs after overnight incubation with a **b**) CCR5-tropic HIV-1_{YU2} or **c**) CXCR4-tropic HIV-1_{HxBc2} pseudovirus carrying a Vpr-BlaM fusion protein. BlaM cleaves the FRET substrate CCF2-AM in infected cells resulting in a shift of its emission spectrum from green (520 nm) to blue (447 nm).

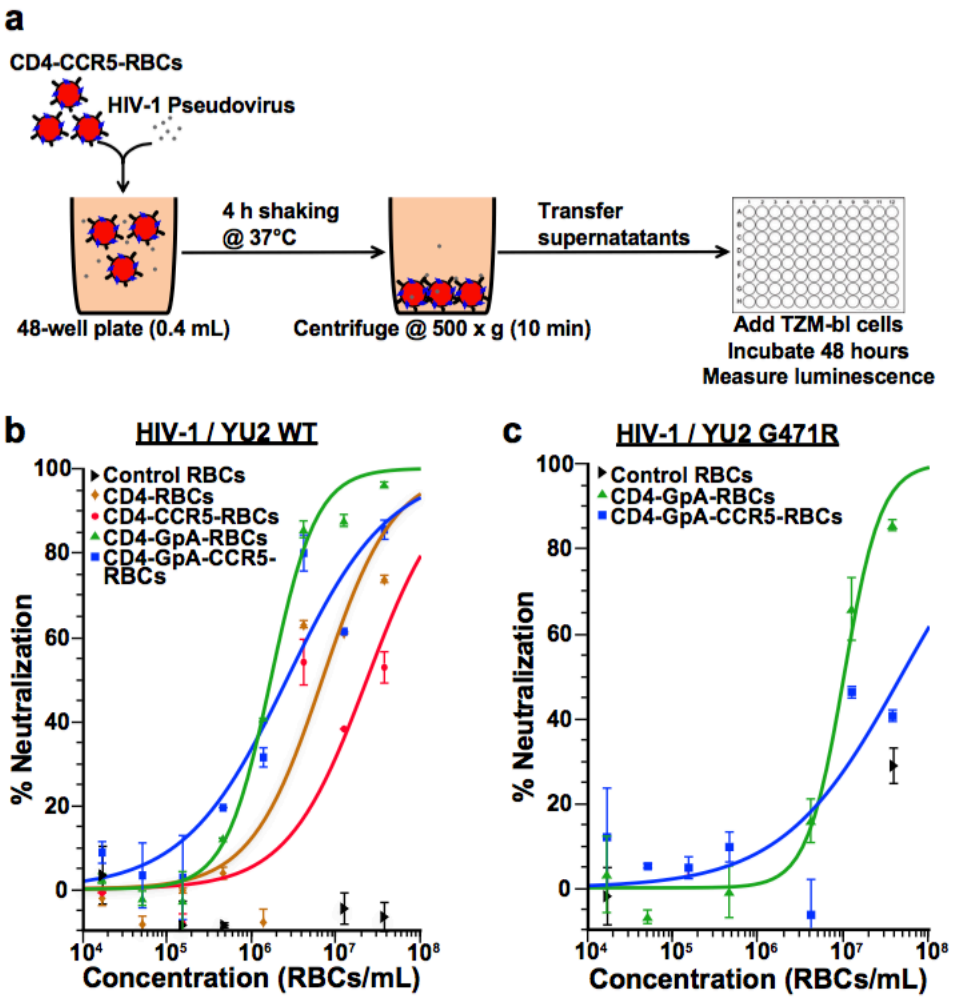

Figure 3. RBC viral traps potently neutralize HIV-1 in vitro. a) Schematic illustrating the workflow for the modified neutralization assay used to evaluate the neutralization activity of engineered RBC viral traps. **b**) In vitro neutralization assay against HIV-1_{YU2} pseudovirus comparing control RBCs (black), CD4-RBCs (brown), CD4-CCR5-RBCs (red), CD4-GpA-RBCs (green), and CD4-GpA-CCR5-RBCs (blue). Data points are the mean and SD of duplicate measurements. **c**) In vitro neutralization assay against mutant HIV-1_{YU2} Env G471R pseudovirus comparing

control RBCs (black), CD4-GpA-RBCs (green), and CD4-GpA-CCR5-RBCs (blue). Data points are the mean and SD of duplicate measurements.

	IC_{50} (x 10^6 RBCs/mL)				
Engineered RBCs	**Assay 1**	**Assay 2**	**Assay 3**	**Average**	**SD**
Control RBCs	ND	ND	ND	ND	ND
CD4-RBCs	7.8	3.3	6.9	6.0	2.2
CD4-CCR5-RBCs	19	5.9	23	16	8.9
CD4-GpA-RBCs	3.0	0.9	1.7	1.9	1.1
CD4-GpA-CCR5-RBCs	3.8	1.4	2.6	2.6	1.2

Table 1. Neutralization potencies of RBC viral traps. IC_{50}s from three independent in vitro neutralization assays from three independent in vitro RBC differentiations are shown as x10^6 RBCs/mL for control RBCs, CD4-RBCs, CD4-CCR5-RBCs, CD4-GpA-RBCs, and CD4-GpA-CCR5-RBCs. Arithmetic mean IC_{50}s and standard deviations (SD) derived from the three experiments are shown.

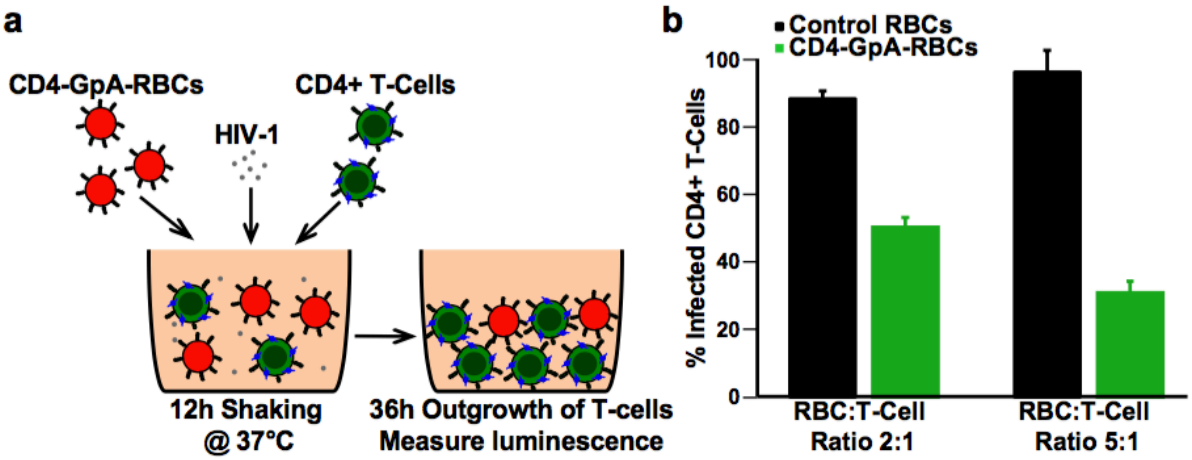

Figure 4. RBC viral traps prevent infection of CD4+ T-cells in vitro. a) Schematic illustrating the workflow for co-incubation of CD4-GpA-RBCs, Rev-A3R5 CD4+ T-cells, and HIV-1_{YU2} pseudovirus to assess the ability of RBC viral traps to prevent infection of HIV-1 target cells in vitro. **b**) Bar chart comparing the ability of control RBCs (black) and CD4-GpA-RBCs (green) to reduce the infection rate of Rev-A3R5 CD4+ T-cells at RBC:T-cell ratios or 2:1 (left) and 5:1 (right), respectively.

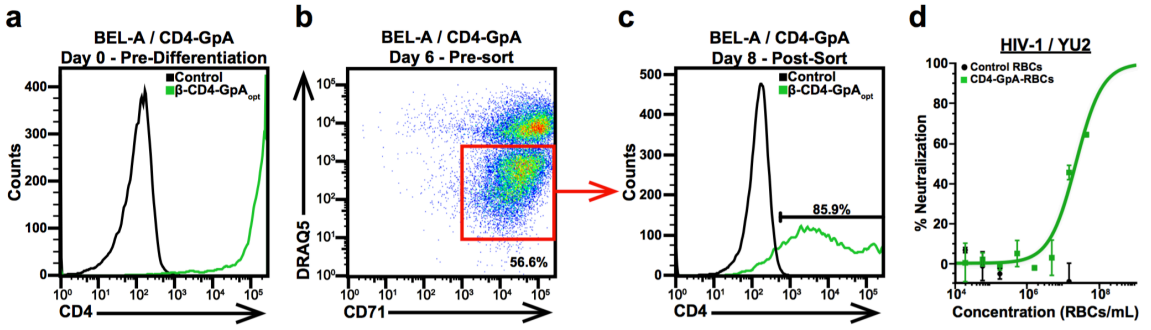

Figure 5. BEL-A erythroblast cell lines stably express CD4-GpA to produce potent RBC viral traps against HIV-1. a) Flow cytometry measurement of CD4-GpA expression on BEL-A / CD4-GpA cells pre-differentiation. **b**) Flow cytometry analysis of enucleated CD4-GpA-RBCs on day 6 of differentiation. Enucleated RBCs expressed CD71 and did not stain for the nuclear dye DRAQ5. **c**) Flow cytometry analysis of CD4-GpA expression on CD71+/DRAQ5- BEL-A / CD4-GpA cells post-sorting on day 8 of differentiation. **d**) In vitro neutralization assay against HIV-1_{YU2} pseudovirus comparing control RBCs (black) and CD4-GpA-RBCs (green). Data points are the mean and SD of duplicate measurements.

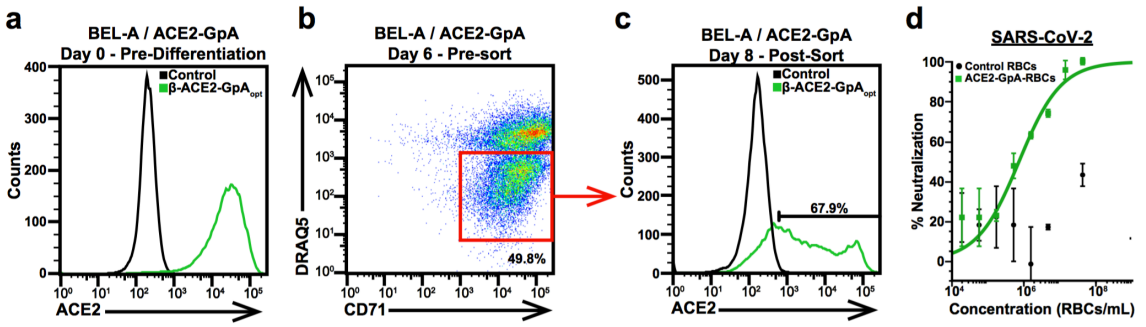

Figure 6. BEL-A erythroblast cell lines stably express ACE2-GpA to produce potent RBC viral traps against SARS-CoV-2. a) Flow cytometry analysis of ACE2-GpA expression on BEL-A / ACE2-GpA cells pre-differentiation. **b**) Flow cytometry analysis of enucleated ACE2-GpA-RBCs on day 6 of differentiation. Enucleated RBCs expressed CD71 and did not stain for the nuclear dye DRAQ5. **c**) Flow cytometry measurement of ACE2-GpA expression on CD71+/DRAQ5- BEL-A / ACE2-GpA cells post-sorting on day 8 of differentiation. **d**) In vitro neutralization assay against lentivirus-based SARS-CoV-2 pseudovirus comparing control RBCs (black) and ACE2-GpA-RBCs (green). Data points are the mean and SD of duplicate measurements.

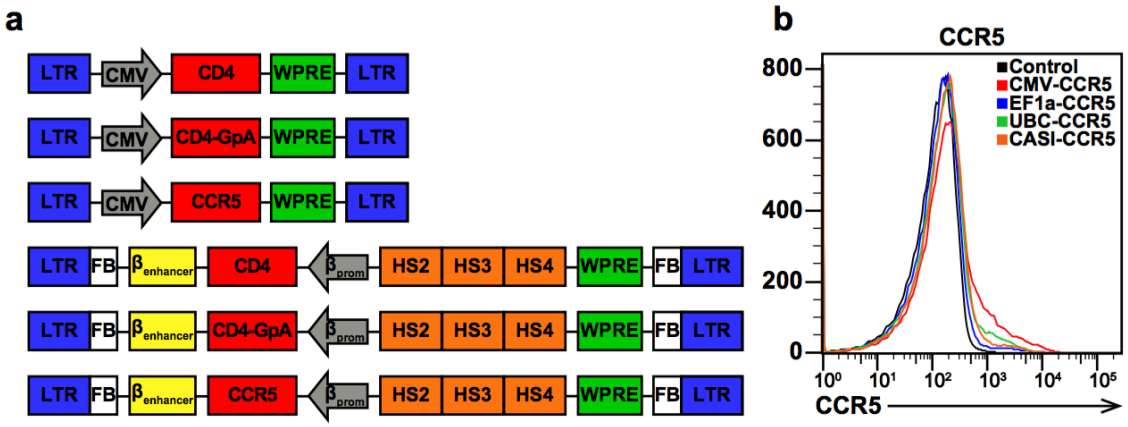

Figure S1. Lentiviral vector constructs for engineering RBCs. a) Schematic of pHAGE-based and pCCL-FB-based lentiviral vector constructs used for the delivery of CD4, CD4-GpA, and CCR5 transgenes. **b**) Comparison of ubiquitous CMV, EF1-α, UBC, and CASI promoters for the expression of CCR5 in erythroid progenitor cells on day 13 of differentiation.

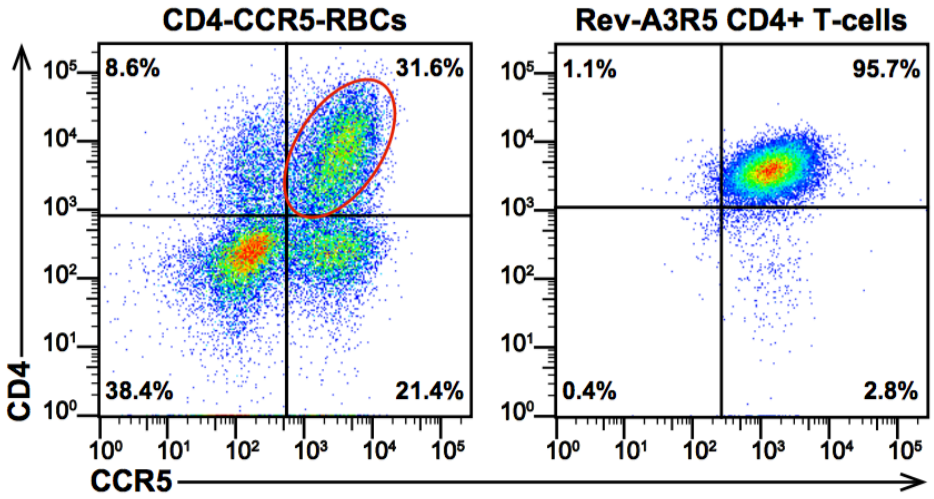

Figure S2. Comparison of HIV-1 receptor expression levels on CD4-CCR5-RBCs and CD4+ T-cells. Flow cytometry analysis of CD4 and CCR5 expression on enucleated CD4-CCR5-RBCs and Rev-A3R5 CD4+ T-cells.

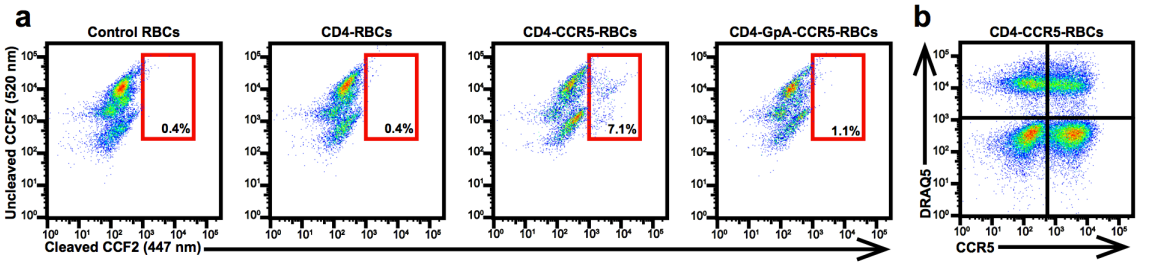

Figure S3. BlaM assay reproducibly shows that HIV-1 enters RBC viral traps.

a) Flow cytometry analysis of HIV-1 infection of engineered RBCs after overnight incubation with a CCR5-tropic HIV-1_{YU2} pseudovirus carrying a Vpr-BlaM fusion protein. These results represent an independent biological replicate of the experiment shown in Fig. 2b using engineered RBCs from a different in vitro differentiation culture. **b**) Comparison of CCR5 expression on enucleated (DRAQ5-) and nucleated (DRAQ5+) CD4-CCR5-RBCs.

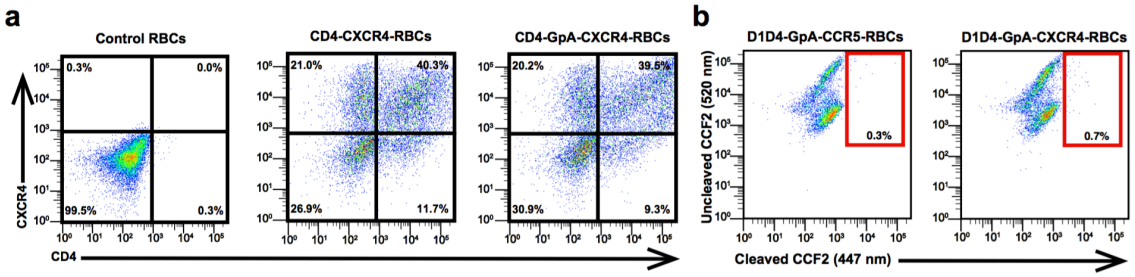

Figure S4. Engineered RBCs express CD4 and CXCR4 and can be infected by X4-tropic HIV-1. a) Flow cytometry measurement of CD4 and CXCR4 expression at the end of differentiation for control RBCs, CD4-CXCR4-RBCs, and CD4-GpA-CXCR4-RBCs. **b**) Flow cytometry analysis of HIV-1 infection of RBCs expressing a chimeric D1D4-GpA fusion protein that contained the CD4 D1D4 domains to evaluate if addition of the CD4 D3D4 domains enhanced infection. BlaM assays were performed with R5-tropic HIV-1_{YU2} and X4-tropic HIV-1_{HxBc2} pseudovirus on D1D4-GpA-CCR5-RBCs (left) and D1D4-GpA-CXCR4-RBCs (right), respectively.

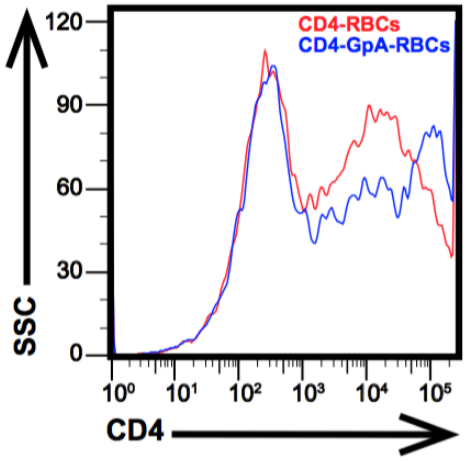

Figure S5. Comparison of expression levels between CD4-RBCs and CD4-GpA-RBCs. Flow cytometry analysis of CD4 and CD4-GpA expression levels on CD4-RBCs and CD4-GpA-RBCs, respectively, at the end of differentiation.

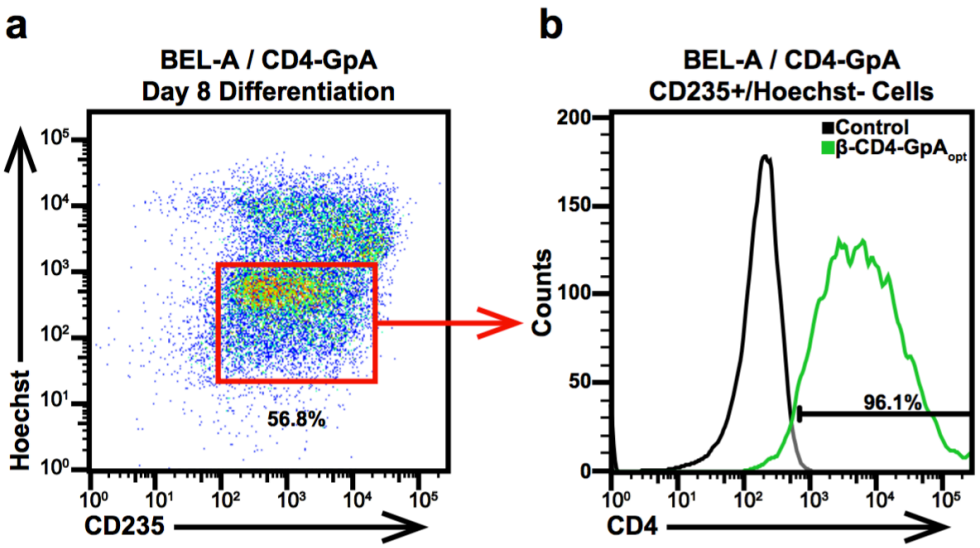

Figure S6. In vitro differentiation of BEL-A / CD4-GpA cells consistently produces RBC viral traps. a) Flow cytometry analysis of enucleated CD4-GpA-RBCs on day 8 of in vitro differentiation. Enucleated RBCs expressed CD235 and did not stain for the nuclear dye Hoechst. **b**) Flow cytometry analysis of CD4-GpA expression on CD235+/Hoechst- BEL-A / CD4-GpA cells. These results represent an independent biological replicate of the experiment shown in Fig. 5.

Chapter 5

SELF-ASSEMBLING VIRAL SPIKE-EBRNANOPARTICLES AS A VACCINE PLATFORM TECHNOLOGY

Abstract

The COVID-19 pandemic represents the 3rd outbreak caused by zoonotic transmission of a beta-coronavirus (beta-CoV) in the last 20 years. Hence there is an urgent need for new vaccine strategies to control the ongoing pandemic and prevent future CoV outbreaks. mRNA vaccines have emerged as an ideal platform for the development of rapid-response vaccines, but clinical studies have shown that neutralizing antibody titers elicited by mRNA vaccines are ~10-fold lower than titers elicited by protein nanoparticle (NP) vaccines. This is a concern with regards to the emergence of SARS-CoV-2 variants of concern (VOCs) that are less sensitive to vaccine-induced antibodies. In addition, less than 25% of the world population is fully vaccinated. Thus, rapid-response vaccine technologies are needed that elicit potent antibody responses with a single injection and/or lower doses, to ensure lasting protection against VOCs, reduce costs, and accelerate global distribution. Moreover, prevention of future CoV pandemics requires the development of a universal CoV vaccine that elicits cross-reactive immune responses against a broad spectrum of CoV strains by focusing responses to conserved epitopes. The scope of the proposed research is to design and evaluate new vaccine strategies to enhance the potency of mRNA-based rapid-response vaccines and facilitate universal CoV vaccine development. The proposal is based on the EBR NP technology, which modifies membrane proteins such as CoV spike (S) proteins to self-assemble into virus-resembling NPs that bud from the cell surface. NP assembly is induced by inserting a short amino acid sequence into the

cytoplasmic tail designed to recruit proteins from the endosomal sorting complex required for transport (ESCRT) pathway. Initial studies in mice showed that low-dose injections of EBR NPs presenting the SARS-CoV-2 S protein elicited 10-fold higher neutralizing antibody titers than soluble S protein and protein-based NPs that displayed the receptor-binding domain (RBD) of the S protein. The EBR NP technology will be applied to accomplish three goals: i) Design a hybrid mRNA vaccine encoding the modified SARS-CoV-2 S-EBR construct that would be expressed at the cell surface and self-assemble into virus-resembling NPs to elicit more potent antibody responses than the approved Pfizer/Moderna vaccines, while retaining the manufacturing properties and T-cell activation of mRNA vaccines. ii) Engineer S-EBR NPs to package and deliver S or S-EBR mRNA vaccines as an alternative to lipid NPs. This delivery approach would enhance mRNA vaccine potency as S proteins presented on S-EBR NPs induce potent antibody responses, facilitate efficient intracellular delivery, and target mRNA vaccines to tissues that are naturally infected by SARS-CoV-2 to induce local immune responses. iii) Design and evaluate mosaic S-EBR NP-based universal CoV vaccine candidates that present full-length membrane-associated S proteins from multiple CoV strains to elicit cross-reactive immune responses against a broad spectrum of CoVs and protect against future outbreaks. The proposed vaccine strategies could have direct impact on the COVID-19 global health crisis and advance our emergency preparedness for the next pandemic.

This chapter was adapted from my application for the NIH Director's Early Independence Award and our provisional patent application for the EBR NP technology:

Hoffmann MAG, Bjorkman PJ (2021). Self-assembling viral spike-EBR nanoparticles as a vaccine platform technology. *US Patent Application No. 63/208,889. US Patent and Trademark Office.*

Research challenge

The ongoing COVID-19 pandemic has caused over 200 million infections and 4 million deaths worldwide[238] and represents the third outbreak triggered by zoonotic transmission of a beta-CoV in the last two decades. The causative agent of COVID-19 is SARS-CoV-2, which is related to SARS-CoV and Middle East Respiratory Syndrome coronavirus (MERS-CoV), the CoVs responsible for the outbreaks in 2002 and 2012, respectively[239]. While the origin of SARS-CoV-2 is still being investigated, bats have been identified as the natural reservoir for SARS-CoV and MERS-CoV, and human transmission required intermediate hosts such as civets and camels[240]. Various CoV strains are known to cause disease in other animal species[241] and a small number of mutations might be sufficient to enable human transmission posing a risk for future CoV outbreaks[242]. Once a zoonotic CoV strain has spilled over to humans, the virus will continue to evolve leading to the emergence of new variants that could become resistant to vaccines and therapeutics, a major concern for a number of recently-identified SARS-CoV-2 VOCs[243,244]. Two types of vaccine strategies could protect against emerging SARS-CoV-2 VOCs and prevent future CoV pandemics: i) rapid-response vaccines and ii) universal CoV vaccines.

Rapid-response vaccines

These vaccines could be rapidly developed once human transmission of a zoonotic CoV has been detected and would be specific to the newly-identified CoV strain. This type of vaccine requires a technology that enables fast, scalable, and adaptable production to ensure rapid global distribution. During the COVID-19

pandemic, mRNA vaccines have emerged as an ideal platform for rapid-response vaccine development[245]. The mRNA vaccines produced by Pfizer and Moderna encode the SARS-CoV-2 S protein, the main target of antibody responses during natural infections[246]. Clinical studies demonstrated that mRNA vaccines are highly effective, preventing >90% of symptomatic and severe SARS-CoV-2 infections[247,248]. However, pre-clinical and clinical studies have shown that neutralizing antibody titers elicited by mRNA vaccines[245,249] are ~10-fold lower than titers elicited by protein NP-based vaccines[250,251]. This is concerning with regards to the emergence of SARS-CoV-2 VOCs that have been shown to be ~5-fold less sensitive to antibodies elicited by mRNA vaccines[252-254]. Thus, vaccinated individuals may need additional doses to ensure lasting protection.

It is even more alarming that less than 25% of the world population are fully vaccinated and only 1.3% of people in low-income countries have received at least one dose[255]. Faster production and global distribution could be achieved by increasing the potency of rapid-response vaccines. More potent vaccines could elicit protective immune responses with lower doses and/or even just a single injection, resulting in reduced costs and accelerated large-scale manufacturing of vaccine doses. Thus, potent vaccine technologies are needed that elicit higher neutralizing antibody responses at lower doses to ensure lasting protection against viral escape variants and expedite global vaccine distribution during the ongoing and future CoV pandemics.

Universal CoV vaccine

The aim of a universal CoV vaccine is to confer broad immunity against a wide range of CoV strains before human transmission occurred. Broad immunity could be achieved by guiding the immune response to epitopes that are conserved among CoVs. Even weak immune responses elicited by a universal CoV vaccine could be sufficient to prevent severe infections and rapid spread following future zoonotic transmission events. It has been suggested that cross-reactive B-cells that recognize conserved epitopes could preferentially be activated through avidity effects by mosaic protein NPs that present multiple forms of a variable antigen[256]. Recent studies demonstrated that mosaic NPs presenting RBDs, the part of the S protein that interacts with host receptors to enter cells, from eight different SARS-like beta-CoV strains elicited heterologous antibody responses against beta-CoV strains that were not displayed on the mosaic NP[257,258]. However, this strategy is likely limited to closely-related strains as the RBD is not widely conserved among CoV families[259]. Universal vaccine strategies that present full-length S proteins from various CoV strains could be more effective as other parts of the S protein, in particular the S2 subunit, are more conserved than the RBD[260]. For instance, cross-reactive antibodies targeting the stem helix in the S2 subunit have been isolated from COVID-19 convalescent individuals[261] and immunized humanized mice[262] and were shown to neutralize a broad spectrum of beta-CoVs.

The production of mosaic NPs presenting full-length S proteins would be difficult to achieve using conventional mosaic NP approaches as they require viral surface proteins to be modified into soluble proteins[256,257]. Full-length CoV S proteins

are membrane proteins, and soluble versions of S protein trimers are unstable in the prefusion conformation in the absence of stabilizing mutations[263], which in our lab's experience, only work for a subset of CoV strains to express stable, soluble S protein trimers. Large-scale expression of eight or more different soluble CoV S proteins to generate mosaic NPs might therefore be unrealistic since effective stabilizing mutations for many CoV S proteins have not been identified. In addition, multiple production steps would be required as all components, including the eight or more CoV S proteins and the NP-assembling proteins need to be individually expressed and purified prior to mosaic NP assembly, followed by a final purification step. Hence NP vaccine technologies are needed that can display a wide range of full-length CoV S proteins without the need for extensive protein engineering and numerous manufacturing steps.

The scope of the proposed research is to design and evaluate new vaccine strategies that have the potential to enhance the potency of mRNA-based rapid-response vaccines and facilitate the development of a universal CoV vaccine. This proposal is based on the EBR NP technology, which modifies membrane proteins such as CoV S proteins to self-assemble into enveloped NPs without the need for additional proteins. For Aims 1 and 2, this technology will be applied to design two hybrid vaccine approaches that combine advantages of mRNA and protein-NP vaccines to produce highly potent rapid-response vaccines. For Aim 3, the EBR NP technology will be used to generate mosaic NPs presenting S proteins from a diverse set of CoV strains and evaluate their ability to elicit cross-reactive immune responses against a broad spectrum of CoVs. These vaccine strategies could enable faster

distribution of rapid-response vaccines and facilitate the development of an effective universal CoV vaccine.

EBR NP technology

Multivalent display of viral surface proteins on NPs is widely known to enhance antibody responses[264]. Conventional protein-NP vaccines require two components: i) the surface protein itself and ii) a structural scaffold protein that self-assembles to form the NP such as the Gag protein from lentiviruses[265]. Here we present a strategy to engineer the surface protein itself to self-assemble into densely-coated NPs without the need for additional proteins. NP assembly is achieved by inserting a short amino acid sequence at the end of the cytoplasmic tail of the surface protein, which recruits host proteins from the endosomal sorting complex required for transport (ESCRT) pathway that has been shown to drive the viral budding process for a number of enveloped viruses[68] (Fig. 1a). The inserted ESCRT binding region (EBR) interacts with the ESCRT proteins TSG101 and ALIX.

We evaluated this technology by fusing the EBR domain to the C-terminus of the SARS-CoV-2 S protein. This version of the S protein contained a D614G mutation that has been shown to increase infectivity of SARS-CoV-2[266]. Two previously described proline substitutions (2P) were introduced into the S2 subunit to stabilize the prefusion conformation[267]. To ensure efficient cell surface

expression, the C-terminal 21 residues were truncated from the cytoplasmic tail of S as it contains an endoplasmic reticulum (ER)-retention signal[268].

Expi293 cells were transiently-transfected to generate S-EBR NPs. After 48 hours, supernatants were collected, and NPs were purified by ultracentrifugation on a 20% sucrose cushion. Cryo-electron tomograms showed that S-EBR NPs are 20-40 nm in diameter and are densely-coated with spikes (Fig. 1b). Western blot analysis demonstrated that purified S-EBR NPs contained >20-fold more S protein than NPs produced by co-expression of S and HIV-1 Gag or S and the SARS-CoV-2 structural proteins, M, N, and E (Fig. 1c), suggesting that S-EBR NPs incorporate S more efficiently than conventional strategies. The EBR domain was >10-fold more effective at generating S-containing NPs than viral ESCRT-interacting proteins such as EIAV p9, EBOV VP40, and HIV-1 p6 (Fig. 1d).

SARS-CoV-2 S-EBR NPs elicit potent neutralizing antibody responses in mice

The efficacy of S-EBR NPs as a vaccine candidate against SARS-CoV-2 was evaluated in C57BL/6 mice. S-EBR NPs were purified by ultracentrifugation on a 20% sucrose cushion followed by size exclusion chromatography. All immunogens were administered by subcutaneous injection in the presence of adjuvant (Sigma adjuvant). A single injection of 0.1 μg of S-EBR NPs elicited robust neutralizing antibody titers against SARS-CoV-2 S, which were similar to titers elicited by SpyCatcher-mi3 NPs that displayed SARS-CoV-2 S-6P (Fig. 2a). In contrast, no neutralizing antibody responses were detected for the soluble S-2P

protein and SpyCatcher-mi3 NPs that displayed the SARS-CoV-2 RBD (Fig. 2a). This dose was 10-50-fold lower than doses used in previous protein-based SARS-CoV-2 immunization studies[250,257], highlighting the high potency of the S-EBR NPs. After the second injection, neutralizing antibody titers increased by >10-fold and were significantly higher than titers measured for soluble S-2P and RBD-mi3 NPs (Fig. 2b). Neutralizing antibody titers were ~10-100-fold higher than titers reported for a SARS-CoV-2 mRNA vaccine in mice[245].

Additional stabilizing proline substitutions[263] were introduced into the S2 subunit to generate S-6P-EBR NPs, which elicited similar antibody responses compared to S-2P-EBR NPs (Fig. 2c). Due to their enhanced stability, purified S-6P-EBR NPs retained their efficacy after storage at 4ºC for 2 months (Fig. 2c). S-2P-EBR NPs elicited similar antibody responses when administered in the presence of Sigma or AddaVax adjuvants (Fig. 2d).

Advantages of the EBR NP technology

Taken together, the EBR NP technology exhibits a number of key advantages over existing vaccine NP approaches that make it ideally suited for the design of rapid-response and universal vaccines against CoVs, as well as potentially other pathogens:

- Conventional approaches to generate enveloped NPs such as co-expression of lentiviral Gag proteins and viral surface proteins result in

inefficient incorporation of surface proteins into NPs as the two proteins do not interact (Fig. 1a). In contrast, the EBR-modified surface protein itself drives NP assembly and is directly incorporated into the NP (Fig. 1a) leading to more efficient production of densely-coated and highly immunogenic NPs (Fig. 1b-d; 2a-d).

- While non-enveloped NP technologies normally require expression and purification of multiple components to generate NPs for vaccine applications[250,269], the EBR NP technology only requires expression of a single component, and the self-assembling NPs can be purified directly from culture supernatants.

- Enveloped EBR NPs are ideally suited for repeated immunizations to focus immune responses to desired epitopes on viral surface proteins, which can be challenging with non-enveloped NP-based vaccines as repeated immunizations elicit off-target immune responses against undesired epitopes such as the NP scaffold[192,270,271].

- A key advantage of the EBR NP technology is that viral surface proteins are maintained in their natural membrane-associated conformation without the need for extensive protein engineering. Other NP technologies require surface proteins to be modified into soluble proteins, which can be unstable and express poorly in the absence of extensive stabilizing mutations[267,272]. As a result, NP-based vaccine approaches against SARS-CoV-2 have focused on displaying the RBD

subunit[250,257,269], which is more stable than the full-length S protein. Although RBD-EBR NPs can also be generated with this technology (Fig. 3a), our in vivo results suggest that the full-length S protein is a more potent immunogen than the RBD (Fig. 2a-b), and other parts of the S protein are more conserved among CoV strains than the RBD[260]. The EBR NP technology is therefore the ideal approach for developing a universal CoV vaccine, and we have already been able to generate S-EBR NPs for a wide range of CoV strains, including the SARS-CoV-2 variant B.1.351 (Fig. 3b), SARS, HKU-1 (Fig. 3c), Rf1, HKU-4 (Fig. 3d), 229E, BtKY72 (Fig. 3e), MERS (Fig. 3f), and NL63 (Fig. 3g). We have also generated two mosaic S-EBR NPs by co-expressing S-EBR constructs from 6 different CoV strains: mosaic NP-1 (SARS, Rf1, BtKY72, HKU-1, HKU-4, 229E) (Fig. 3h) and mosaic NP-2 (SHC014, HKU-3, HKU-5, HKU-8, HKU-24, BM48-31) (Fig. 3i).

- Unlike other NP technologies that require expression and purification of multiple components, the engineered SARS-CoV-2 S-EBR construct could be delivered as an mRNA vaccine as it only requires expression of a single component. In comparison to the SARS-CoV-2 S constructs used in the Pfizer and Moderna vaccines, mRNA-mediated delivery of the S-EBR construct could greatly enhance activation of B-cells, because S-EBR proteins will be expressed at the cell surface and self-assemble into S-EBR NPs that bud from the plasma membrane.

In addition to the development of fast-response and universal vaccines against CoVs, the EBR NP technology could also be applicable to the design of protein- and/or nucleic acid-based vaccines against a wide range of viral pathogens. This includes but is not limited to HIV, influenza, flaviviruses (e.g., zika, dengue, yellow fever, hepatitis C), filoviruses (EBOV, Marburg), and emerging viral pathogens such as Hantavirus and Nipah virus. HIV-1 Env-EBR NPs have already been generated, and the purified Env-EBR NPs contained a greater amount of Env than NPs produced by co-expression of HIV-1 Gag and Env, suggesting that HIV-1 Env was incorporated more efficiently into Env-EBR NPs (Fig. 4). The EBR NP technology could also be used to develop vaccines against non-viral infectious diseases such as malaria and tuberculosis. The potential to incorporate and deliver specific cargoes in EBR NPs could also be an attractive property for therapeutic applications such as targeted drug delivery to cancer or infected cells.

Future directions

Aim 1. Design a hybrid approach between mRNA and protein NP vaccines to enhance the potency of rapid-response vaccines.

In contrast to conventional NP technologies, engineered EBR constructs could be delivered as mRNA vaccines since NP assembly only requires a single genetically-encoded component. In comparison to the SARS-CoV-2 S constructs used in the Pfizer and Moderna vaccines, mRNA-mediated delivery of the S-EBR construct should greatly enhance activation of B-cells, the cells responsible for

secreting antibodies, because S-EBR proteins will be expressed at cell surfaces and would also self-assemble into virus-resembling NPs that are secreted from cells (Fig. 5a-b). Both S and S-EBR mRNAs would be expressed inside host cells and localize to the cell surface, which elicits potent T-cell, but only moderate B-cell, responses, respectively. However, formation and secretion of self-assembling S-EBR NPs by the S-EBR mRNA, but not by the S mRNA, would potentiate B-cell activation because the NPs would widely distribute inside the body to engage a large number of immune cells, thereby more accurately mimicking a natural infection. Increased immune responses could ensure protection against SARS-CoV-2 VOCs and lower vaccine doses might be needed, which would reduce costs and expedite global vaccine distribution.

Proof-of-Concept Studies to Evaluate Hybrid Vaccine Approach

To evaluate the potential of this hybrid vaccine approach, we performed a pilot study in mice. mRNAs encoding the SARS-CoV-2 S and S-EBR constructs were synthesized at the RNA core of the Houston Methodist Research Center and encapsulated using a standard LNP formulation (Precision NanoSystems). Groups of six mice received two intramuscular (IM) injections in weeks 0 and 4 of either 1 μg of the unmodified S mRNA vaccine alone (similar to the Pfizer/Moderna vaccine) or 1 μg of a 1:1 combination of the S and S-EBR mRNAs (0.5 μg S mRNA + 0.5 μg S-EBR mRNA). Due to shortage of reagents, the S-EBR mRNA could not be evaluated on its own in this study, but this condition will be included in the next

experiment. Both mRNA vaccines were compared to 1 μg doses of purified S-EBR NPs (similar to the Novavax vaccine) that were administered subcutaneously in weeks 0 and 4 in the presence of adjuvant (Sigma adjuvant).

Two weeks post-boost injections, we evaluated serum neutralizing antibody responses by in vitro neutralization assays against lentivirus-based S-pseudotyped pseudoviruses for SARS-CoV-2 and the Delta VOC. The conventional S mRNA vaccine elicited neutralizing antibody responses against SARS-CoV-2 and the Delta VOC in only 3 of 6 and 2 of 6 mice, respectively (Fig. 6a-b). In contrast, potent neutralizing antibody responses against SARS-CoV-2 were detected for all mice that received the S + S-EBR mRNA combination vaccine (Fig. 6a). Moreover, 5 of 6 serum samples neutralized the Delta VOC (Fig. 6b). Geometric means for serum half-maximal inhibitory dilutions (ID_{50}s) against SARS-CoV-2 and the Delta VOC were 21- ($p = 0.0577$) and 7-fold higher, respectively, for the S + S-EBR mRNA combination compared to the conventional S mRNA vaccine. Neutralizing antibody titers elicited by the S + S-EBR mRNA combination were comparable to responses observed for the purified S-EBR NPs suggesting that hybrid mRNA vaccines can induce similarly potent antibody responses in the absence of adjuvants. Consistent with previous results from preclinical[245,250] and clinical studies[249,251], neutralizing antibody titers elicited by the conventional S mRNA vaccine (similar to the Pfizer/Moderna vaccine) were 30- ($p < 0.05$) and 9-fold lower than responses induced by purified S-EBR NPs (similar to the Novavax vaccine) against SARS-CoV-2 and the Delta VOC, respectively. Statistical

significance was not achieved for this pilot experiment due to the small group sizes; group sizes will be increased in our follow-up studies.

The results obtained from this proof-of-concept study were promising, suggesting that the proposed hybrid mRNA vaccine approach has the potential to substantially enhance the potency of mRNA vaccines. The potency of S-EBR mRNA vaccines could be further improved as we recently designed optimized EBR sequences that self-assemble ~5-fold more efficiently (data not shown). Future experiments will include the optimized S-EBR mRNA vaccines alone and in combination with the S mRNA, evaluate all mRNA vaccines at various doses, and use larger cohorts of mice. We will also investigate whether hybrid mRNA vaccines induce more potent T-cell responses than conventional mRNA and protein NP vaccines using T cell assays as described[273].

As mRNA synthesis and LNP encapsulation are expensive and time-consuming, we also tested plasmid-based DNA vaccines encoding SARS-CoV-2 S or S-EBR in mice. 10 μg doses of plasmid DNA were administered IM in weeks 0 and 3. The DNA vaccines were compared to 1 μg purified S-EBR NPs that were also injected IM in weeks 0 and 3 in the presence of adjuvant (Addavax). Two weeks post-boost immunizations, serum neutralizing antibody responses were analyzed by in vitro neutralization assays against lentivirus-based S-pseudotyped SARS-CoV-2 pseudovirus. The S-EBR DNA vaccine elicited 9-fold more potent neutralizing antibody titers compared to the S DNA vaccine ($p < 0.05$) (Fig. 6c). Since DNA vaccines are generally less potent than mRNA vaccines, serum

neutralizing antibody responses induced by the S-EBR DNA vaccine were 4-fold lower compared to purified S-EBR NPs (Fig. 6c). Nevertheless, these results provided additional evidence that nucleic acid-based vaccines encoding the self-assembling S-EBR construct elicit significantly more potent neutralizing antibody responses than conventional nucleic acid-based vaccines. This study also demonstrated that the S-EBR construct alone is sufficient to induce enhanced neutralizing antibody responses and does not have to be delivered in combination with the unmodified S construct.

Aim 2. Engineer EBR NPs as an alternative to lipid NPs (LNPs) for efficient, targeted, and cost-effective mRNA vaccine delivery.

The state-of-the-art delivery strategy for mRNA vaccines is to encapsulate mRNAs in LNPs composed of a complex mixture of ionizable lipids, structural helper lipids, cholesterol, and PEGylated lipids[274]. LNPs protect mRNAs from enzymatic degradation in vivo and are rapidly endocytosed to facilitate intracellular delivery[275]. However, endosomal escape is inefficient; it has been estimated that <2% of RNA molecules reach the cytoplasm[275-277]. I propose to develop an alternative mRNA delivery strategy by engineering EBR NPs to specifically interact with and encapsulate mRNA payloads (Fig. 7a). Such protein-RNA interactions can be designed by introducing structural RNA motifs into the 3' untranslated region (UTR) of the mRNA that are specifically recognized by small proteins such as the archaeal ribosomal protein L7Ae[278] or the MS2 bacteriophage

capsid protein (MCP)[279]. Insertion of L7Ae or MCP upstream of the EBR domain would ensure efficient mRNA incorporation into budding EBR NPs (Fig. 7b, left). As a proof-of-concept, we applied this strategy to generate S-L7Ae-EBR NPs that delivered luciferase mRNA to ACE2-expressing target cells. Luciferase expression was comparable to a lentivirus-based S-pseudotyped pseudovirus (Fig. 7c).

EBR NP-mediated delivery of mRNA vaccines has the potential to enhance their potency in multiple ways. First, EBR NPs themselves elicit strong immune responses by displaying the viral surface antigen of interest, e.g., the SARS-CoV-2 S protein (Fig. 7a). Viral surface proteins also enable efficient intracellular mRNA delivery by interacting with host receptors and facilitating endosomal escape. Targeting mRNA vaccine delivery to tissues that express viral host receptors and are naturally infected by the virus might also stimulate local immune responses at mucosal entry sites. Finally, combining strategies from Aims 1 and 2 could maximize the potency of mRNA vaccines potentially leading to substantial dose reductions.

Aim 3. Design and evaluate EBR NP-based universal CoV vaccine candidates.

Another key advantage of the EBR NP technology is that viral surface proteins are maintained in their natural membrane-associated conformation without the need for extensive protein engineering. The EBR technology is therefore the ideal approach for developing a universal CoV vaccine, and I have already generated S-EBR NPs for a wide range of CoV strains including SARS, HKU1,

MERS, and 229E (Fig. 8a). The presentation of full-length S proteins on S-EBR NPs ensures that highly conserved regions in the S2 subunit are displayed to the immune system to potentially elicit cross-reactive antibodies that neutralize a broad spectrum of CoV strains.

In addition, I have generated mosaic S-EBR NPs that displayed S proteins from multiple CoV strains on the same NP by co-expressing S-EBR constructs from 6 different CoV strains, including three beta-CoV strains from the sarbecovirus family (SARS, Rf1, BtKY72), one beta-CoV strain from the embecovirus family (HKU1), one beta-CoV strain from the merbecovirus family (HKU4), and one alpha-CoV strain (229E) (Fig. 8a). Whereas mosaic NP production requires expression and purification of individual components for conventional NP technologies, mosaic S-EBR NPs can be harvested directly from culture supernatants and purified in a single step. Compared to SARS S-EBR NPs and the corresponding cocktail of six individual S-EBR NPs (Fig. 8b), mosaic S-EBR NPs elicited increased heterologous antibody responses in mice against CoV strains that were not displayed on mosaic NPs, including SARS-CoV-2, MERS, and SHC014 (Fig. 8c-e).

As initial mosaic S-EBR NP designs predominantly focused on sarbecoviruses, future designs will aim to enhance antibody responses against alpha-CoVs, beta-CoVs from the embeco-, merbeco-, and nobecovirus lineages, and potentially gamma- and delta-CoVs. It will also be important to test if universal CoV vaccine efforts should focus on eliciting cross-reactive antibodies that

recognize epitopes conserved among all CoV strains, or whether it's more effective and feasible to elicit distinct sets of antibodies in parallel with each set recognizing members of a different CoV genus (e.g., beta-CoVs) or subgenus (e.g., sarbecoviruses). To identify the best strategy, I will compare three mosaic S-EBR NP combinations: i) display all alpha- and beta-CoV S proteins on a single mosaic S-EBR NP; ii) display only alpha- or beta-CoV S proteins on two separate S-EBR NPs; iii) display only alpha-CoV, embeco-, sarbeco-, merbeco-, or nobecovirus S proteins on multiple S-EBR NPs.

The efficacy of universal CoV vaccines will be assessed in multiple ways. First, cross-reactive serum antibody responses will be analyzed by enzyme-linked immunosorbent assays (ELISAs) and neutralization assays against a panel of heterologous CoV strains. Second, cross-reactive monoclonal antibodies recognizing a broad spectrum of CoVs will be isolated by single B-cell screening and characterized by ELISAs, neutralization assays, and single-particle cryo-electron microscopy (cryo-EM). Third, heterologous T-cell responses will be measured by enzyme-linked immune absorbent spot (ELISpot) assays and T-cell-mediated cytotoxicity assays. Finally, promising universal CoV vaccine candidates could be evaluated in heterologous CoV challenge studies.

Dependencies

None of the proposed aims are dependent on the success of a separate aim, and all aims can be started in parallel. However, outcomes could be maximized by

integrating individual aims. For example, the strategies outlined for Aims 1 and 2 could work synergistically and the combination of both approaches could result in a highly potent rapid-response vaccine technology (Fig. 7a). Initial experiments for Aim 3 will use purified S-EBR NPs, but the strategies proposed in Aims 1 and 2 could also be applied to designing universal CoV vaccines. Comparing the ability of different vaccine approaches to elicit cross-reactive responses could provide insight into how immunogen delivery and presentation affect immune recognition of conserved epitopes.

Experimental plan and milestones

Aim 1. Based on the results from our pilot experiment, we will perform large-scale in vivo studies in mice to evaluate our hybrid mRNA vaccine approach. mRNAs encoding the unmodified SARS-CoV-2 S protein or the engineered S-EBR protein will be synthesized at the RNA core of the Houston Methodist Research Institute. mRNA synthesis will include addition of 5' cap analogs and long polyA tails for optimal mammalian expression, as well as pseudouridine substitution and HPLC purification to remove double-stranded RNA to minimize innate immune responses[280]. S-EBR mRNA constructs will include the original S-EBR design that was used in the pilot experiment (Fig. 6a-b), as well as various optimized S-EBR versions designed to self-assemble more efficiently (data not shown) and/or prevent endocytosis of S-EBR proteins to remain on the cell surface for extended durations (Fig. 8f).

To ensure efficient delivery into host cells, S, S-EBR, and optimized S-EBR mRNAs will be encapsulated into state-of-the-art LNPs in collaboration with Acuitas Therapeutics. As described for the initial pilot study, combinations of the S and optimized S-EBR mRNA constructs will also be generated. S-EBR mRNA-LNPs will be tested in vitro to ensure that S-EBR NPs are efficiently assembled and secreted from cells. Mice will initially receive 1 or 2 IM injections of 0.01, 0.1, or 1 μg mRNA, and immune responses will be compared to SC injections of 1 μg purified S-EBR NPs in the presence or absence of adjuvant. Serum antibody titers will be determined by ELISA and pseudovirus neutralization assays against SARS-CoV-2 and VOCs. Neutralization titers will also be evaluated against authentic viruses by plaque reduction neutralization test (PRNT) (performed at Bioqual). CD4+ and CD8+ T-cell responses elicited by mRNA vaccines will be compared by ELISpot[273]. Additional studies could evaluate hybrid mRNA vaccines encoding VOC-based S-EBR constructs, e.g., Delta.

Milestone: Achieve ≥ 10-fold higher antibody responses and/or demonstrate neutralizing antibody responses (ID_{50} ≤ 1:200) at ≥ 10-fold lower doses for hybrid S-EBR mRNA vaccines compared to the conventional S mRNA vaccine against SARS-CoV-2 and VOCs.

Aim 2. To engineer EBR NPs as a delivery strategy for mRNA vaccines, various construct designs will be evaluated in vitro. In addition to L7Ae, we will test the MS2 MCP protein and the HIV-1 Tat protein that both specifically interact with structural RNA stem loop motifs, which can be inserted into the 3' UTR of the

mRNA[279,281]. Alternatively, CRISPR-Cas13 with a deactivated version of the Cas13 enzyme (dCas13) binds specific RNA sequences[282] and could be used to enable sequence-specific mRNA incorporation into EBR NPs. Minimal versions of L7Ae, MCP, Tat, and dCas13 will be inserted into the cytoplasmic tail of the SARS-CoV-2 S-EBR construct, upstream or downstream of the EBR domain. mRNA packaging and delivery will be validated in ACE2-293T cells and test mRNAs will encode GFP, SARS-CoV-2 S, or S-EBR. Expression will be analyzed by flow cytometry and compared to conventional LNP-mediated mRNA delivery. The best S-EBR constructs will be compared to standard LNPs for mRNA vaccine delivery in mice. To test if approaches proposed for Aims 1 and 2 could work synergistically, S-EBR NPs will be compared to LNPs for the delivery of the self-assembling S-EBR mRNA vaccine (Fig. 7a). Immune responses will be assessed by ELISA, neutralization assay, and ELISpot.

Milestone: Achieve ≥ 5-fold higher neutralizing antibody responses for S and/or S-EBR mRNA vaccines delivered by S-EBR NPs compared to conventional LNPs.

Aim 3. The EBR NP technology will be applied to design and evaluate mosaic S-EBR NPs for the development of a universal CoV vaccine. Initial designs will include an 8-strain mosaic S-EBR NP that displays two sarbecovirus strains (SARS-CoV, Rf1), two embecovirus strains (HKU1, MHV), two merbecovirus strains (HKU4, HKU5), and two alpha-CoV strains (229E, HKU8). A 12-strain mosaic S-EBR NP could achieve even broader coverage by including additional

sarbecovirus (BtKY72), nobecovirus (HKU9), alpha-CoV (PDEV), and delta-CoV (HKU13) strains. The effect of using different CoV strains on mosaic S-EBR NPs for prime and boost injections to increase diversity will also be assessed. To investigate the effect of separating alpha- and beta-CoV strains on mosaic NPs, a 12-strain mosaic S-EBR NP that displays 6 alpha- and 6 beta-CoV strains will be compared against the combination of two 6-strain mosaic S-EBR NPs that either present 6 alpha- or 6 beta-CoV strains. Additional mosaic S-EBR NP designs could assess if separating alpha-CoV, sarbeco-, embeco-, and merbecovirus beta-CoV strains could have beneficial effects on eliciting potent cross-reactive responses.

All mosaic S-EBR NPs will be generated by co-transfecting Expi293 cells with the respective S-EBR constructs and purified by ultracentrifugation on a 20% sucrose cushion and size-exclusion chromatography. Initial in vivo studies will be performed in mice and mosaic S-EBR NPs will be compared to the corresponding cocktails of individual S-EBR NPs (Fig. 8b). Cross-reactive immune responses will be evaluated by ELISAs, pseudovirus neutralization assays, and ELISpot assays against a panel of heterologous alpha- and beta-CoV strains that were not presented on the mosaic S-EBR NPs, including pandemic MERS-CoV and SARS-CoV-2 strains as well as SARS-CoV-2 VOCs, the common cold-causing human CoVs OC43 and NL63, as well as zoonotic sarbecovirus (SHC014, WIV1), embecovirus (BCoV), alpha-CoV (CCoV, TGEV), and delta-CoV (PDCoV) strains. If successful, the hybrid mRNA vaccine strategies outlined for Aims 1 and 2 will also

be applied to designing universal CoV vaccine candidates and will be directly compared to purified mosaic S-EBR NPs.

Sequences of cross-reactive monoclonal antibodies from immunized mice will be obtained from single B cells using a Berkeley Lights Beacon Optofluidic System available at Caltech as described[283]. B cells will be harvested from spleens and lymph nodes and selected based on interactions with fluorescently-labeled SARS-CoV-2, MERS, OC43, and NL63 S trimer proteins. The breadth and potency of cross-neutralizing antibodies will be assessed by ELISAs and neutralization assays against the heterologous CoV panel. Single-particle cryo-EM structures of antibody Fab-S trimer complexes will be solved to characterize epitopes of the isolated antibodies. Structural insights could guide CoV strain selection for more effective mosaic S-EBR NPs and inform immunogen design strategies such as masking of undesired epitopes to focus responses to conserved regions. Isolated antibodies could also serve as a starting point for developing pan-neutralizing antibodies as potential 1st-line treatments against future CoV pandemics.

Milestone: Demonstrate neutralizing antibody responses at serum dilutions of at least 1:200 against 7 of 10 heterologous CoV strains, T-cell responses against 9 of 10 heterologous CoV strains, and isolate at least one monoclonal antibody that neutralizes 7 of 10 heterologous CoV strains.

Animal models and challenge studies

Studies for Aims 1-3 will initially be performed in wild-type mice. The efficacy and safety of promising vaccine candidates could also be evaluated in

NHPs in collaboration with Malcolm Martin's laboratory (NIH). Protection studies against CoV challenges could also be performed in transgenic mice expressing human ACE2, hamsters, or NHPs.

Risk mitigation and alternative strategies

Aim 1. mRNA-mediated S-EBR expression might be relatively low, which could reduce the efficiency of S-EBR NP assembly. S-EBR expression could be optimized by inserting a short amino acid sequence upstream of the EBR domain designed to prevent endocytosis by tethering the cytoplasmic tail to the cytoskeleton (Fig. 8f). S-EBR expression could be further increased through stabilizing mutations[263] and mutating the furin cleavage site[284]. If these measures are insufficient, the number of mRNA molecules per LNP could be increased by changing the size of LNPs. This would ensure that multiple S-EBR mRNA molecules get delivered into the same cell, thereby enhancing S-EBR expression and NP production. The potency of hybrid mRNA vaccines could be further improved by using self-amplifying mRNA constructs[285,286] or by combining the strategies proposed for Aims 1 and 2 to deliver S-EBR mRNA vaccines in S-EBR NPs.

Aim 2. Insertion of L7Ae, MCP, Tat, or dCas13 upstream or downstream of the EBR domain could reduce S-EBR expression and/or NP assembly. As suggested for Aim 1, S-EBR expression could be increased by inserting a short endocytosis-preventing sequence upstream of the EBR domain (Fig. 8f). Another strategy would be to separate S-EBR and L7Ae by adding a myristoylation motif

to the N-terminus of L7Ae (Myr-L7Ae) to tether L7Ae to the cytoplasmic side of the plasma membrane. Co-expression of S-EBR and Myr-L7Ae leads to incorporation of L7Ae-mRNA complexes into budding S-EBR NPs (Fig. 7b, right) that efficiently infected ACE2-expressing target cells (Fig. 7c). Additional approaches to improve the mRNA delivery efficiency and potency of S-EBR NPs include the use of self-amplifying mRNA constructs[285,286] and co-display of a fusogenic molecule[287] on S-EBR NPs that induces membrane fusion at low pH to further enhance endosomal escape of the mRNA.

Aim 3. Focusing antibody responses to conserved epitopes on CoV S proteins could be challenging. Immune responses could initially be primed by injecting NPs presenting highly conserved linear epitopes from the S2 subunit[261]. Immunodominant antibody responses to undesired regions could be prevented by mutating or masking these epitopes with glycans. Another strategy to focus antibody responses to conserved epitopes could be to use different strains on mosaic S-EBR NPs for prime and boost injections. Universal CoV vaccine candidates based on the hybrid mRNA vaccine strategies outlined in Aims 1 and 2 could also enhance cross-reactive immune responses through potent activation of both, T-cells and B-cells. mRNA-mediated expression of S-EBR NPs would also lead to prolonged antigen presentation, which could have positive effects on the frequency and potency of cross-reactive antibodies. However, the success of using hybrid mRNA vaccine approaches for universal CoV vaccine applications will depend on achieving simultaneous delivery of most or all CoV S-EBR mRNA constructs to

the same cell to ensure assembly of mosaic S-EBR NPs. This could be accomplished by using polycistronic mRNAs encoding 4 or more S-EBR constructs and by adjusting the size of LNPs to ensure encapsulation of multiple mRNA molecules per LNP.

Innovation

The vaccine strategy proposed for Aim 1 has the potential to become a leading vaccine technology as it combines the best attributes of mRNA vaccines and protein NP vaccines. This hybrid approach could elicit stronger antibody responses than conventional mRNA vaccines while retaining their excellent manufacturing properties and potent activation of T-cells. The enhanced potency of hybrid mRNA vaccines could have commercial advantages as protective immune responses might be achieved with a single injection and/or substantially lower mRNA doses, resulting in reduced costs and faster global vaccine distribution. Hybrid mRNA vaccines could be the ideal platform technology to elicit effective, targeted, and long-lasting immune responses because they mimic natural infections more accurately than other vaccine approaches as antigens are presented on the cell surface resembling an infected cell, as well as on secreted NPs resembling free virions.

Engineering EBR NPs to package and deliver mRNAs as proposed for Aim 2 has the potential to revolutionize mRNA delivery for vaccine and therapeutic applications. EBR NPs have a number of advantages over conventional LNPs: i)

EBR NPs induce potent antibody responses by presenting the viral surface antigen of interest; ii) viral surface antigens on EBR NPs facilitate cellular uptake and endosomal escape of mRNA payloads; iii) EBR NPs target mRNA vaccine delivery to tissues that are naturally infected by the virus and could induce local immune responses. Combining the strategies outlined for Aims 1 and 2 has the potential to lower protective mRNA doses by several orders of magnitude to expedite global vaccine supply for COVID-19 and future pandemics. EBR NPs could also be used for targeted delivery of mRNA-based therapeutics to specific tissues, e.g., cancer cells. This could be accomplished by designing antibody-EBR NPs that display antibodies recognizing specific cancer surface markers such as the human epidermal growth factor receptor 2 (HER-2). Moreover, since EBR NP production is relatively simple, this delivery strategy would provide more researchers with the opportunity to test their mRNA-based vaccines and therapeutics as the manufacturing of conventional mRNA-LNP formulations requires considerable know-how and resources, thereby limiting accessibility.

Finally, the EBR NP technology is ideally suited for the production of mosaic NPs that present multiple antigens on the same NP. In contrast to conventional NP technologies, full-length viral surface antigens can be incorporated without extensive protein modifications, and the production of mosaic EBR NPs only requires single expression and purification steps. An additional advantage of the EBR technology is that NPs are enveloped, which prevents off-target antibody responses to the NP scaffold after repeated administrations. EBR

NPs have already been expressed for a wide range of membrane proteins, including HIV-1 Env (Fig. 8g), and the modularity of this technology will be valuable for the production of mosaic NPs in research efforts to develop universal vaccines against CoVs and influenza, as well as an effective vaccine against HIV-1.

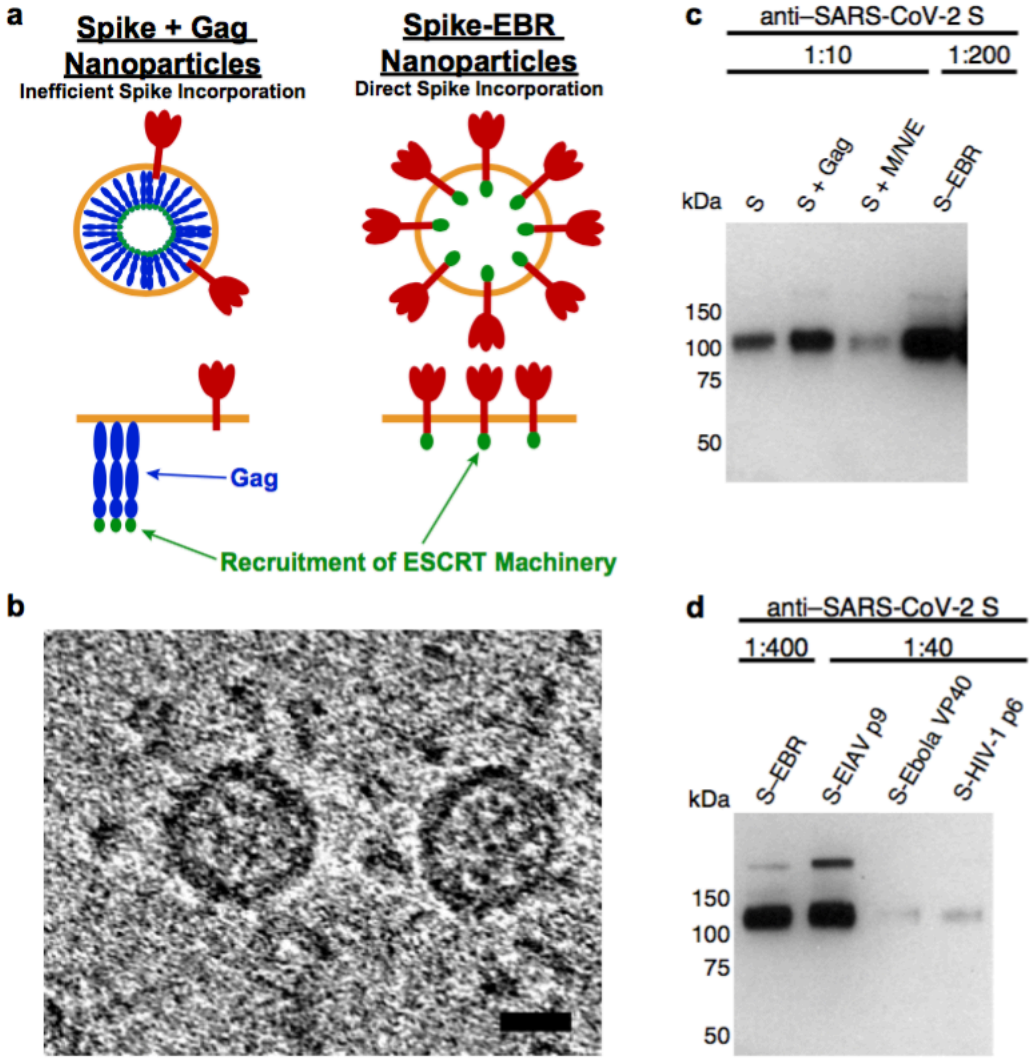

Figure 1. Generation of self-assembling SARS-CoV-2 S-EBR NPs. a) Schematic presenting the mechanism of the self-assembling S-EBR NP technology compared to a conventional approach that requires co-expression of a structural scaffold protein that assembles the NP, e.g., Gag. b) Cryo-electron tomogram showing S-EBR NPs that were purified by sucrose ultracentrifugation and size-exclusion chromatography. Scale bar = 20 nm. c) Western blot analysis of SARS-CoV-2 S-containing NPs that were generated by transfecting Expi293 cells with S (lane 1), S + Gag (lane 2), S +

SARS-CoV-2 structural proteins M, N, and E (lane 3), or S-EBR (lane 4). NPs were purified from culture supernatants by sucrose ultracentrifugation. Samples in lanes 1-3 were diluted 1:10-fold, while samples in lanes 4-5 were diluted 1:200-fold. d) Western blot analysis of purified SARS-CoV-2 S-containing NPs that were generated by transfecting Expi293 cells with S-EBR (lane 1), S fused to the EIAV p9 protein (lane 2), S fused to the EBOV VP40 protein (lane 3), or S fused to the HIV-1 p6 protein (lane 4). The sample in lane 1 was diluted 1:400-fold, while samples in lanes 2-4 were diluted 1:40-fold.

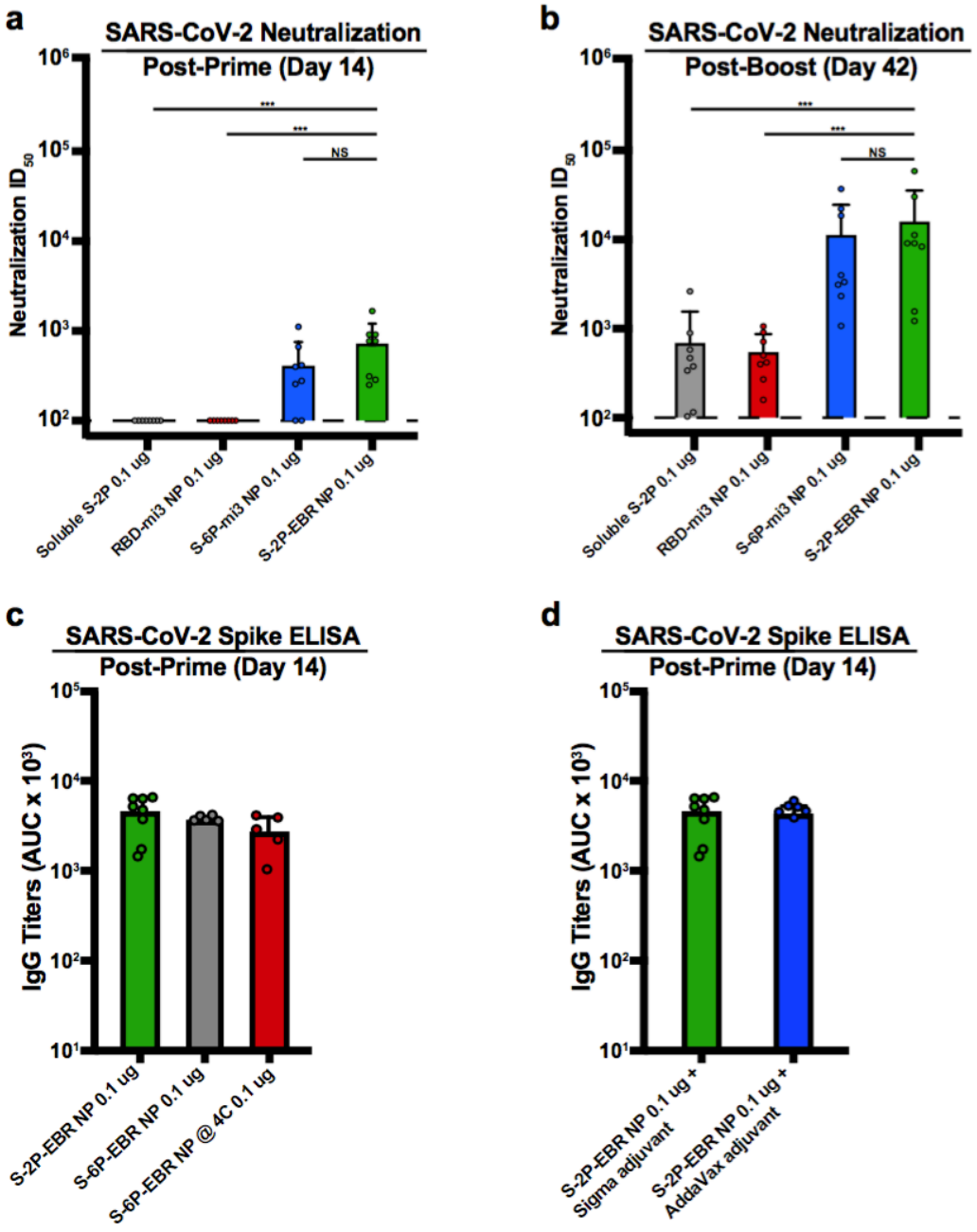

Figure 2. SARS-CoV-2 S-2P-EBR NPs elicit potent antibody responses in vivo. a-b) SARS-CoV-2 neutralization for serum samples from mice immunized with soluble S-2P (gray), RBD-mi3 NPs (red), S-6P-mi3 NPs (blue), and S-2P-EBR NPs (green). Potencies are presented as half-maximal inhibitory dilutions (ID_{50} values)

and are shown for a) post-prime (day 14) and b) post-boost (day 42) samples. The dashed horizontal line corresponds to the limit of detection. Data points represent ID_{50}s for individual animals and rectangles represent mean ID_{50}s for 8 animals per group with SDs shown as vertical lines. Statistical significance ($p < 0.05$) between groups linked by horizontal lines are indicated by asterisks. c) ELISA data for IgG responses against SARS-CoV-2 S for serum samples from mice immunized with S-2P-EBR NPs (green), S-6P-EBR NPs (gray), and S-6P-EBR NPs that were stored at 4ºC for 2 months (red). d) ELISA data for IgG responses against SARS-CoV-2 S for serum samples from mice immunized with S-2P-EBR NPs using either Sigma adjuvant (green) or AddaVax adjuvant (blue). All analyzed serum samples were taken 14 days after a single injection of the respective immunogen and results are shown as area under the curve (AUC) for individual animals and rectangles represent mean AUC for 6-8 animals per group with SDs shown as vertical lines.

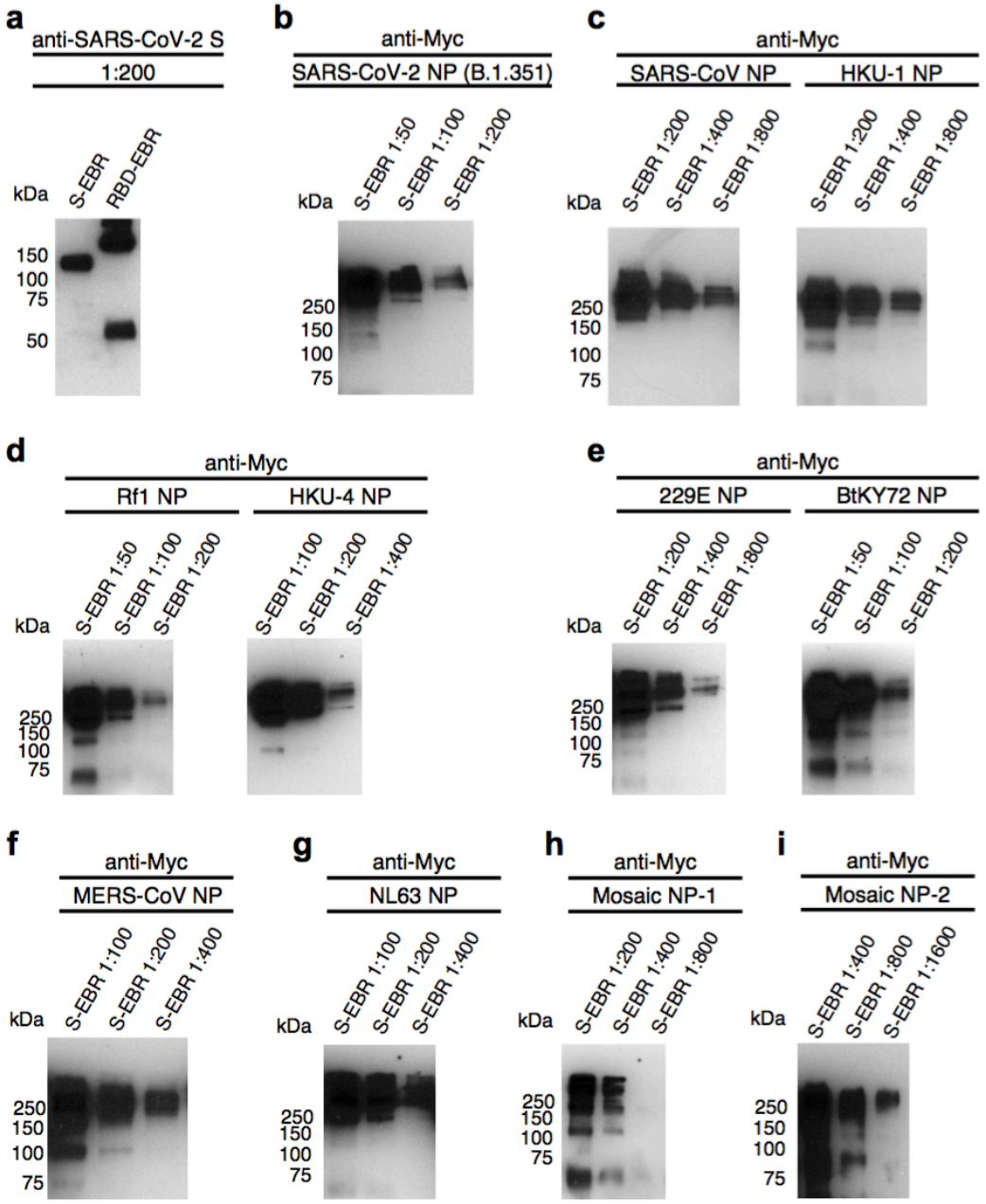

Figure 3. Production of S-EBR NPs for various CoV strains. Western blot analysis for purified a) SARS-CoV-2 RBD-EBR NPs, b) SARS-CoV-2 S-2P-EBR NPs (B.1.351 variant), c) SARS-CoV and HKU-1 S-EBR NPs, d) Rf1 and HKU-4 S-EBR NPs, e) 229E and BtKY72 S-EBR NPs, f) MERS-CoV S-EBR NPs, and g) NL63 S-EBR NPs. h-i) Western blot analysis for purified mosaic S-EBR NPs

consisting of h) SARS-CoV, Rf1, BtKY72, HKU-1, HKU-4, and 229E S-EBR or i) SHC014, HKU-3, HKU-5, HKU-8, HKU-24, and BM48-31 S-EBR. All S-EBR NPs were purified by sucrose ultracentrifugation and size-exclusion chromatography.

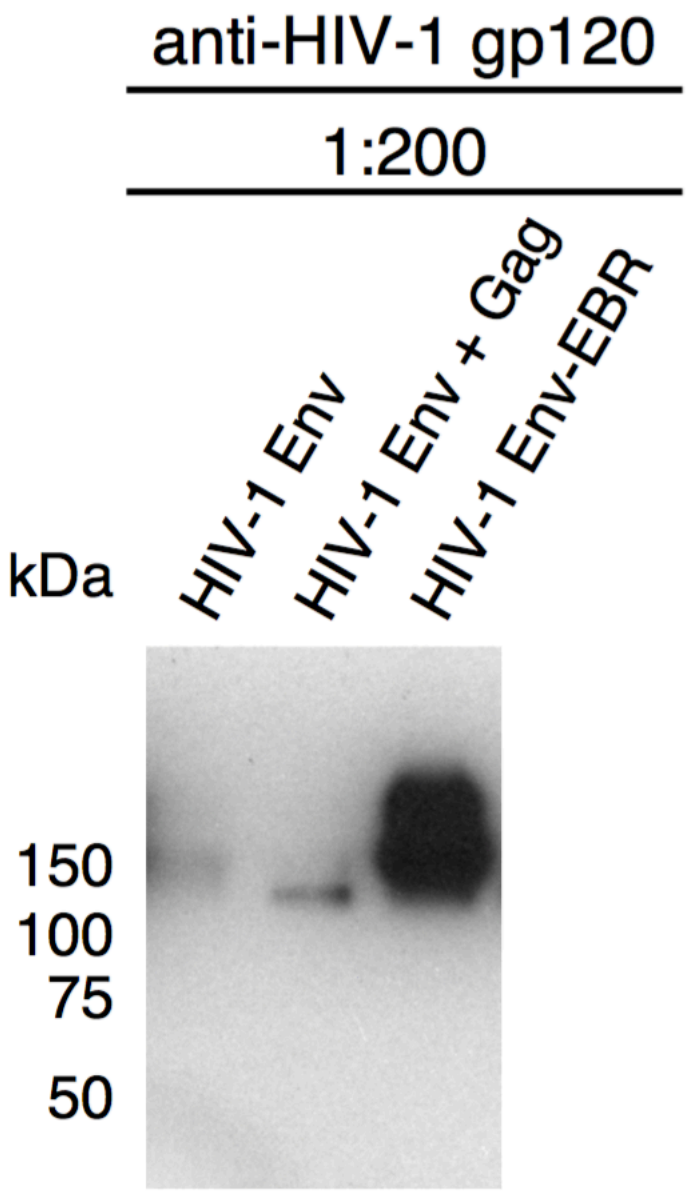

Figure 4. HIV-1 Env-presenting NPs can be generated using EBR NP technology. Western blot analysis for HIV-1 Env-containing NPs that were generated by transfecting Expi293 cells with HIV-1 Env (lane 1), Env + Gag (lane 2), or Env-EBR (lane 3). The HIV-1 YU2 strain was used for transfections and NPs were purified from culture supernatants by sucrose ultracentrifugation. All samples

were diluted 1:200 and gp120 bands were detected using the V3 glycan patch-targeting antibody 10-1074.

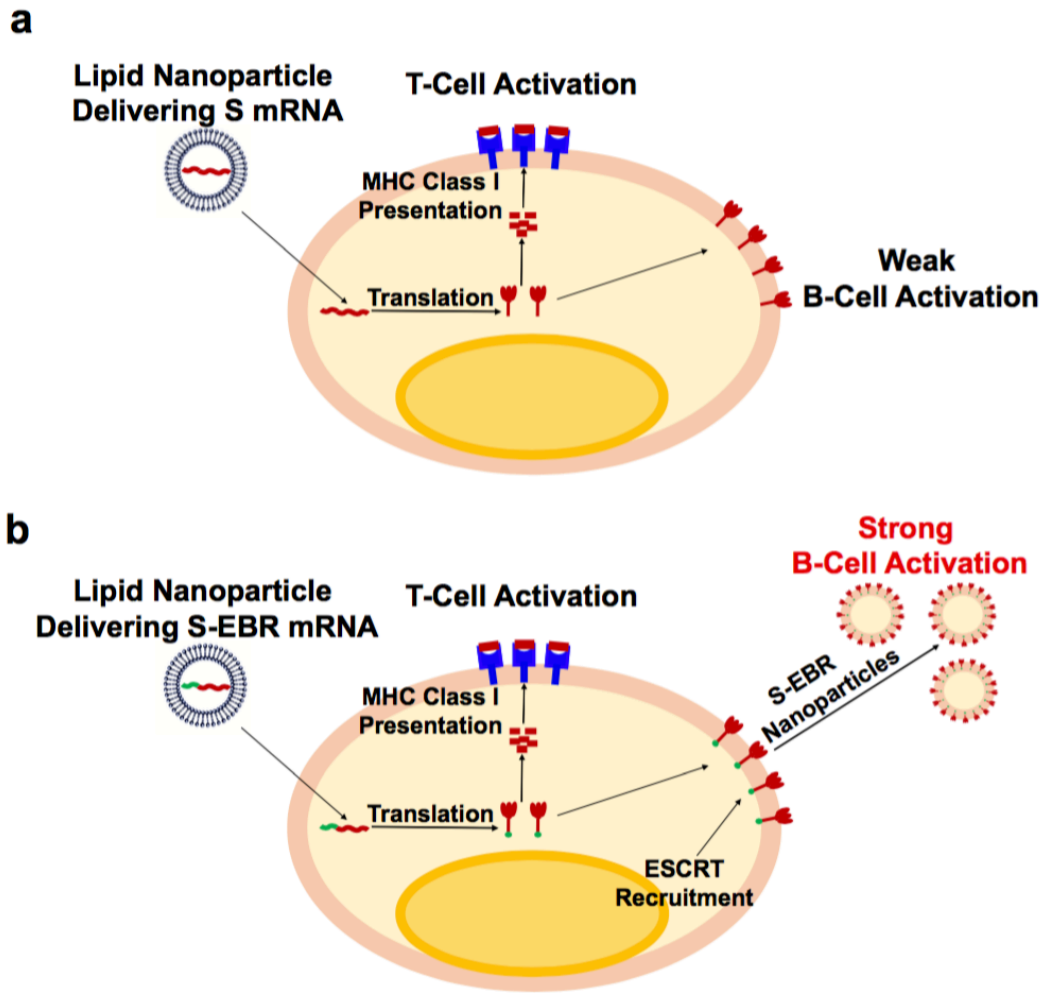

Figure 5. Hybrid vaccine strategies to enhance the potency of rapid-response mRNA vaccines. a-b) Schematics showing immune activation mechanisms for **a)** S and **b)** S-EBR mRNA vaccines delivered by lipid nanoparticles (LNPs), respectively.

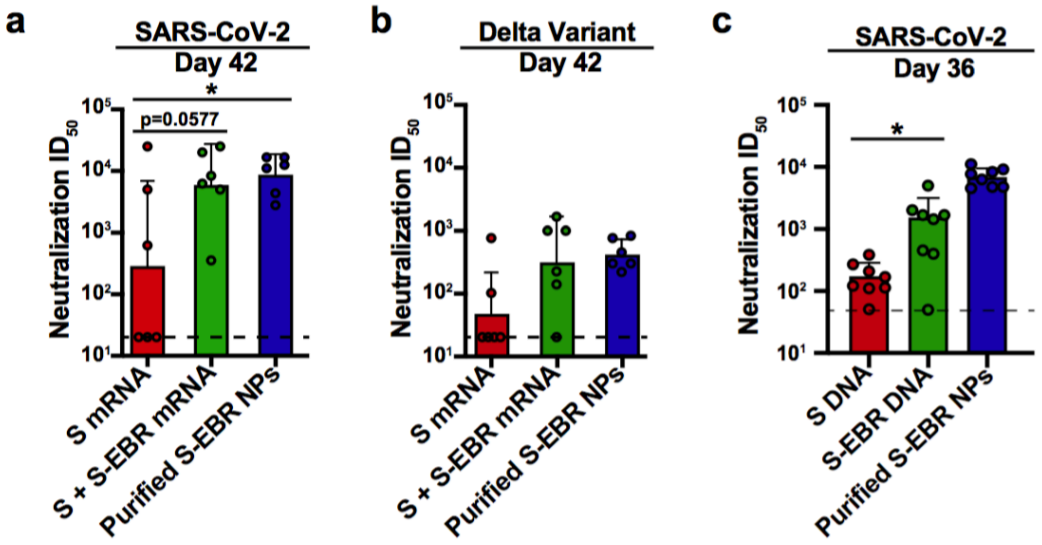

Figure 6. Hybrid mRNA and DNA vaccines elicit more potent neutralizing antibody responses than conventional nucleic acid-based vaccines. **a-b)** Post-boost (day 42) neutralization against **a)** SARS-CoV-2 and the **b)** Delta VOC for serum samples from mice immunized with 1 μg S mRNA (red), 1 μg of the combination of S + S-EBR mRNA (0.5 μg S + 0.5 μg S-EBR; green), or 1 μg purified S-EBR NPs plus adjuvant (blue). **c)** Post-boost (day 36) neutralization against SARS-CoV-2 for serum samples from mice immunized with 10 μg S DNA (red), 10 μg of S-EBR DNA (0.5 μg S + 0.5 μg S-EBR; green), or 1 μg purified S-EBR NPs plus adjuvant (blue). Potencies are presented as half-maximal inhibitory dilutions (ID_{50} values). Dashed horizontal lines correspond to the detection limit. Data points represent ID_{50}s for individual animals and rectangles represent geometric mean ID_{50}s for 6-8 animals per group with SDs shown as vertical lines. Statistical significance ($p < 0.05$) between groups linked by a horizontal line is indicated by an asterisk.

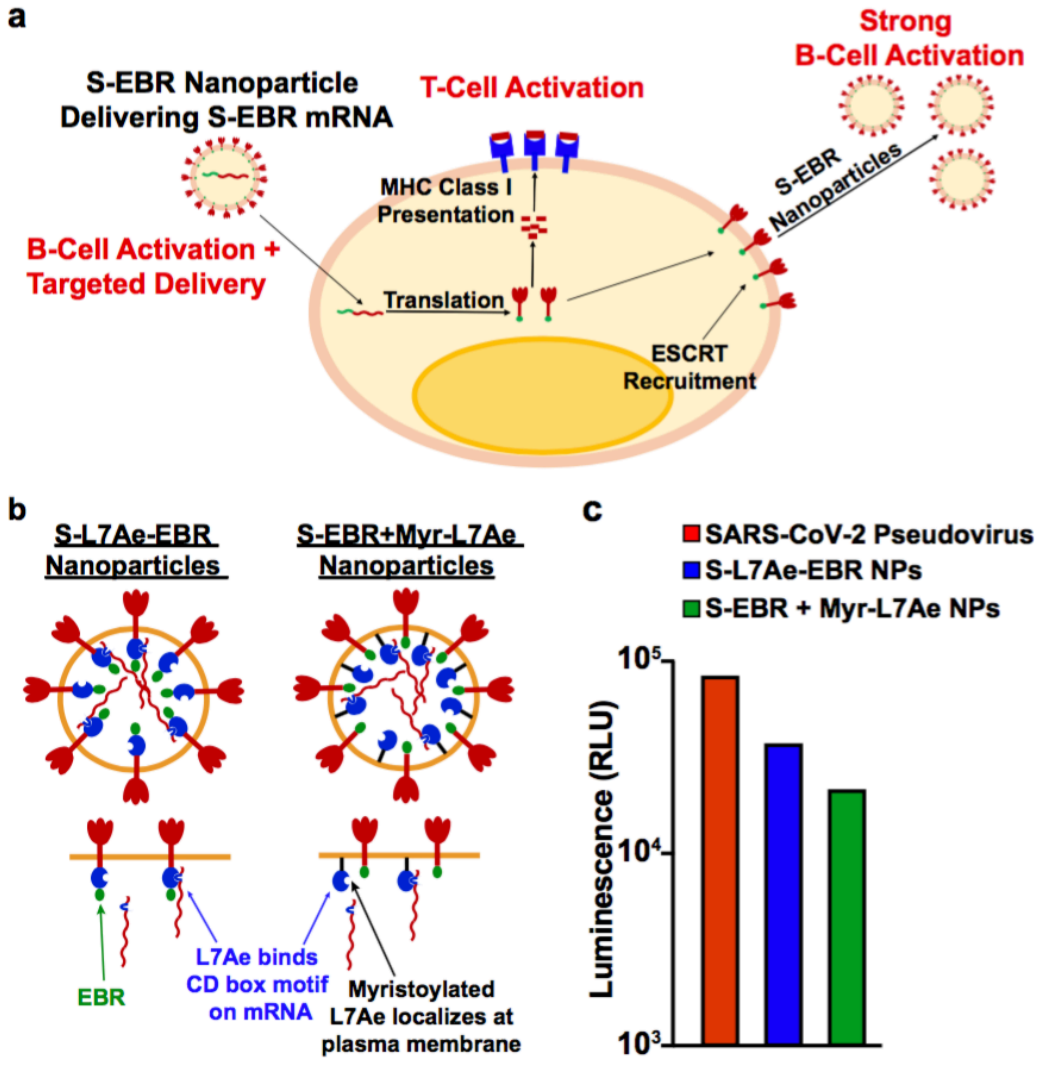

Figure 7. S-EBR NPs as an alternative to LNPs for targeted delivery of mRNA vaccines. a) Schematic presenting immune activation mechanisms for the S-EBR mRNA vaccine delivered by S-EBR NPs. **b)** Schematic showing two approaches to engineer S-EBR NPs to incorporate specific mRNAs. Left: The L7Ae protein is inserted upstream of the EBR domain and interacts with a CD box motif in the 3'UTR of the mRNA. Right: A myristoylation motif is added to the N-terminus of L7Ae (Myr-L7Ae) to tether L7Ae to the cytoplasmic side of the plasma membrane. L7Ae-

mRNA complexes get incorporated into budding S-EBR NPs. **c)** Infectivity assay measuring luminescence in ACE2-293T cells to compare lentivirus-based SARS-CoV-2 S-pseudotyped pseudovirus (red), S-L7Ae-EBR NPs (blue), and S-EBR + Myr-L7Ae NPs (green). The firefly luciferase gene was inserted into the lentiviral backbone for the pseudovirus. S-L7Ae-EBR NPs and S-EBR + Myr-L7Ae NPs delivered luciferase mRNA that contained a CD box motif in the 3'UTR.

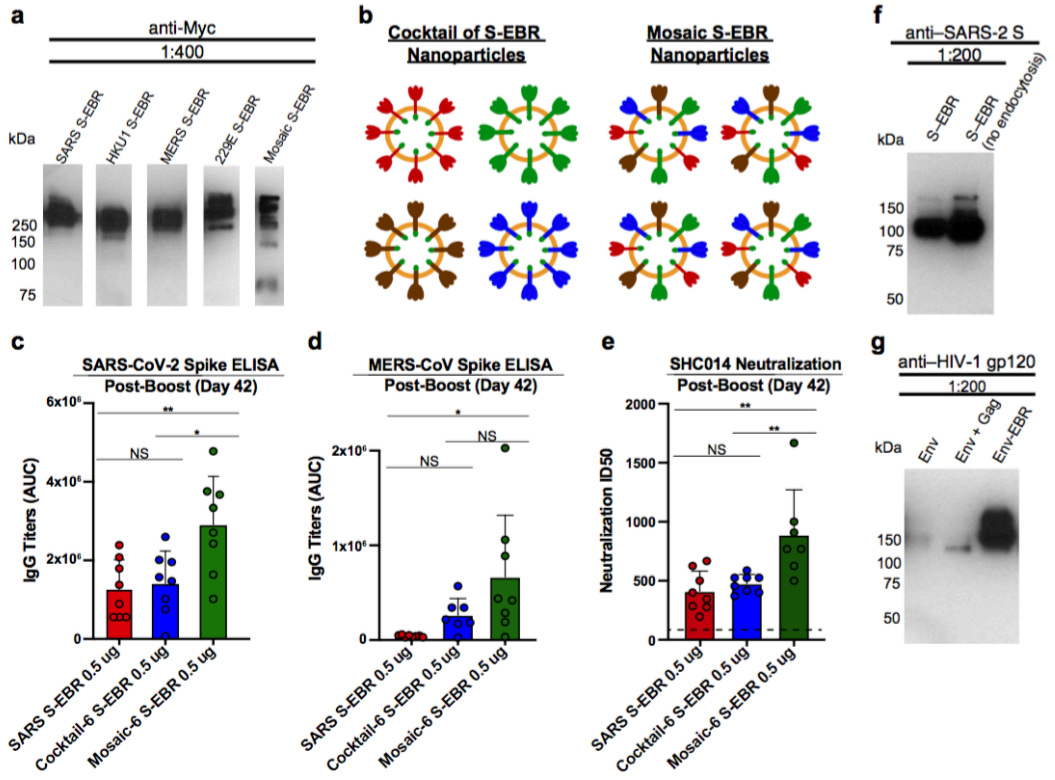

Figure 8. S-EBR NPs as a platform for designing a universal CoV vaccine. a) Western blot analysis for purified SARS, HKU1, MERS, 229E, and mosaic S-EBR NPs. All S-EBR constructs were detected through a C-terminal myc-tag. **b)** Schematic comparing different approaches to designing a universal CoV vaccine. Left side: Cocktail of homotypic CoV S-EBR NPs that present the S protein from a single CoV strain. Right side: Heterotypic mosaic CoV S-EBR NPs that display S proteins from multiple CoV strains. **c-e)** ELISA results against **c)** SARS-CoV-2 S and **d)** MERS-CoV S, and neutralization data against **e)** lentivirus-based SHC014 pseudovirus for post-boost (day 42) serum samples from mice immunized with SARS S-EBR NPs (red), a cocktail of SARS, Rf1, BtKY72, HKU1, HKU4, and 229E S-EBR NPs (blue), or mosaic S-EBR NPs generated by co-transfection of

SARS, Rf1, BtKY72, HKU1, HKU4, and 229E S-EBR (red). Results are shown as area under the curve (AUC) for ELISAs and half-maximal inhibitory dilutions (ID_{50} values) for neutralization assays for individual animals, and rectangles represent mean values for 8 animals per group with SDs shown as vertical lines. Statistical significance ($p < 0.05$) between groups linked by horizontal lines are indicated by asterisks. **f)** Western blot analysis comparing S-containing NPs after transfecting Expi293 cells with S-EBR (lane 1) or a modified S-EBR construct that contains an insertion designed to prevent endocytosis (lane 2). **g)** Western blot analysis for purified HIV-1 Env NPs generated by transfecting Expi293 cells with HIV-1 Env (lane 1), Env + Gag (lane 2), or Env-EBR (lane 3).

BIBLIOGRAPHY

1 Gottlieb, M. S. *et al.* Pneumocystis-Carinii Pneumonia and Mucosal Candidiasis in Previously Healthy Homosexual Men - Evidence of a New Acquired Cellular Immunodeficiency. *New Engl J Med* **305**, 1425-1431, doi:Doi 10.1056/Nejm198112103052401 (1981).

2 Friedman-Kien, A. E. Disseminated Kaposi's sarcoma syndrome in young homosexual men. *J Am Acad Dermatol* **5**, 468-471, doi:10.1016/s0190-9622(81)80010-2 (1981).

3 AIDS.gov. *A Timeline of HIV/AIDS*, <https://www.hiv.gov/sites/default/files/aidsgov-timeline.pdf> (2021).

4 Barre-Sinoussi, F. *et al.* Isolation of a T-lymphotropic retrovirus from a patient at risk for acquired immune deficiency syndrome (AIDS). *Science* **220**, 868-871, doi:10.1126/science.6189183 (1983).

5 Gallo, R. C. & Montagnier, L. The discovery of HIV as the cause of AIDS. *N Engl J Med* **349**, 2283-2285, doi:10.1056/NEJMp038194 (2003).

6 Dalgleish, A. G. *et al.* The CD4 (T4) antigen is an essential component of the receptor for the AIDS retrovirus. *Nature* **312**, 763-767, doi:10.1038/312763a0 (1984).

7 Poiesz, B. J. *et al.* Detection and isolation of type C retrovirus particles from fresh and cultured lymphocytes of a patient with cutaneous T-cell lymphoma. *Proc Natl Acad Sci U S A* **77**, 7415-7419, doi:10.1073/pnas.77.12.7415 (1980).

8 Temin, H. M. & Mizutani, S. RNA-dependent DNA polymerase in virions of Rous sarcoma virus. *Nature* **226**, 1211-1213, doi:10.1038/2261211a0 (1970).

9 Baltimore, D. RNA-dependent DNA polymerase in virions of RNA tumour viruses. *Nature* **226**, 1209-1211, doi:10.1038/2261209a0 (1970).

10 Gallo, R. C. *et al.* Frequent detection and isolation of cytopathic retroviruses (HTLV-III) from patients with AIDS and at risk for AIDS. *Science* **224**, 500-503, doi:10.1126/science.6200936 (1984).

11 Levy, J. A. *et al.* Isolation of lymphocytopathic retroviruses from San Francisco patients with AIDS. *Science* **225**, 840-842, doi:10.1126/science.6206563 (1984).

12 UNAIDS. *90-90-90: Treatment for all (update)*, <https://www.unaids.org/en/resources/presscentre/featurestories/2020/september/20200921_90-90-90> (2021).

13 World-Health-Organization. *HIV/AIDS Key Facts*, <https://www.who.int/news-room/fact-sheets/detail/hiv-aids> (2020).

14 Clavel, F. *et al.* Isolation of a new human retrovirus from West African patients with AIDS. *Science* **233**, 343-346, doi:10.1126/science.2425430 (1986).

15 Diwan, B., Saxena, R. & Tiwari, A. HIV-2 and its role in conglutinated approach towards Acquired Immunodeficiency Syndrome (AIDS) Vaccine Development. *Springerplus* **2**, 7, doi:10.1186/2193-1801-2-7 (2013).

16 Huet, T., Cheynier, R., Meyerhans, A., Roelants, G. & Wain-Hobson, S. Genetic organization of a chimpanzee lentivirus related to HIV-1. *Nature* **345**, 356-359, doi:10.1038/345356a0 (1990).

17 Hirsch, V. M., Olmsted, R. A., Murphey-Corb, M., Purcell, R. H. & Johnson, P. R. An African primate lentivirus (SIVsm) closely related to HIV-2. *Nature* **339**, 389-392, doi:10.1038/339389a0 (1989).

18 Hahn, B. H., Shaw, G. M., De Cock, K. M. & Sharp, P. M. AIDS as a zoonosis: scientific and public health implications. *Science* **287**, 607-614, doi:10.1126/science.287.5453.607 (2000).

19 Motomura, K., Chen, J. & Hu, W. S. Genetic recombination between human immunodeficiency virus type 1 (HIV-1) and HIV-2, two distinct human lentiviruses. *J Virol* **82**, 1923-1933, doi:10.1128/JVI.01937-07 (2008).

20 Sharp, P. M. & Hahn, B. H. Origins of HIV and the AIDS pandemic. *Cold Spring Harb Perspect Med* **1**, a006841, doi:10.1101/cshperspect.a006841 (2011).

21 Taylor, B. S., Sobieszczyk, M. E., McCutchan, F. E. & Hammer, S. M. The challenge of HIV-1 subtype diversity. *N Engl J Med* **358**, 1590-1602, doi:10.1056/NEJMra0706737 (2008).

22 Tyor, W., Fritz-French, C. & Nath, A. Effect of HIV clade differences on the onset and severity of HIV-associated neurocognitive disorders. *J Neurovirol* **19**, 515-522, doi:10.1007/s13365-013-0206-6 (2013).

23 Santoro, M. M. & Perno, C. F. HIV-1 Genetic Variability and Clinical Implications. *ISRN Microbiol* **2013**, 481314, doi:10.1155/2013/481314 (2013).

24 Roberts, J. D., Bebenek, K. & Kunkel, T. A. The accuracy of reverse transcriptase from HIV-1. *Science* **242**, 1171-1173, doi:10.1126/science.2460925 (1988).

25 Rawson, J. M., Landman, S. R., Reilly, C. S. & Mansky, L. M. HIV-1 and HIV-2 exhibit similar mutation frequencies and spectra in the absence of G-to-A hypermutation. *Retrovirology* **12**, 60, doi:10.1186/s12977-015-0180-6 (2015).

26 Charpentier, C., Nora, T., Tenaillon, O., Clavel, F. & Hance, A. J. Extensive recombination among human immunodeficiency virus type 1 quasispecies makes an important contribution to viral diversity in individual patients. *J Virol* **80**, 2472-2482, doi:10.1128/JVI.80.5.2472-2482.2006 (2006).

27 Moutouh, L., Corbeil, J. & Richman, D. D. Recombination leads to the rapid emergence of HIV-1 dually resistant mutants under selective drug pressure. *Proc Natl Acad Sci U S A* **93**, 6106-6111, doi:10.1073/pnas.93.12.6106 (1996).

28 Sundquist, W. I. & Krausslich, H. G. HIV-1 assembly, budding, and maturation. *Cold Spring Harb Perspect Med* **2**, a006924, doi:10.1101/cshperspect.a006924 (2012).

29 Zhu, P. *et al.* Distribution and three-dimensional structure of AIDS virus envelope spikes. *Nature* **441**, 847-852, doi:10.1038/nature04817 (2006).

30 Lee, B., Sharron, M., Montaner, L. J., Weissman, D. & Doms, R. W. Quantification of CD4, CCR5, and CXCR4 levels on lymphocyte subsets, dendritic cells, and differentially conditioned monocyte-derived macrophages. *Proc Natl Acad Sci U S A* **96**, 5215-5220 (1999).

31 Artyomov, M. N., Lis, M., Devadas, S., Davis, M. M. & Chakraborty, A. K. CD4 and CD8 binding to MHC molecules primarily acts to enhance Lck delivery. *Proc Natl Acad Sci U S A* **107**, 16916-16921, doi:10.1073/pnas.1010568107 (2010).

32 Shaik, M. M. *et al.* Structural basis of coreceptor recognition by HIV-1 envelope spike. *Nature* **565**, 318-323, doi:10.1038/s41586-018-0804-9 (2019).

33 Gijsbers, E. F. *et al.* The presence of CXCR4-using HIV-1 prior to start of antiretroviral therapy is an independent predictor of delayed viral suppression. *PLoS One* **8**, e76255, doi:10.1371/journal.pone.0076255 (2013).

34 Harrison, S. C. Viral membrane fusion. *Virology* **479-480**, 498-507, doi:10.1016/j.virol.2015.03.043 (2015).

35 Roche, J., Louis, J. M., Aniana, A., Ghirlando, R. & Bax, A. Complete dissociation of the HIV-1 gp41 ectodomain and membrane proximal regions upon phospholipid binding. *J Biomol NMR* **61**, 235-248, doi:10.1007/s10858-015-9900-4 (2015).

36 McDonald, D. *et al.* Visualization of the intracellular behavior of HIV in living cells. *J Cell Biol* **159**, 441-452, doi:10.1083/jcb.200203150 (2002).

37 Sarafianos, S. G. *et al.* Structure and function of HIV-1 reverse transcriptase: molecular mechanisms of polymerization and inhibition. *J Mol Biol* **385**, 693-713, doi:10.1016/j.jmb.2008.10.071 (2009).

38 Burdick, R. C. *et al.* HIV-1 uncoats in the nucleus near sites of integration. *Proc Natl Acad Sci U S A* **117**, 5486-5493, doi:10.1073/pnas.1920631117 (2020).

39 Zila, V. *et al.* Cone-shaped HIV-1 capsids are transported through intact nuclear pores. *Cell* **184**, 1032-1046 e1018, doi:10.1016/j.cell.2021.01.025 (2021).

40 Delelis, O., Carayon, K., Saib, A., Deprez, E. & Mouscadet, J. F. Integrase and integration: biochemical activities of HIV-1 integrase. *Retrovirology* **5**, 114, doi:10.1186/1742-4690-5-114 (2008).

41 Barre-Sinoussi, F., Ross, A. L. & Delfraissy, J. F. Past, present and future: 30 years of HIV research. *Nat Rev Microbiol* **11**, 877-883, doi:10.1038/nrmicro3132 (2013).

42 Li, G. & De Clercq, E. HIV Genome-Wide Protein Associations: a Review of 30 Years of Research. *Microbiol Mol Biol Rev* **80**, 679-731, doi:10.1128/MMBR.00065-15 (2016).

43 Yang, Q., Lucas, A., Son, S. & Chang, L. J. Overlapping enhancer/promoter and transcriptional termination signals in the lentiviral long terminal repeat. *Retrovirology* **4**, 4, doi:10.1186/1742-4690-4-4 (2007).

44 Hiscott, J., Kwon, H. & Genin, P. Hostile takeovers: viral appropriation of the NF-kappaB pathway. *J Clin Invest* **107**, 143-151, doi:10.1172/JCI11918 (2001).

45 Sertznig, H., Hillebrand, F., Erkelenz, S., Schaal, H. & Widera, M. Behind the scenes of HIV-1 replication: Alternative splicing as the dependency factor on the quiet. *Virology* **516**, 176-188, doi:10.1016/j.virol.2018.01.011 (2018).

46 Molle, D. *et al.* A real-time view of the TAR:Tat:P-TEFb complex at HIV-1 transcription sites. *Retrovirology* **4**, 36, doi:10.1186/1742-4690-4-36 (2007).

47 Jain, C. & Belasco, J. G. A structural model for the HIV-1 Rev-RRE complex deduced from altered-specificity rev variants isolated by a rapid genetic strategy. *Cell* **87**, 115-125, doi:10.1016/s0092-8674(00)81328-8 (1996).

48 Love, D. C., Sweitzer, T. D. & Hanover, J. A. Reconstitution of HIV-1 rev nuclear export: independent requirements for nuclear import and export. *Proc Natl Acad Sci U S A* **95**, 10608-10613, doi:10.1073/pnas.95.18.10608 (1998).

49 Leblanc, J., Weil, J. & Beemon, K. Posttranscriptional regulation of retroviral gene expression: primary RNA transcripts play three roles as pre-mRNA, mRNA, and genomic RNA. *Wiley Interdiscip Rev RNA* **4**, 567-580, doi:10.1002/wrna.1179 (2013).

50 Kobayashi, Y., Zhuang, J., Peltz, S. & Dougherty, J. Identification of a cellular factor that modulates HIV-1 programmed ribosomal frameshifting. *J Biol Chem* **285**, 19776-19784, doi:10.1074/jbc.M109.085621 (2010).

51 Moulard, M. & Decroly, E. Maturation of HIV envelope glycoprotein precursors by cellular endoproteases. *Biochim Biophys Acta* **1469**, 121-132, doi:10.1016/s0304-4157(00)00014-9 (2000).

52 Shen, R., Raska, M., Bimczok, D., Novak, J. & Smith, P. D. HIV-1 envelope glycan moieties modulate HIV-1 transmission. *J Virol* **88**, 14258-14267, doi:10.1128/JVI.02164-14 (2014).

53 Seabright, G. E., Doores, K. J., Burton, D. R. & Crispin, M. Protein and Glycan Mimicry in HIV Vaccine Design. *J Mol Biol* **431**, 2223-2247, doi:10.1016/j.jmb.2019.04.016 (2019).

54 Klein, J. S. & Bjorkman, P. J. Few and far between: how HIV may be evading antibody avidity. *PLoS Pathog* **6**, e1000908, doi:10.1371/journal.ppat.1000908 (2010).

55 Galimidi, R. P. *et al.* Intra-spike crosslinking overcomes antibody evasion by HIV-1. *Cell* **160**, 433-446, doi:10.1016/j.cell.2015.01.016 (2015).

56 Zhang, X., Zhou, T., Frabutt, D. A. & Zheng, Y. H. HIV-1 Vpr increases Env expression by preventing Env from endoplasmic reticulum-associated protein degradation (ERAD). *Virology* **496**, 194-202, doi:10.1016/j.virol.2016.06.002 (2016).

57 Ohno, H. *et al.* Interaction of endocytic signals from the HIV-1 envelope glycoprotein complex with members of the adaptor medium chain family. *Virology* **238**, 305-315, doi:10.1006/viro.1997.8839 (1997).

58 Lubben, N. B. *et al.* HIV-1 Nef-induced down-regulation of MHC class I requires AP-1 and clathrin but not PACS-1 and is impeded by AP-2. *Mol Biol Cell* **18**, 3351-3365, doi:10.1091/mbc.e07-03-0218 (2007).

59 Lama, J., Mangasarian, A. & Trono, D. Cell-surface expression of CD4 reduces HIV-1 infectivity by blocking Env incorporation in a Nef- and Vpu-inhibitable manner. *Curr Biol* **9**, 622-631, doi:10.1016/s0960-9822(99)80284-x (1999).

60 Armitage, A. E. *et al.* APOBEC3G-induced hypermutation of human immunodeficiency virus type-1 is typically a discrete "all or nothing" phenomenon. *PLoS Genet* **8**, e1002550, doi:10.1371/journal.pgen.1002550 (2012).

61 Feng, Y., Baig, T. T., Love, R. P. & Chelico, L. Suppression of APOBEC3-mediated restriction of HIV-1 by Vif. *Front Microbiol* **5**, 450, doi:10.3389/fmicb.2014.00450 (2014).

62 Perez-Caballero, D. *et al.* Tetherin inhibits HIV-1 release by directly tethering virions to cells. *Cell* **139**, 499-511, doi:10.1016/j.cell.2009.08.039 (2009).

63 Umviligihozo, G. *et al.* Differential Vpu-Mediated CD4 and Tetherin Downregulation Functions among Major HIV-1 Group M Subtypes. *J Virol* **94**, doi:10.1128/JVI.00293-20 (2020).

64 Guenzel, C. A., Herate, C. & Benichou, S. HIV-1 Vpr-a still "enigmatic multitasker". *Front Microbiol* **5**, 127, doi:10.3389/fmicb.2014.00127 (2014).

65 Freed, E. O. HIV-1 assembly, release and maturation. *Nat Rev Microbiol* **13**, 484-496, doi:10.1038/nrmicro3490 (2015).

66 Resh, M. D. A myristoyl switch regulates membrane binding of HIV-1 Gag. *Proc Natl Acad Sci U S A* **101**, 417-418, doi:10.1073/pnas.0308043101 (2004).

67 Alfadhli, A. *et al.* Analysis of HIV-1 Matrix-Envelope Cytoplasmic Tail Interactions. *J Virol* **93**, doi:10.1128/JVI.01079-19 (2019).

68 Votteler, J. & Sundquist, W. I. Virus budding and the ESCRT pathway. *Cell Host Microbe* **14**, 232-241, doi:10.1016/j.chom.2013.08.012 (2013).

69 Davis, D. A. *et al.* Activity of human immunodeficiency virus type 1 protease inhibitors against the initial autocleavage in Gag-Pol polyprotein processing. *Antimicrob Agents Chemother* **56**, 3620-3628, doi:10.1128/AAC.00055-12 (2012).

70 Adamson, C. S. Protease-Mediated Maturation of HIV: Inhibitors of Protease and the Maturation Process. *Mol Biol Int* **2012**, 604261, doi:10.1155/2012/604261 (2012).

71 Moir, S., Chun, T. W. & Fauci, A. S. Pathogenic mechanisms of HIV disease. *Annu Rev Pathol* **6**, 223-248, doi:10.1146/annurev-pathol-011110-130254 (2011).

72 Patel, P. *et al.* Estimating per-act HIV transmission risk: a systematic review. *AIDS* **28**, 1509-1519, doi:10.1097/QAD.0000000000000298 (2014).

73 Gonzalez, S. M., Aguilar-Jimenez, W., Su, R. C. & Rugeles, M. T. Mucosa: Key Interactions Determining Sexual Transmission of the HIV Infection. *Front Immunol* **10**, 144, doi:10.3389/fimmu.2019.00144 (2019).

74 Manches, O., Frleta, D. & Bhardwaj, N. Dendritic cells in progression and pathology of HIV infection. *Trends Immunol* **35**, 114-122, doi:10.1016/j.it.2013.10.003 (2014).

75 Kaplan, E. H. & Heimer, R. A model-based estimate of HIV infectivity via needle sharing. *J Acquir Immune Defic Syndr (1988)* **5**, 1116-1118 (1992).

76 Santmyire, B. R. Vertical transmission of HIV from mother to child in sub-Saharan Africa: modes of transmission and methods for prevention. *Obstet Gynecol Surv* **56**, 306-312, doi:10.1097/00006254-200105000-00026 (2001).

77 Rodger, A. J. *et al.* Risk of HIV transmission through condomless sex in serodifferent gay couples with the HIV-positive partner taking suppressive antiretroviral therapy (PARTNER): final results of a multicentre, prospective, observational study. *Lancet* **393**, 2428-2438, doi:10.1016/S0140-6736(19)30418-0 (2019).

78 Pinkerton, S. D. & Abramson, P. R. Effectiveness of condoms in preventing HIV transmission. *Soc Sci Med* **44**, 1303-1312, doi:10.1016/s0277-9536(96)00258-4 (1997).

79 Baeten, J. M., Haberer, J. E., Liu, A. Y. & Sista, N. Preexposure prophylaxis for HIV prevention: where have we been and where are we going? *J Acquir*

Immune Defic Syndr **63 Suppl 2**, S122-129, doi:10.1097/QAI.0b013e3182986f69 (2013).

80 Fauci, A. S., Pantaleo, G., Stanley, S. & Weissman, D. Immunopathogenic mechanisms of HIV infection. *Ann Intern Med* **124**, 654-663, doi:10.7326/0003-4819-124-7-199604010-00006 (1996).

81 Moss, A. R. & Bacchetti, P. Natural history of HIV infection. *AIDS* **3**, 55-61, doi:10.1097/00002030-198902000-00001 (1989).

82 Mindel, A. & Tenant-Flowers, M. ABC of AIDS: Natural history and management of early HIV infection. *BMJ* **322**, 1290-1293, doi:10.1136/bmj.322.7297.1290 (2001).

83 Shepherd, J. C. *et al.* Emergence and persistence of CXCR4-tropic HIV-1 in a population of men from the multicenter AIDS cohort study. *J Infect Dis* **198**, 1104-1112, doi:10.1086/591623 (2008).

84 Huang, L. & Crothers, K. HIV-associated opportunistic pneumonias. *Respirology* **14**, 474-485, doi:10.1111/j.1440-1843.2009.01534.x (2009).

85 Sabin, C. A. Do people with HIV infection have a normal life expectancy in the era of combination antiretroviral therapy? *BMC Med* **11**, 251, doi:10.1186/1741-7015-11-251 (2013).

86 Marcus, J. L. *et al.* Comparison of Overall and Comorbidity-Free Life Expectancy Between Insured Adults With and Without HIV Infection, 2000-2016. *JAMA Netw Open* **3**, e207954, doi:10.1001/jamanetworkopen.2020.7954 (2020).

87 Arts, E. J. & Hazuda, D. J. HIV-1 antiretroviral drug therapy. *Cold Spring Harb Perspect Med* **2**, a007161, doi:10.1101/cshperspect.a007161 (2012).

88 Qian, K., Morris-Natschke, S. L. & Lee, K. H. HIV entry inhibitors and their potential in HIV therapy. *Med Res Rev* **29**, 369-393, doi:10.1002/med.20138 (2009).

89 Perelson, A. S. *et al.* Decay characteristics of HIV-1-infected compartments during combination therapy. *Nature* **387**, 188-191, doi:10.1038/387188a0 (1997).

90 Montessori, V., Press, N., Harris, M., Akagi, L. & Montaner, J. S. Adverse effects of antiretroviral therapy for HIV infection. *CMAJ* **170**, 229-238 (2004).

91 Chen, Y., Chen, K. & Kalichman, S. C. Barriers to HIV Medication Adherence as a Function of Regimen Simplification. *Ann Behav Med* **51**, 67-78, doi:10.1007/s12160-016-9827-3 (2017).

92 Nachega, J. B. *et al.* HIV treatment adherence, drug resistance, virologic failure: evolving concepts. *Infect Disord Drug Targets* **11**, 167-174, doi:10.2174/18715261179558966 3 (2011).

93 Gonzalo, T., Garcia Goni, M. & Munoz-Fernandez, M. A. Socio-economic impact of antiretroviral treatment in HIV patients. An economic review of cost savings after introduction of HAART. *AIDS Rev* **11**, 79-90 (2009).

94 Landais, E. & Moore, P. L. Development of broadly neutralizing antibodies in HIV-1 infected elite neutralizers. *Retrovirology* **15**, 61, doi:10.1186/s12977-018-0443-0 (2018).

95 Burton, D. R. & Hangartner, L. Broadly Neutralizing Antibodies to HIV and Their Role in Vaccine Design. *Annu Rev Immunol* **34**, 635-659, doi:10.1146/annurev-immunol-041015-055515 (2016).

96 Escolano, A. *et al.* Immunization expands B cells specific to HIV-1 V3 glycan in mice and macaques. *Nature* **570**, 468-473, doi:10.1038/s41586-019-1250-z (2019).

97 Dosenovic, P. *et al.* Immunization for HIV-1 Broadly Neutralizing Antibodies in Human Ig Knockin Mice. *Cell* **161**, 1505-1515, doi:10.1016/j.cell.2015.06.003 (2015).

98 Escolano, A. *et al.* Sequential Immunization Elicits Broadly Neutralizing Anti-HIV-1 Antibodies in Ig Knockin Mice. *Cell* **166**, 1445-1458 e1412, doi:10.1016/j.cell.2016.07.030 (2016).

99 Steichen, J. M. *et al.* A generalized HIV vaccine design strategy for priming of broadly neutralizing antibody responses. *Science* **366**, doi:10.1126/science.aax4380 (2019).

100 Xu, K. *et al.* Epitope-based vaccine design yields fusion peptide-directed antibodies that neutralize diverse strains of HIV-1. *Nat Med* **24**, 857-867, doi:10.1038/s41591-018-0042-6 (2018).

101 Wu, X. & Kong, X. P. Antigenic landscape of the HIV-1 envelope and new immunological concepts defined by HIV-1 broadly neutralizing antibodies. *Curr Opin Immunol* **42**, 56-64, doi:10.1016/j.coi.2016.05.013 (2016).

102 West, A. P., Jr. *et al.* Structural insights on the role of antibodies in HIV-1 vaccine and therapy. *Cell* **156**, 633-648, doi:10.1016/j.cell.2014.01.052 (2014).

103 Liu, Y., Cao, W., Sun, M. & Li, T. Broadly neutralizing antibodies for HIV-1: efficacies, challenges and opportunities. *Emerg Microbes Infect* **9**, 194-206, doi:10.1080/22221751.2020.1713707 (2020).

104 Caskey, M. *et al.* Viraemia suppressed in HIV-1-infected humans by broadly neutralizing antibody 3BNC117. *Nature* **522**, 487-491, doi:10.1038/nature14411 (2015).

105 Caskey, M. *et al.* Antibody 10-1074 suppresses viremia in HIV-1-infected individuals. *Nat Med* **23**, 185-191, doi:10.1038/nm.4268 (2017).

106 Scheid, J. F. *et al.* HIV-1 antibody 3BNC117 suppresses viral rebound in humans during treatment interruption. *Nature* **535**, 556-560, doi:10.1038/nature18929 (2016).

107 Mendoza, P. *et al.* Combination therapy with anti-HIV-1 antibodies maintains viral suppression. *Nature* **561**, 479-484, doi:10.1038/s41586-018-0531-2 (2018).

108 Klein, F. *et al.* HIV therapy by a combination of broadly neutralizing antibodies in humanized mice. *Nature* **492**, 118-122, doi:10.1038/nature11604 (2012).

109 Hutter, G. *et al.* Long-term control of HIV by CCR5 Delta32/Delta32 stem-cell transplantation. *N Engl J Med* **360**, 692-698, doi:10.1056/NEJMoa0802905 (2009).

110 Gupta, R. K. *et al.* HIV-1 remission following CCR5 Delta 32/Delta 32 haematopoietic stem-cell transplantation. *Nature* **568**, 244-+, doi:10.1038/s41586-019-1027-4 (2019).

111 Lopalco, L. CCR5: From Natural Resistance to a New Anti-HIV Strategy. *Viruses* **2**, 574-600, doi:10.3390/v2020574 (2010).

112 Liu, C., Ma, X., Liu, B., Chen, C. & Zhang, H. HIV-1 functional cure: will the dream come true? *BMC Med* **13**, 284, doi:10.1186/s12916-015-0517-y (2015).

113 Siliciano, R. F. & Greene, W. C. HIV latency. *Cold Spring Harb Perspect Med* **1**, a007096, doi:10.1101/cshperspect.a007096 (2011).

114 Abner, E. & Jordan, A. HIV "shock and kill" therapy: In need of revision. *Antiviral Res* **166**, 19-34, doi:10.1016/j.antiviral.2019.03.008 (2019).

115 Halper-Stromberg, A. *et al.* Broadly neutralizing antibodies and viral inducers decrease rebound from HIV-1 latent reservoirs in humanized mice. *Cell* **158**, 989-999, doi:10.1016/j.cell.2014.07.043 (2014).

116 Bullen, C. K., Laird, G. M., Durand, C. M., Siliciano, J. D. & Siliciano, R. F. New ex vivo approaches distinguish effective and ineffective single agents for reversing HIV-1 latency in vivo. *Nat Med* **20**, 425-429, doi:10.1038/nm.3489 (2014).

117 Lucera, M. B. *et al.* The histone deacetylase inhibitor vorinostat (SAHA) increases the susceptibility of uninfected CD4+ T cells to HIV by increasing the kinetics and efficiency of postentry viral events. *J Virol* **88**, 10803-10812, doi:10.1128/JVI.00320-14 (2014).

118 Jones, R. B. *et al.* Histone deacetylase inhibitors impair the elimination of HIV-infected cells by cytotoxic T-lymphocytes. *PLoS Pathog* **10**, e1004287, doi:10.1371/journal.ppat.1004287 (2014).

119 Gama, L. *et al.* Reactivation of simian immunodeficiency virus reservoirs in the brain of virally suppressed macaques. *AIDS* **31**, 5-14, doi:10.1097/QAD.0000000000001267 (2017).

120 Wallet, C. *et al.* Microglial Cells: The Main HIV-1 Reservoir in the Brain. *Front Cell Infect Microbiol* **9**, 362, doi:10.3389/fcimb.2019.00362 (2019).

121 Katlama, C. *et al.* Barriers to a cure for HIV: new ways to target and eradicate HIV-1 reservoirs. *Lancet* **381**, 2109-2117, doi:10.1016/S0140-6736(13)60104-X (2013).

122 Gebara, N. Y., El Kamari, V. & Rizk, N. HIV-1 elite controllers: an immunovirological review and clinical perspectives. *J Virus Erad* **5**, 163-166 (2019).

123 Fellay, J. *et al.* A whole-genome association study of major determinants for host control of HIV-1. *Science* **317**, 944-947, doi:10.1126/science.1143767 (2007).

124 Casado, C. *et al.* Permanent control of HIV-1 pathogenesis in exceptional elite controllers: a model of spontaneous cure. *Sci Rep* **10**, 1902, doi:10.1038/s41598-020-58696-y (2020).

125 Haworth, K. G., Peterson, C. W. & Kiem, H. P. CCR5-edited gene therapies for HIV cure: Closing the door to viral entry. *Cytotherapy* **19**, 1325-1338, doi:10.1016/j.jcyt.2017.05.013 (2017).

126 Mehmetoglu-Gurbuz, T., Yeh, R., Garg, H. & Joshi, A. Combination gene therapy for HIV using a conditional suicidal gene with CCR5 knockout. *Virol J* **18**, 31, doi:10.1186/s12985-021-01501-7 (2021).

127 Ahlenstiel, C. L., Symonds, G., Kent, S. J. & Kelleher, A. D. Block and Lock HIV Cure Strategies to Control the Latent Reservoir. *Front Cell Infect Microbiol* **10**, 424, doi:10.3389/fcimb.2020.00424 (2020).

128 Balazs, A. B. *et al.* Antibody-based protection against HIV infection by vectored immunoprophylaxis. *Nature* **481**, 81-84, doi:10.1038/nature10660 (2011).

129 Johnson, P. R. *et al.* Vector-mediated gene transfer engenders long-lived neutralizing activity and protection against SIV infection in monkeys. *Nat Med* **15**, 901-906, doi:10.1038/nm.1967 (2009).

130 Gardner, M. R. *et al.* AAV-expressed eCD4-Ig provides durable protection from multiple SHIV challenges. *Nature* **519**, 87-U173, doi:10.1038/nature14264 (2015).

131 Martinez-Navio, J. M. *et al.* Adeno-Associated Virus Delivery of Anti-HIV Monoclonal Antibodies Can Drive Long-Term Virologic Suppression. *Immunity* **50**, 567-575 e565, doi:10.1016/j.immuni.2019.02.005 (2019).

132 Gardner, M. R. *et al.* Anti-drug Antibody Responses Impair Prophylaxis Mediated by AAV-Delivered HIV-1 Broadly Neutralizing Antibodies. *Mol Ther* **27**, 650-660, doi:10.1016/j.ymthe.2019.01.004 (2019).

133 Choudhary, S. K. & Margolis, D. M. Curing HIV: Pharmacologic approaches to target HIV-1 latency. *Annu Rev Pharmacol Toxicol* **51**, 397-418, doi:10.1146/annurev-pharmtox-010510-100237 (2011).

134 Bruel, T. & Schwartz, O. Markers of the HIV-1 reservoir: facts and controversies. *Curr Opin HIV AIDS* **13**, 383-388, doi:10.1097/COH.0000000000000482 (2018).

135 Gardner, M. R. & Farzan, M. Engineering antibody-like inhibitors to prevent and treat HIV-1 infection. *Curr Opin HIV AIDS* **12**, 294-301, doi:10.1097/COH.0000000000000367 (2017).

136 Falkenhagen, A. & Joshi, S. Further Characterization of the Bifunctional HIV Entry Inhibitor sCD4-FIT45. *Mol Ther Nucleic Acids* **7**, 387-395, doi:10.1016/j.omtn.2017.04.017 (2017).

137 Schooley, R. T. *et al.* Recombinant soluble CD4 therapy in patients with the acquired immunodeficiency syndrome (AIDS) and AIDS-related complex. A phase I-II escalating dosage trial. *Ann Intern Med* **112**, 247-253, doi:10.7326/0003-4819-112-4-247 (1990).

138 Schacker, T. *et al.* Phase-I Study of High-Dose, Intravenous Rscd4 in Subjects with Advanced Hiv-1 Infection. *J Acq Immun Def Synd* **9**, 145-152 (1995).

139 Daar, E. S., Li, X. L., Moudgil, T. & Ho, D. D. High concentrations of recombinant soluble CD4 are required to neutralize primary human immunodeficiency virus type 1 isolates. *Proc Natl Acad Sci U S A* **87**, 6574-6578 (1990).

140 Klasse, P. J. & McKeating, J. A. Soluble CD4 and CD4 immunoglobulin-selected HIV-1 variants: a phenotypic characterization. *AIDS Res Hum Retroviruses* **9**, 595-604, doi:10.1089/aid.1993.9.595 (1993).

141 McKeating, J. A. *et al.* Resistance of a human serum-selected human immunodeficiency virus type 1 escape mutant to neutralization by CD4 binding site monoclonal antibodies is conferred by a single amino acid change in gp120. *J Virol* **67**, 5216-5225 (1993).

142 Grupping, K. *et al.* MiniCD4 protein resistance mutations affect binding to the HIV-1 gp120 CD4 binding site and decrease entry efficiency. *Retrovirology* **9**, 36, doi:10.1186/1742-4690-9-36 (2012).

143 Arthos, J. *et al.* Biochemical and biological characterization of a dodecameric CD4-Ig fusion protein: implications for therapeutic and vaccine strategies. *J Biol Chem* **277**, 11456-11464, doi:10.1074/jbc.M111191200 (2002).

144 Traunecker, A., Schneider, J., Kiefer, H. & Karjalainen, K. Highly efficient neutralization of HIV with recombinant CD4-immunoglobulin molecules. *Nature* **339**, 68-70, doi:10.1038/339068a0 (1989).

145 Amitai, A., Chakraborty, A. K. & Kardar, M. The low spike density of HIV may have evolved because of the effects of T helper cell depletion on affinity maturation. *PLoS Comput Biol* **14**, e1006408, doi:10.1371/journal.pcbi.1006408 (2018).

146 Gheysen, D. *et al.* Assembly and release of HIV-1 precursor Pr55gag virus-like particles from recombinant baculovirus-infected insect cells. *Cell* **59**, 103-112, doi:10.1016/0092-8674(89)90873-8 (1989).

147 Carlson, L. A. *et al.* Three-dimensional analysis of budding sites and released virus suggests a revised model for HIV-1 morphogenesis. *Cell Host Microbe* **4**, 592-599, doi:10.1016/j.chom.2008.10.013 (2008).

148 Goicochea, N. L. *et al.* Structure and stoichiometry of template-directed recombinant HIV-1 Gag particles. *J Mol Biol* **410**, 667-680, doi:10.1016/j.jmb.2011.04.012 (2011).

149 Montefiori, D. C. Evaluating neutralizing antibodies against HIV, SIV, and SHIV in luciferase reporter gene assays. *Curr Protoc Immunol* **Chapter 12**, Unit 12 11, doi:10.1002/0471142735.im1211s64 (2005).

150 Tkach, M. & Thery, C. Communication by Extracellular Vesicles: Where We Are and Where We Need to Go. *Cell* **164**, 1226-1232, doi:10.1016/j.cell.2016.01.043 (2016).

151 deCamp, A. *et al.* Global panel of HIV-1 Env reference strains for standardized assessments of vaccine-elicited neutralizing antibodies. *J Virol* **88**, 2489-2507, doi:10.1128/JVI.02853-13 (2014).

152 Cohen, Y. Z. *et al.* Relationship between latent and rebound viruses in a clinical trial of anti-HIV-1 antibody 3BNC117. *J Exp Med* **215**, 2311-2324, doi:10.1084/jem.20180936 (2018).

153 Kolchinsky, P. *et al.* Adaptation of a CCR5-using, primary human immunodeficiency virus type 1 isolate for CD4-independent replication. *J Virol* **73**, 8120-8126 (1999).

154 Gorry, P. R. *et al.* Increased CCR5 affinity and reduced CCR5/CD4 dependence of a neurovirulent primary human immunodeficiency virus type

1 isolate. *J Virol* **76**, 6277-6292, doi:10.1128/jvi.76.12.6277-6292.2002 (2002).

155 Lauren, A., Vincic, E., Hoshino, H., Thorstensson, R. & Fenyo, E. M. CD4-independent use of the CCR5 receptor by sequential primary SIVsm isolates. *Retrovirology* **4**, 50, doi:10.1186/1742-4690-4-50 (2007).

156 Mates, J. M. *et al.* Mouse Liver Sinusoidal Endothelium Eliminates HIV-Like Particles from Blood at a Rate of 100 Million per Minute by a Second-Order Kinetic Process. *Front Immunol* **8**, 35, doi:10.3389/fimmu.2017.00035 (2017).

157 Dreja, H., Pade, C., Chen, L. & McKnight, A. CD4 binding site broadly neutralizing antibody selection of HIV-1 escape mutants. *J Gen Virol* **96**, 1899-1905, doi:10.1099/vir.0.000120 (2015).

158 Lynch, R. M. *et al.* HIV-1 fitness cost associated with escape from the VRC01 class of CD4 binding site neutralizing antibodies. *J Virol* **89**, 4201-4213, doi:10.1128/JVI.03608-14 (2015).

159 McLinden, R. J. *et al.* Detection of HIV-1 neutralizing antibodies in a human CD4(+)/CXCR4(+)/CCR5(+) T-lymphoblastoid cell assay system. *PLoS One* **8**, e77756, doi:10.1371/journal.pone.0077756 (2013).

160 Fellinger, C. H. *et al.* eCD4-Ig Limits HIV-1 Escape More Effectively than CD4-Ig or a Broadly Neutralizing Antibody. *J Virol* **93**, doi:10.1128/JVI.00443-19 (2019).

161 Roh, K. H., Lillemeier, B. F., Wang, F. & Davis, M. M. The coreceptor CD4 is expressed in distinct nanoclusters and does not colocalize with T-cell

receptor and active protein tyrosine kinase p56lck. *Proc Natl Acad Sci U S A* **112**, E1604-1613, doi:10.1073/pnas.1503532112 (2015).

162 Singer, II *et al.* CCR5, CXCR4, and CD4 are clustered and closely apposed on microvilli of human macrophages and T cells. *J Virol* **75**, 3779-3790, doi:10.1128/JVI.75.8.3779-3790.2001 (2001).

163 Sougrat, R. *et al.* Electron tomography of the contact between T cells and SIV/HIV-1: implications for viral entry. *PLoS Pathog* **3**, e63, doi:10.1371/journal.ppat.0030063 (2007).

164 Chojnacki, J. *et al.* Maturation-dependent HIV-1 surface protein redistribution revealed by fluorescence nanoscopy. *Science* **338**, 524-528, doi:10.1126/science.1226359 (2012).

165 Sullivan, N. *et al.* Determinants of human immunodeficiency virus type 1 envelope glycoprotein activation by soluble CD4 and monoclonal antibodies. *J Virol* **72**, 6332-6338 (1998).

166 Ishikawa, F. *et al.* Development of functional human blood and immune systems in NOD/SCID/IL2 receptor {gamma} chain(null) mice. *Blood* **106**, 1565-1573, doi:10.1182/blood-2005-02-0516 (2005).

167 Saito, Y., Ellegast, J. M. & Manz, M. G. Generation of Humanized Mice for Analysis of Human Dendritic Cells. *Methods Mol Biol* **1423**, 309-320, doi:10.1007/978-1-4939-3606-9_22 (2016).

168 Hammonds, J. *et al.* Gp120 stability on HIV-1 virions and Gag-Env pseudovirions is enhanced by an uncleaved Gag core. *Virology* **314**, 636-649, doi:10.1016/s0042-6822(03)00467-7 (2003).

169 Gach, J. S. *et al.* Human immunodeficiency virus type-1 (HIV-1) evades antibody-dependent phagocytosis. *PLoS Pathog* **13**, e1006793, doi:10.1371/journal.ppat.1006793 (2017).

170 Vink, C. A. *et al.* Eliminating HIV-1 Packaging Sequences from Lentiviral Vector Proviruses Enhances Safety and Expedites Gene Transfer for Gene Therapy. *Mol Ther* **25**, 1790-1804, doi:10.1016/j.ymthe.2017.04.028 (2017).

171 Diskin, R. *et al.* Increasing the potency and breadth of an HIV antibody by using structure-based rational design. *Science* **334**, 1289-1293, doi:10.1126/science.1213782 (2011).

172 Lorenzi, J. C. *et al.* Paired quantitative and qualitative assessment of the replication-competent HIV-1 reservoir and comparison with integrated proviral DNA. *Proc Natl Acad Sci U S A* **113**, E7908-E7916, doi:10.1073/pnas.1617789113 (2016).

173 Brandenberg, O. F. *et al.* Partial rescue of V1V2 mutant infectivity by HIV-1 cell-cell transmission supports the domain's exceptional capacity for sequence variation. *Retrovirology* **11**, 75, doi:10.1186/s12977-014-0075-y (2014).

174 Li, H. *et al.* Envelope residue 375 substitutions in simian-human immunodeficiency viruses enhance CD4 binding and replication in rhesus macaques. *Proc Natl Acad Sci U S A* **113**, E3413-3422, doi:10.1073/pnas.1606636113 (2016).

175 Zhang, Y. J. *et al.* Envelope-dependent, cyclophilin-independent effects of glycosaminoglycans on human immunodeficiency virus type 1 attachment

and infection. *J Virol* **76**, 6332-6343, doi:10.1128/jvi.76.12.6332-6343.2002 (2002).

176 West, A. P., Jr. *et al.* Computational analysis of anti-HIV-1 antibody neutralization panel data to identify potential functional epitope residues. *Proc Natl Acad Sci U S A* **110**, 10598-10603, doi:10.1073/pnas.1309215110 (2013).

177 Sanders, R. W. *et al.* A next-generation cleaved, soluble HIV-1 Env trimer, BG505 SOSIP.664 gp140, expresses multiple epitopes for broadly neutralizing but not non-neutralizing antibodies. *PLoS Pathog* **9**, e1003618, doi:10.1371/journal.ppat.1003618 (2013).

178 West, A. P., Jr. *et al.* Evaluation of CD4-CD4i antibody architectures yields potent, broadly cross-reactive anti-human immunodeficiency virus reagents. *J Virol* **84**, 261-269, doi:10.1128/JVI.01528-09 (2010).

179 Wang, H. *et al.* Cryo-EM structure of a CD4-bound open HIV-1 envelope trimer reveals structural rearrangements of the gp120 V1V2 loop. *Proc Natl Acad Sci U S A* **113**, E7151-E7158, doi:10.1073/pnas.1615939113 (2016).

180 Mastronarde, D. N. Automated electron microscope tomography using robust prediction of specimen movements. *J Struct Biol* **152**, 36-51, doi:10.1016/j.jsb.2005.07.007 (2005).

181 Hagen, W. J. H., Wan, W. & Briggs, J. A. G. Implementation of a cryo-electron tomography tilt-scheme optimized for high resolution subtomogram averaging. *J Struct Biol* **197**, 191-198, doi:10.1016/j.jsb.2016.06.007 (2017).

182 Kremer, J. R., Mastronarde, D. N. & McIntosh, J. R. Computer visualization of three-dimensional image data using IMOD. *J Struct Biol* **116**, 71-76, doi:10.1006/jsbi.1996.0013 (1996).

183 Scharf, L. *et al.* Broadly Neutralizing Antibody 8ANC195 Recognizes Closed and Open States of HIV-1 Env. *Cell* **162**, 1379-1390, doi:10.1016/j.cell.2015.08.035 (2015).

184 Horwitz, J. A. *et al.* Non-neutralizing Antibodies Alter the Course of HIV-1 Infection In Vivo. *Cell* **170**, 637-648 e610, doi:10.1016/j.cell.2017.06.048 (2017).

185 Salazar-Gonzalez, J. F. *et al.* Deciphering human immunodeficiency virus type 1 transmission and early envelope diversification by single-genome amplification and sequencing. *J Virol* **82**, 3952-3970, doi:10.1128/JVI.02660-07 (2008).

186 McCoy, L. E. & Burton, D. R. Identification and specificity of broadly neutralizing antibodies against HIV. *Immunol Rev* **275**, 11-20, doi:10.1111/imr.12484 (2017).

187 Hoffmann, M. A. G. *et al.* Nanoparticles presenting clusters of CD4 expose a universal vulnerability of HIV-1 by mimicking target cells. *Proc Natl Acad Sci U S A* **117**, 18719-18728, doi:10.1073/pnas.2010320117 (2020).

188 Kessler, P. D. *et al.* Gene delivery to skeletal muscle results in sustained expression and systemic delivery of a therapeutic protein. *Proc Natl Acad Sci U S A* **93**, 14082-14087, doi:10.1073/pnas.93.24.14082 (1996).

189 Rivera, V. M. *et al.* Long-term regulated expression of growth hormone in mice after intramuscular gene transfer. *Proc Natl Acad Sci U S A* **96**, 8657-8662, doi:10.1073/pnas.96.15.8657 (1999).

190 Hemphill, D. D., McIlwraith, C. W., Slayden, R. A., Samulski, R. J. & Goodrich, L. R. Adeno-associated virus gene therapy vector scAAVIGF-I for transduction of equine articular chondrocytes and RNA-seq analysis. *Osteoarthritis Cartilage* **24**, 902-911, doi:10.1016/j.joca.2015.12.001 (2016).

191 Pastuzyn, E. D. *et al.* The Neuronal Gene Arc Encodes a Repurposed Retrotransposon Gag Protein that Mediates Intercellular RNA Transfer (vol 172, pg 275, 2018). *Cell* **173**, 275-275, doi:10.1016/j.cell.2018.03.024 (2018).

192 Sliepen, K. *et al.* Structure and immunogenicity of a stabilized HIV-1 envelope trimer based on a group-M consensus sequence. *Nat Commun* **10**, 2355, doi:10.1038/s41467-019-10262-5 (2019).

193 Liu, Z. *et al.* Systematic comparison of 2A peptides for cloning multi-genes in a polycistronic vector. *Sci Rep* **7**, 2193, doi:10.1038/s41598-017-02460-2 (2017).

194 Sarcar, S. *et al.* Next-generation muscle-directed gene therapy by in silico vector design. *Nat Commun* **10**, 492, doi:10.1038/s41467-018-08283-7 (2019).

195 Fuchs, S. P., Martinez-Navio, J. M., Rakasz, E. G., Gao, G. & Desrosiers, R. C. Liver-Directed but Not Muscle-Directed AAV-Antibody Gene Transfer

Limits Humoral Immune Responses in Rhesus Monkeys. *Mol Ther Methods Clin Dev* **16**, 94-102, doi:10.1016/j.omtm.2019.11.010 (2020).

196 McClure, M. O. *et al.* HIV infection of primate lymphocytes and conservation of the CD4 receptor. *Nature* **330**, 487-489, doi:10.1038/330487a0 (1987).

197 Challis, R. C. *et al.* Systemic AAV vectors for widespread and targeted gene delivery in rodents. *Nat Protoc* **14**, 379-414, doi:10.1038/s41596-018-0097-3 (2019).

198 Hoffmann, M. A. G., Kieffer, C. & Bjorkman, P. J. In vitro characterization of engineered red blood cells as viral traps against HIV-1 and SARS-CoV-2. *Mol Ther Methods Clin Dev* **21**, 161-170, doi:10.1016/j.omtm.2021.03.003 (2021).

199 Rossi, L., Fraternale, A., Bianchi, M. & Magnani, M. Red Blood Cell Membrane Processing for Biomedical Applications. *Front Physiol* **10**, 1070, doi:10.3389/fphys.2019.01070 (2019).

200 Villa, C. H., Cines, D. B., Siegel, D. L. & Muzykantov, V. Erythrocytes as Carriers for Drug Delivery in Blood Transfusion and Beyond. *Transfus Med Rev* **31**, 26-35, doi:10.1016/j.tmrv.2016.08.004 (2017).

201 Oldenborg, P. A. *et al.* Role of CD47 as a marker of self on red blood cells. *Science* **288**, 2051-2054, doi:10.1126/science.288.5473.2051 (2000).

202 Zeira, M. *et al.* Full-length CD4 electroinserted in the erythrocyte membrane as a long-lived inhibitor of infection by human immunodeficiency virus. *Proc Natl Acad Sci U S A* **88**, 4409-4413, doi:10.1073/pnas.88.10.4409 (1991).

203 Idziorek, T. & Klatzmann, D. Functional expression of the CD4 protein after cross-linking to red blood cells with a bifunctional reagent. *Biochim Biophys Acta* **1062**, 39-45, doi:10.1016/0005-2736(91)90332-3 (1991).

204 Asher, D. R., Cerny, A. M. & Finberg, R. W. The erythrocyte viral trap: transgenic expression of viral receptor on erythrocytes attenuates coxsackievirus B infection. *Proc Natl Acad Sci U S A* **102**, 12897-12902, doi:10.1073/pnas.0506211102 (2005).

205 Halder, U. C. Bone marrow stem cells to destroy circulating HIV: a hypothetical therapeutic strategy. *J Biol Res (Thessalon)* **25**, 3, doi:10.1186/s40709-018-0075-5 (2018).

206 Herbst, F. *et al.* Extensive methylation of promoter sequences silences lentiviral transgene expression during stem cell differentiation in vivo. *Mol Ther* **20**, 1014-1021, doi:10.1038/mt.2012.46 (2012).

207 Alvarez-Dominguez, J. R., Zhang, X. & Hu, W. Widespread and dynamic translational control of red blood cell development. *Blood* **129**, 619-629, doi:10.1182/blood-2016-09-741835 (2017).

208 Nguyen, A. T. *et al.* UBE2O remodels the proteome during terminal erythroid differentiation. *Science* **357**, doi:10.1126/science.aan0218 (2017).

209 Shi, J. H. *et al.* Engineered red blood cells as carriers for systemic delivery of a wide array of functional probes. *P Natl Acad Sci USA* **111**, 10131-10136, doi:10.1073/pnas.1409861111 (2014).

210 Huang, N. J. *et al.* Genetically engineered red cells expressing single domain camelid antibodies confer long-term protection against botulinum neurotoxin. *Nat Commun* **8**, 423, doi:10.1038/s41467-017-00448-0 (2017).

211 Popik, W., Alce, T. M. & Au, W. C. Human immunodeficiency virus type 1 uses lipid raft-colocalized CD4 and chemokine receptors for productive entry into CD4(+) T cells. *J Virol* **76**, 4709-4722, doi:10.1128/jvi.76.10.4709-4722.2002 (2002).

212 Romero, Z. *et al.* beta-globin gene transfer to human bone marrow for sickle cell disease. *J Clin Invest*, doi:10.1172/JCI67930 (2013).

213 Cavrois, M., De Noronha, C. & Greene, W. C. A sensitive and specific enzyme-based assay detecting HIV-1 virion fusion in primary T lymphocytes. *Nat Biotechnol* **20**, 1151-1154, doi:10.1038/nbt745 (2002).

214 Shao, B. *et al.* O-glycans direct selectin ligands to lipid rafts on leukocytes. *Proc Natl Acad Sci U S A* **112**, 8661-8666, doi:10.1073/pnas.1507712112 (2015).

215 Dennehy, J. J., Friedenberg, N. A., Yang, Y. W. & Turner, P. E. Virus population extinction via ecological traps. *Ecol Lett* **10**, 230-240, doi:10.1111/j.1461-0248.2006.01013.x (2007).

216 Trakarnsanga, K. *et al.* An immortalized adult human erythroid line facilitates sustainable and scalable generation of functional red cells. *Nat Commun* **8**, 14750, doi:10.1038/ncomms14750 (2017).

217 Daniels, D. E. *et al.* Comparing the two leading erythroid lines BEL-A and HUDEP-2. *Haematologica* **105**, e389-e394, doi:10.3324/haematol.2019.229211 (2020).

218 Hoffmann, M. *et al.* SARS-CoV-2 Cell Entry Depends on ACE2 and TMPRSS2 and Is Blocked by a Clinically Proven Protease Inhibitor. *Cell*, doi:10.1016/j.cell.2020.02.052 (2020).

219 Crawford, K. H. D. *et al.* Protocol and Reagents for Pseudotyping Lentiviral Particles with SARS-CoV-2 Spike Protein for Neutralization Assays. *Viruses-Basel* **12**, doi:ARTN 513

10.3390/v12050513 (2020).

220 Glassman, P. M. *et al.* Vascular Drug Delivery Using Carrier Red Blood Cells: Focus on RBC Surface Loading and Pharmacokinetics. *Pharmaceutics* **12**, doi:10.3390/pharmaceutics12050440 (2020).

221 Villa, C. H., Anselmo, A. C., Mitragotri, S. & Muzykantov, V. Red blood cells: Supercarriers for drugs, biologicals, and nanoparticles and inspiration for advanced delivery systems. *Adv Drug Deliv Rev* **106**, 88-103, doi:10.1016/j.addr.2016.02.007 (2016).

222 Scott, M. D., Murad, K. L., Koumpouras, F., Talbot, M. & Eaton, J. W. Chemical camouflage of antigenic determinants: stealth erythrocytes. *Proc Natl Acad Sci U S A* **94**, 7566-7571, doi:10.1073/pnas.94.14.7566 (1997).

223 Sternberg, N., Georgieva, R., Duft, K. & Baumler, H. Surface-modified loaded human red blood cells for targeting and delivery of drugs. *J Microencapsul* **29**, 9-20, doi:10.3109/02652048.2011.629741 (2012).

224 Zhao, Z. *et al.* Systemic tumour suppression via the preferential accumulation of erythrocyte-anchored chemokine-encapsulating nanoparticles in lung metastases. *Nat Biomed Eng*, doi:10.1038/s41551-020-00644-2 (2020).

225 Murciano, J. C. *et al.* Prophylactic fibrinolysis through selective dissolution of nascent clots by tPA-carrying erythrocytes. *Nat Biotechnol* **21**, 891-896, doi:10.1038/nbt846 (2003).

226 Zaitsev, S. *et al.* Sustained thromboprophylaxis mediated by an RBC-targeted pro-urokinase zymogen activated at the site of clot formation. *Blood* **115**, 5241-5248, doi:10.1182/blood-2010-01-261610 (2010).

227 Villa, C. H. *et al.* Biocompatible coupling of therapeutic fusion proteins to human erythrocytes. *Blood Adv* **2**, 165-176, doi:10.1182/bloodadvances.2017011734 (2018).

228 Carnemolla, R. *et al.* Targeting thrombomodulin to circulating red blood cells augments its protective effects in models of endotoxemia and ischemia-reperfusion injury. *FASEB J* **31**, 761-770, doi:10.1096/fj.201600912R (2017).

229 Wu, Y., Beddall, M. H. & Marsh, J. W. Rev-dependent indicator T cell line. *Curr HIV Res* **5**, 394-402, doi:10.2174/157016207781024018 (2007).

230 Giarratana, M. C. *et al.* Proof of principle for transfusion of in vitro-generated red blood cells. *Blood* **118**, 5071-5079, doi:10.1182/blood-2011-06-362038 (2011).

231 Lorentz, K. M., Kontos, S., Diaceri, G., Henry, H. & Hubbell, J. A. Engineered binding to erythrocytes induces immunological tolerance to E. coli asparaginase. *Sci Adv* **1**, e1500112, doi:10.1126/sciadv.1500112 (2015).

232 Pishesha, N. *et al.* Engineered erythrocytes covalently linked to antigenic peptides can protect against autoimmune disease. *Proc Natl Acad Sci U S A* **114**, 3157-3162, doi:10.1073/pnas.1701746114 (2017).

233 Zhang, Q. *et al.* Cellular Nanosponges Inhibit SARS-CoV-2 Infectivity. *Nano Lett* **20**, 5570-5574, doi:10.1021/acs.nanolett.0c02278 (2020).

234 Zaitsev, S. *et al.* Targeting recombinant thrombomodulin fusion protein to red blood cells provides multifaceted thromboprophylaxis. *Blood* **119**, 4779-4785, doi:10.1182/blood-2011-12-398149 (2012).

235 Taylor, R. P. *et al.* In vivo binding and clearance of circulating antigen by bispecific heteropolymer-mediated binding to primate erythrocyte complement receptor. *J Immunol* **148**, 2462-2468 (1992).

236 Votteler, J. *et al.* Designed proteins induce the formation of nanocage-containing extracellular vesicles. *Nature* **540**, 292-+, doi:10.1038/nature20607 (2016).

237 Ryan, M. D. & Drew, J. Foot-and-Mouth-Disease Virus 2a Oligopeptide Mediated Cleavage of an Artificial Polyprotein. *Embo J* **13**, 928-933, doi:DOI 10.1002/j.1460-2075.1994.tb06337.x (1994).

238 Organization, W. H. *COVID-19 Dashboard*, <https://covid19.who.int/> (2021).

239 Abdelrahman, Z., Li, M. & Wang, X. Comparative Review of SARS-CoV-2, SARS-CoV, MERS-CoV, and Influenza A Respiratory Viruses. *Front Immunol* **11**, 552909, doi:10.3389/fimmu.2020.552909 (2020).

240 Zhao, J., Cui, W. & Tian, B. P. The Potential Intermediate Hosts for SARS-CoV-2. *Front Microbiol* **11**, 580137, doi:10.3389/fmicb.2020.580137 (2020).

241 Alluwaimi, A. M., Alshubaith, I. H., Al-Ali, A. M. & Abohelaika, S. The Coronaviruses of Animals and Birds: Their Zoonosis, Vaccines, and Models for SARS-CoV and SARS-CoV2. *Front Vet Sci* **7**, 582287, doi:10.3389/fvets.2020.582287 (2020).

242 Li, W. *et al.* Receptor and viral determinants of SARS-coronavirus adaptation to human ACE2. *Embo J* **24**, 1634-1643, doi:10.1038/sj.emboj.7600640 (2005).

243 Altmann, D. M., Boyton, R. J. & Beale, R. Immunity to SARS-CoV-2 variants of concern. *Science* **371**, 1103-1104, doi:10.1126/science.abg7404 (2021).

244 Bernal, J. L. *et al.* Effectiveness of Covid-19 Vaccines against the B.1.617.2 (Delta) Variant. *New Engl J Med*, doi:10.1056/NEJMoa2108891 (2021).

245 Corbett, K. S. *et al.* SARS-CoV-2 mRNA vaccine design enabled by prototype pathogen preparedness. *Nature* **586**, 567-571, doi:10.1038/s41586-020-2622-0 (2020).

246 Barnes, C. O. *et al.* Structures of Human Antibodies Bound to SARS-CoV-2 Spike Reveal Common Epitopes and Recurrent Features of Antibodies. *Cell* **182**, 828-842 e816, doi:10.1016/j.cell.2020.06.025 (2020).

247 Polack, F. P. *et al.* Safety and Efficacy of the BNT162b2 mRNA Covid-19 Vaccine. *N Engl J Med* **383**, 2603-2615, doi:10.1056/NEJMoa2034577 (2020).

248 Baden, L. R. *et al.* Efficacy and Safety of the mRNA-1273 SARS-CoV-2 Vaccine. *N Engl J Med* **384**, 403-416, doi:10.1056/NEJMoa2035389 (2021).

249 Jackson, L. A. *et al.* An mRNA Vaccine against SARS-CoV-2 - Preliminary Report. *N Engl J Med* **383**, 1920-1931, doi:10.1056/NEJMoa2022483 (2020).

250 Walls, A. C. *et al.* Elicitation of Potent Neutralizing Antibody Responses by Designed Protein Nanoparticle Vaccines for SARS-CoV-2. *Cell* **183**, 1367-1382 e1317, doi:10.1016/j.cell.2020.10.043 (2020).

251 Keech, C. *et al.* Phase 1-2 Trial of a SARS-CoV-2 Recombinant Spike Protein Nanoparticle Vaccine. *N Engl J Med* **383**, 2320-2332, doi:10.1056/NEJMoa2026920 (2020).

252 Chen, R. E. *et al.* Resistance of SARS-CoV-2 variants to neutralization by monoclonal and serum-derived polyclonal antibodies. *Nat Med*, doi:10.1038/s41591-021-01294-w (2021).

253 Wu, K. *et al.* Serum Neutralizing Activity Elicited by mRNA-1273 Vaccine. *N Engl J Med*, doi:10.1056/NEJMc2102179 (2021).

254 Planas, D. *et al.* Reduced sensitivity of SARS-CoV-2 variant Delta to antibody neutralization. *Nature* **596**, 276-280, doi:10.1038/s41586-021-03777-9 (2021).

255 Our-World-in-Data. *Coronavirus (COVID-19) Vaccinations*, <https://ourworldindata.org/covid-vaccinations> (2021).

256 A.A. Cohen, Z. Y., P. Gnanapragasam, S. Ou, K. Dam, H. Wang, P. J. Bjorkman. Construction, characterization, and immunization of nanoparticles that display a diverse array of influenza HA trimers. *http://biorxiv.org/lookup/doi/10.1101/2020.01.18.911388* (2020).

257 Cohen, A. A. *et al.* Mosaic nanoparticles elicit cross-reactive immune responses to zoonotic coronaviruses in mice. *Science* **371**, 735-741, doi:10.1126/science.abf6840 (2021).

258 Walls, A. C. *et al.* Elicitation of broadly protective sarbecovirus immunity by receptor-binding domain nanoparticle vaccines. *bioRxiv*, doi:10.1101/2021.03.15.435528 (2021).

259 Premkumar, L. *et al.* The receptor binding domain of the viral spike protein is an immunodominant and highly specific target of antibodies in SARS-CoV-2 patients. *Sci Immunol* **5**, doi:10.1126/sciimmunol.abc8413 (2020).

260 Shah, P., Canziani, G. A., Carter, E. P. & Chaiken, I. The Case for S2: The Potential Benefits of the S2 Subunit of the SARS-CoV-2 Spike Protein as an Immunogen in Fighting the COVID-19 Pandemic. *Front Immunol* **12**, 637651, doi:10.3389/fimmu.2021.637651 (2021).

261 Pinto, D. *et al.* Broad betacoronavirus neutralization by a stem helix-specific human antibody. *Science*, doi:10.1126/science.abj3321 (2021).

262 Wang, C. *et al.* A conserved immunogenic and vulnerable site on the coronavirus spike protein delineated by cross-reactive monoclonal antibodies. *Nat Commun* **12**, 1715, doi:10.1038/s41467-021-21968-w (2021).

263 Hsieh, C. L. *et al.* Structure-based design of prefusion-stabilized SARS-CoV-2 spikes. *Science* **369**, 1501-1505, doi:10.1126/science.abd0826 (2020).

264 Bachmann, M. F. & Jennings, G. T. Vaccine delivery: a matter of size, geometry, kinetics and molecular patterns. *Nat Rev Immunol* **10**, 787-796, doi:10.1038/nri2868 (2010).

265 Kushnir, N., Streatfield, S. J. & Yusibov, V. Virus-like particles as a highly efficient vaccine platform: diversity of targets and production systems and advances in clinical development. *Vaccine* **31**, 58-83, doi:10.1016/j.vaccine.2012.10.083 (2012).

266 Daniloski, Z. *et al.* The Spike D614G mutation increases SARS-CoV-2 infection of multiple human cell types. *Elife* **10**, doi:10.7554/eLife.65365 (2021).

267 Pallesen, J. *et al.* Immunogenicity and structures of a rationally designed prefusion MERS-CoV spike antigen. *Proc Natl Acad Sci U S A* **114**, E7348-E7357, doi:10.1073/pnas.1707304114 (2017).

268 McBride, C. E., Li, J. & Machamer, C. E. The cytoplasmic tail of the severe acute respiratory syndrome coronavirus spike protein contains a novel

endoplasmic reticulum retrieval signal that binds COPI and promotes interaction with membrane protein. *J Virol* **81**, 2418-2428, doi:10.1128/JVI.02146-06 (2007).

269 Tan, T. K. *et al.* A COVID-19 vaccine candidate using SpyCatcher multimerization of the SARS-CoV-2 spike protein receptor-binding domain induces potent neutralising antibody responses. *Nat Commun* **12**, 542, doi:10.1038/s41467-020-20654-7 (2021).

270 Marcandalli, J. *et al.* Induction of Potent Neutralizing Antibody Responses by a Designed Protein Nanoparticle Vaccine for Respiratory Syncytial Virus. *Cell* **176**, 1420-1431 e1417, doi:10.1016/j.cell.2019.01.046 (2019).

271 Shukla, G. S., Sun, Y. J., Pero, S. C., Sholler, G. S. & Krag, D. N. Immunization with tumor neoantigens displayed on T7 phage nanoparticles elicits plasma antibody and vaccine-draining lymph node B cell responses. *J Immunol Methods* **460**, 51-62, doi:10.1016/j.jim.2018.06.009 (2018).

272 Sanders, R. W. *et al.* Stabilization of the soluble, cleaved, trimeric form of the envelope glycoprotein complex of human immunodeficiency virus type 1. *J Virol* **76**, 8875-8889, doi:10.1128/jvi.76.17.8875-8889.2002 (2002).

273 Yu, J. *et al.* DNA vaccine protection against SARS-CoV-2 in rhesus macaques. *Science* **369**, 806-811, doi:10.1126/science.abc6284 (2020).

274 Schoenmaker, L. *et al.* mRNA-lipid nanoparticle COVID-19 vaccines: Structure and stability. *Int J Pharm* **601**, 120586, doi:10.1016/j.ijpharm.2021.120586 (2021).

275 Gilleron, J. *et al.* Image-based analysis of lipid nanoparticle-mediated siRNA delivery, intracellular trafficking and endosomal escape. *Nat Biotechnol* **31**, 638-646, doi:10.1038/nbt.2612 (2013).

276 Wang, Y. & Huang, L. A window onto siRNA delivery. *Nat Biotechnol* **31**, 611-612, doi:10.1038/nbt.2634 (2013).

277 Wittrup, A. *et al.* Visualizing lipid-formulated siRNA release from endosomes and target gene knockdown. *Nat Biotechnol* **33**, 870-876, doi:10.1038/nbt.3298 (2015).

278 Huang, L., Ashraf, S. & Lilley, D. M. J. The role of RNA structure in translational regulation by L7Ae protein in archaea. *RNA* **25**, 60-69, doi:10.1261/rna.068510.118 (2019).

279 Prel, A. *et al.* Highly efficient in vitro and in vivo delivery of functional RNAs using new versatile MS2-chimeric retrovirus-like particles. *Mol Ther Methods Clin Dev* **2**, 15039, doi:10.1038/mtm.2015.39 (2015).

280 Pardi, N., Hogan, M. J., Porter, F. W. & Weissman, D. mRNA vaccines - a new era in vaccinology. *Nat Rev Drug Discov* **17**, 261-279, doi:10.1038/nrd.2017.243 (2018).

281 Wang, Q. *et al.* ARMMs as a versatile platform for intracellular delivery of macromolecules. *Nat Commun* **9**, 960, doi:10.1038/s41467-018-03390-x (2018).

282 Cox, D. B. T. *et al.* RNA editing with CRISPR-Cas13. *Science* **358**, 1019-1027, doi:10.1126/science.aaq0180 (2017).

283 Zost, S. J. *et al.* Rapid isolation and profiling of a diverse panel of human monoclonal antibodies targeting the SARS-CoV-2 spike protein. *Nat Med* **26**, 1422-1427, doi:10.1038/s41591-020-0998-x (2020).

284 Johnson, M. C. *et al.* Optimized Pseudotyping Conditions for the SARS-COV-2 Spike Glycoprotein. *J Virol* **94**, doi:10.1128/JVI.01062-20 (2020).

285 Beissert, T. *et al.* A Trans-amplifying RNA Vaccine Strategy for Induction of Potent Protective Immunity. *Mol Ther* **28**, 119-128, doi:10.1016/j.ymthe.2019.09.009 (2020).

286 McKay, P. F. *et al.* Self-amplifying RNA SARS-CoV-2 lipid nanoparticle vaccine candidate induces high neutralizing antibody titers in mice. *Nat Commun* **11**, 3523, doi:10.1038/s41467-020-17409-9 (2020).

287 Yang, L., Bailey, L., Baltimore, D. & Wang, P. Targeting lentiviral vectors to specific cell types in vivo. *Proc Natl Acad Sci U S A* **103**, 11479-11484, doi:10.1073/pnas.0604993103 (2006).